Mg/Hydroxyapatite composites for potential bio-medical applications

Zibiao Li

Thesis submitted for the degree of

M. Phil

at the

Brunel University

Brunel Centre for Advanced Solidification Technology

(BCAST)

August 2010

Contents

Key words explanation

Undercooling: also known as supercooling**,** is the process of lowering the temperature of a liquid or a gas below its freezing point, without it becoming a solid. Below this temperature liquid gets solidified.

Solid-solution strengthening: a type of alloying that can be used to improve the strength of a pure metal. The technique works by adding atoms of one element (the alloying element) to the crystalline lattice of another element (the base metal). The alloying element diffuses into the matrix, forming a solid solution.

Dispersion strengthening: also called age hardening, is a heat treatment technique used to increase the yield strength of malleable materials, including most structural alloys of aluminium, magnesium, nickel and titanium, and some stainless steels. It relies on changes in solid solubility with temperature to produce fine particles of an impurity phase, which impede the movement of dislocations, or defects in a crystal's lattice. Since dislocations are often the dominant carriers of plasticity, this serves to harden the material.

Yield strength (YS): defined in engineering and materials science as the stress at which a material begins to deform plastically.

Ultimate tensile strength (UTS): indicated by the maximum of a stress-strain curve and, in general, indicates when necking will occur.

Elongation: a test to measure the ductility. When a material is tested for tensile strength it elongates a certain amount before fracture takes place.

In vivo: experimentation using a whole, living organism as opposed to a partial or dead organism, or an *in vitro* controlled environment. Animal testing and clinical trials are two forms of *in vivo* research.

In vitro: performed not in a living organism but in a controlled environment. **Cytotoxicity**: the quality of being toxic to cells. Examples of toxic agents are a

chemical substance, an immune cell or some types of venom.

Lysis: refers to the breaking down of a cell, often by viral, enzymic or osmotic mechanisms that compromise its integrity.

Osteoconductivity: refers to ability of any structure that facilitates the formation of bone structure.

MTT assay: colorimetric assays for measuring the activity of enzymes that reduce MTT or close dyes (XTT, MTS, WSTs) to formazan dyes, giving a purple color.

Acidosis: an increased acidity in the blood. (i.e., an increased hydronium ion concentration). It usually refers to acidity of the blood plasma.

Osteoblast: mononucleate cells that are responsible for bone formation; in essence, osteoblasts are sophisticated fibroblasts that express all genes that fibroblasts (a type of cell that plays a critical role in wound healing) express, with the addition of the genes for bone sialoprotein and osteocalcin.

Anti-corrosion: refers to the protection of metal surfaces from corroding in aggressive (corroding) environments.

Galvanic corrosion: an electrochemical process in which one metal corrodes preferentially when in electrical contact with a different type of metal and both metals are immersed in an electrolyte.

Synovial tissue: the soft tissue that lines the non-cartilaginous surfaces within joints with cavities (synovial joints).

Histology: is the study of the microscopic anatomy of cells and tissues of plants and animals. It is performed by examining a thin slice (section) of tissue under a light microscope or electron microscope.

Osteogenesis: the process of laying down new bone material by cells called osteoblasts.

List of figures

Chapter 2 – Literature review

Chapter 3 – Experimental Techniques & Procedure

Chapter 4 – Results and Discussions

List of tables

Chapter 1
Introduction

1.1 Background

Depending on an excellent combination of high mechanical property and fracture toughness, metallic biomaterials have been widely accepted for clinical application of bone fixation. However, some prominent disadvantages such as stress shielding effect due to their high elastic modulus, poisonous ions released by corrosion or mechanical wear [Puleo and Huh, 1995] definitely restrict their effective performance in-service. In addition, patients also have to bear the pain resulted from second surgery for removing implants. Although bio-degradable polymers and ceramics seem to solve the tough problem as promising substitutes, the low mechanical property and rapid corrosion rate make them fail to qualify against the bear-loading requirement in body. Therefore, we desperately look for a non-toxic suitable material for medical application which possesses appropriate mechanical properties, and favourable corrosion resistance.

1.1.1 Mg and its alloys for medical application

In light of the moderate elastic modulus and density which are quite similar to natural bone, magnesium and its alloys of non-toxic composition can be regarded as potential bio-resorbable material, which not only avoid the second surgery and minimize the patient's pain but also contribute to accelerating bone restoration. As a result, over the last decade, a large number of researchers have investigated their properties in order to achieve the purpose of clinical application.

Generally speaking, magnesium alloys available nowadays are designed for commercial industrial applications, which contain other bio-poisonous elements such as Al, and rare earth elements. Moreover, since those alloys are susceptible to Cl ion

containing physiological environment, the subcutaneous cavity formed by the rapid evolution of hydrogen gas can negatively affect osteoconductivity. Hence, it is necessary to select alloying elements based on their influence on mechanical properties, biocompatibility and corrosion resistance.

Zinc is one of the most abundant nutritionally essential elements in the human body, and considered as a safe element for biomedical applications. When alloyed with Mg, it can improve the corrosion resistance and mechanical properties. Additionally, due to low density and biological function, calcium is regarded as an indispensable bio-alloying element. Therefore, we strongly believe that the ternary alloy of Mg-Zn-Ca synthesized with optimized composition may be able to perfectly suit load-bearing application.

1.1.2 Metal matrix composites

In the past, although magnesium alloys were identified as potentially suitable bio-degradable medical material, either their mechanical properties or corrosion resistance failed to satisfy the strict requirement in-service. Currently, it is therefore necessary to investigate a novel method by which designed magnesium alloys possess a controllable corrosion rate in physiological condition without compromising their mechanical properties.

Metal matrix composites (MMC) based on magnesium alloys seem to be a feasible approach to work out the tough problem. A metal matrix composite (MMC) generally consists of at least two constituent parts, one is a metal as matrix and the other constituent is possibly another metal or different kind of material, such as a ceramic or organic compound as reinforcement. Moreover, according to the form of reinforcement in the matrix, the composite microstructures are also divided in to three types, which are monofilaments, whisker fibres and particulate composition. In the last decade, MMCs have been paid more attention in automotive and general transportation industry due to their relative high stiffness, strength, creep resistance

and favourable corrosion behaviour [Clyne, 2000]. On the basis of Mg-Zn-Ca alloy as the metal matrix, if we choose an appropriate reinforcement particle, a good combination of corrosion resistance and mechanical properties may be achieved.

As a composition of natural bone, hydroxyapatite (HA) has been widely employed in medical applications. In addition, HA possesses a low solubility in the body environment [Fulmer et al., 2002]. Hence, it is reasonable to suggest that HA can be a suitable reinforcement in Mg-based MMCs.

1.2 Aim and objectives

In this study, the main objective is to prepare metal matrix composites based on Mg-Zn-Ca alloy as the matrix and HA particles as reinforcement for potential bio-medical application. Since the alloyed elements in this study and HA reinforcement are absolutely bio-safe, it is now important to enhance mechanical property and corrosion behaviour. The key approach to achieve the aim is to refine the microstructure, especially for improving the distribution of HA particles.

An impeller is designed according to crucible dimension and is employed to stir the Mg/HA slurry, which should impact on the uniform distribution of the reinforcement. Therefore, the mixing procedure is carefully conducted prior to directly cast or other processes. Due to the high cooling rate, high pressure die-casting (HPDC) process can refine the microstructure. In order to improve the mechanical properties and corrosion behaviour, we have used the HPDC process. In addition, intensive shearing the Mg/HA slurry using melt conditioning by advanced shear technology (MCAST) process has been adopted to improve homogeneous dispersion of intermetallic particles and HA particles.

In this thesis, the effect of HA particle addition on refining the grain size of Mg-Zn-Ca and AZ91D magnesium alloys is also systematically investigated. For this study, to maintain a constant cooling rate in casting process and to simulate cooling

conditions that are normally achieved in industrial practice such as in direct chill casting process, the standard test procedure-1 (TP1) mould is used for casting and investigated the grain refinement characteristics in detailed.

1.3 Thesis outline

This thesis is divided into 6 Chapters. Chapter 1 presents a brief introduction, aims, objectives and thesis outline. In Chapter 2, a literature review is presented, which consist of two parts. Part 1 reviews in detail the current research and relevant technology development in the field of bio-degradable medical materials. Part 2 of this chapter mainly discusses the metallurgical aspects of Mg alloys. Chapter 3 presents experimental procedure and working principles of techniques used in this work. The experimental results obtained in this research are presented in Chapter 4, which include the optical microscopy studies, XRD investigation, micro-hardness investigation, tensile properties, cooling curve measurements and detailed measurements of average grain size. Moreover, the discussion of the corresponding results is also given in this chapter.

In Chapter 5, we have concluded the results. The recommendation for further work related to process improvement that can effectively further improve distribution of HA in Mg alloy, and the detailed experimental plan in association with characterization of bio-medical properties of these materials are presented in Chapter 6.

Chapter 2
Literature Review
Part 1: Biomaterials

2.1.1 Introduction

Since metallic biomaterials possess a good combination of high mechanical properties and fracture toughness, they are widely being used in load-bearing bio-medical applications. However, some clinical limitations of these materials such as cobalt chromium alloys, stainless steel 316L, pure titanium and titanium alloys [Frosch and Stürme, 2006] confine their application. For instance, the stress shielding effect is induced due to the much higher elastic modulus of metal in-service in comparison with that of natural bone [Harvey et al., 1999]. This phenomenon could contribute to accelerate the resorption of bone in vicinity of the implant, resulting in unbalanced load supported by the metal instead of the surrounding bone. Eventually, the implant will fail to satisfy the requirement of load-bearing fixation. Moreover, the surface of metallic implants is impossible to match perfectly with bone surface, while the toxic ions released by corrosion or mechanical wear [Puleo and Huh, 1995] could cause deleterious influence on the bone and tissue response (e.g. less bone formation and inflammation). On the basis of those negative effects, biodegradable polymers and resorbable ceramics have widely been developed as alternatives to permanent metallic implants, whereas the low mechanical properties retarded their clinical application.

Currently, iron and magnesium are two promising candidates for bio-medical application. If we take the elastic modulus and density of iron (91 GPa and 7.8 $g.cm^{-3}$ respectively) into account, it is obviously noted that Fe does not seem to be an excellent option for bone fixation because of the prominent deviation from those of

natural bone (10-15 GPa and 1.5-2.0 $g.cm^{-3}$ respectively). However, according to some specific advantages of iron, it may conform to the requirement of specific applications such as biodegradable vascular stents [Waksman et al., 2008]. Therefore, despite Mg yield strength (55 MPa) being lower than that of natural bone (e.g. femur ≈110 MPa) [Gu et al., 2009; Li et al., 2008], the elastic modulus and density of magnesium are similar to human bone.

The bio-medical implant based on magnesium and its alloys offer a novel vehicle to relieve the patient's pain due to avoiding second surgery for removing the bone fixation. Normally speaking, the physiological concentration of magnesium ions released by corrosion will sustain a relative constant standard in serum via storage in the muscle and the bone, while the excess magnesium ions in the serum are excreted by the kidney [Lothar, 2000]. As a result, the toxic reaction caused by the excess quantity of Mg ions could be efficiently avoided. Moreover, during the corrosion process of magnesium alloys, the complicated protective layer which consists of the precipitated calcium phosphates and corrosion products like magnesium oxides and magnesium hydroxides formed on the surface of implants *in vivo* improve the osteoconductivity but retard the corrosion. Nevertheless, as a negative effect on the tissue around the implant, the fast evolution of hydrogen gas caused by corrosion in the physiological condition may result in subcutaneous cavity formation. However, the hydrogen gas produced by the corrosion of Mg alloy implants placed at different locations *in vivo* resulted in different consequences. Depending on the pre-operation and post-operation investigation of Mg alloys, as cardiovascular stents in animals, the hydrogen evolution seems to rarely cause remarkable inflammation. The hydrogen is completely eliminated within two months due to less weight of implants and good transportation by blood circulation [Heublein et al., 2003]. The subcutaneous cavity formation is attributed to the rapid gas generation, and is responsible for the negative effect on bone healing.

On the basis of the enormous progress in the field of synthesis technology, advanced approaches in preparation of alloys have given researchers firm confidence that Mg

and its alloys could be used as bio-medical implants in place of non-corrosion metallic materials like stainless steel and polymeric materials, although polymeric medical implants also possess the capability of degradation in physiological environment and non-toxicity. Nevertheless, the fast corrosion rate and low mechanical properties of polymeric materials cannot offer sufficient support in comparison with magnesium alloys. For instance, the magnesium alloys containing rare earth elements with better corrosion behaviour can provide 2-times higher tensile yield strength (200 MPa) and 4-times higher young's modulus (45 MPa) than the bio-degradable polymeric implants (u-HA/PLLA 50/50) currently in clinical application [Shikinami and Okuno, 1999].

2.1.2 The corrosion mechanism of magnesium in aqueous conditions

Magnesium and its alloys undergo electrochemical reaction easily in aqueous conditions. Magnesium hydroxide and hydrogen are generally observed as corrosion products. The entire corrosion equation of magnesium in aqueous solution is:

$$Mg_{(s)} + 2\,H_2O_{(aq)} \leftrightarrow Mg(OH)_{2\,(s)} + H_{2\,(g)}$$

This reaction could be divided into three partial equations:

$$Mg_{(s)} \leftrightarrow Mg^{2+}_{(aq)} + 2\,e^- \text{ (anodic reaction)}$$

$$2\,H_2O_{(aq)} + 2\,e^- \leftrightarrow H_{2\,(g)} + 2\,OH^-_{(aq)} \text{ (cathodic reaction)}$$

$$Mg^{2+}_{(aq)} + 2\,OH^-_{(aq)} \leftrightarrow Mg(OH)_{2\,(s)} \text{ (product formation)}$$

Although the $Mg(OH)_2$ film formed on the surface of Mg could temporarily retard the corrosion to some extent, it will become susceptible when the concentration of aggressive chloride ions increases above 30 mmol/l [Shaw, 2003] and eventually transform into $MgCl_2$ with high solubility. Therefore, it is worth mentioning that Mg alloys as bio-degradable implants will be subjected to serious corrosion due to the

presence of high Cl^- concentration (150 mmol/l) in physiological conditions [Xu et al., 2007; Witte et al., 2005 and 2006].

2.1.3 Magnesium corrosion in relation to biocompatibility

Yun et al. [Yun et al., 2009] have performed the special investigation of Mg corrosion and osteoblasts cell culture. The corrosion potential of pure magnesium immersed in phosphate-buffered saline (PBS) solution obtained from polarization curves was -1.53 V, which is a little lower than the standard corrosion potential of Mg at 25 ^{O}C. It was associated with the formation of magnesium hydroxide resulting from the dissolution of Mg as protective layers which retarded the process of corrosion in aggressive ion containing environment [Song and Atrens, 2003]. Combined with the results of E_{corr} measured in deionized water (-1.4 V) and McCoy's 5A culture medium (-1.55 V), the most noble corrosion potential of Mg was observed in non-ions water, which indicate that the slowest corrosion occurred in the condition with absence of invasive ions. Nevertheless, although the E_{corr} in PBS was quite similar to that in McCoy's 5A-5% fetal bovine serum (FBS), the corrosion current density was four-fold higher than that in McCoy's 5A-5% FBS, which may be responsible for the positive effect of albumin or other proteins on the corrosion resistance [Rettig and Virtanen, 2007].

The time-dependant tests using open circuit potential and electrochemical impedance in various solutions were performed for Mg. Passivation layer is observed to form on the surfaces of all magnesium samples according to the change of corrosion resistance, whereas the more compact and homogeneous protective layer was observed for the sample in McCoy's 5A-5% FBS. The morphology and composition analysis of corrosion surface after 5 days confirmed the existence of the passivation layer during the corrosion in comparison with non-corroded Mg surface. The energy dispersion analysis (EDS) results indicated that the corrosion films in McCoy's 5A-5% FBS and PBS also contained oxygen, chloride, phosphate and potassium rather than just magnesium like the sample in de-ionized water.

The result of cell culture *in vitro* revealed that no remarkable viability enhancement of U2OS (a human osteosarcoma cell line) cells was observed because of the presence of magnesium, which is slightly different from the proliferation improvement of L-929 cells by magnesium ions as reported previously [Li et al., 2008]. However, the existence of magnesium promoted the mineral deposition process and didn't cause cell lysis or cytotoxicity.

2.1.4 Bone response during the corrosion of bio-degradable implants

The degradation mechanism on the bone-implant interface of different magnesium alloys adjacent to bone and the effect on the surrounding bone has been widely studied by a large number of researchers. However, little information about the impact on the corrosion process by local condition is available. High pH (>11.5) could enhance a stable protective hydroxide layer on the surface of the Mg alloy implants and low pH (<11.5) could increase the corrosion process in aqueous solution [Pourbaix, 1974]. Based on this result, we can speculate that the surface corrosion rate of magnesium alloy implants obviously elevate due to low pH value caused by acidosis after surgery.

Witte et al. [Witte, 2005] have investigated the degradable process happening on the bone-magnesium alloy interface and analyzed bone formation in the vicinity of bio-degradable magnesium implants (AZ31, AZ91, WE43, LAE442) in comparison with currently degradable polymers (SR-PLA96) used in clinical practices. The remarkably better osteoblast activity and a greater deposition rate of mineral in the vicinity of degradable Mg implants relative to a degradable polymer implant were observed. It can be explained that magnesium ions positively affect the synthesis of biological nucleic acids and the activity of enzymes which manage the nucleic acids [Katayanagi et al., 1990] or the protein translation for the extracellular matrix such as collagen type 1 was observed to be enhanced due to the presence of high Mg ion concentration. Furthermore, on the basis of different composition among these alloys,

the magnesium implants possessed different corrosion rate but generate similar calcium phosphates on the surface which could retard corrosion behaviour *in vivo*. As an unavoidable product of corrosion *in vivo*, limited amount of hydrogen gas does not result in adverse impact because of its disappearance caused by blood flux within 2-3 weeks.

2.1.5 Biological stimulus for bone growth

Magnesium alloys as bio-medical degradable implants *in vivo* initiates the process of bone formation [Witte et al., 2005; Xu et al., 2007]. Electrical stimulation during the corrosion of magnesium alloys stimulates the bio-activity of osteoblast and accelerates the deposition of the bone [Xu et al., 2007]. It was responsible for the slow evolution of hydrogen gas which is related to the corrosion rate of Mg alloys containing various alloying elements [Witte et al., 2008]. The surface properties of magnesium alloys such as surface roughness, energy and charge, which can be modified by different post-treatment, are regarded as acceptable reasons that activate the bone healing.

Positive bone response has been observed regardless of the composition of the magnesium alloys. Therefore, the common corrosion product in vivo, magnesium hydroxide, is paid more attention. Due to the susceptible resistance of $Mg(OH)_2$ to Cl^--containing physiological environment, Janning et al. [Janning et al., 2010] presume that the good biological influence on the bone activity around the bio-degradable implant is primarily associated with the local reinforced concentration of Mg ions by dissolution of magnesium hydroxide as well as in collaboration with local alkalosis.

In vivo studies in rabbits [Janning et al., 2010] indicate that the volume of bone in the vicinity of magnesium hydroxide cylinders with low corrosion rate increased, which results from the improvement of osteoblast activity and the temporary reduction of osteoclast number. It is worth noticing that temporary reduction of bone resorption

has never been reported by *in vivo* study previously. Thus, the study supports the hypothesis of "the formation of the bone adjacent to the implant was accelerated by magnesium ions released by corrosion of Mg alloys in combination with local alkalosis". However, due to the limitation of experimental instruments, it is very difficult to exactly measure the local concentration of Mg ions and the local pH value. From the previous assumption, the local pH value should vary in the range of the alkaline between 7.5 and 9.0, although it was never possible to probe the local pH value *in vivo* by a non-destructive method. In this regard, further investigation of the Mg^{2+} effect on the bone growth should be executed.

2.1.6 The effect of the microstructure on the degradable behaviour

The microstructure of Mg alloys as a bio-degradable implant is regarded as an important factor that can influence the corrosion performance when served *in vivo* condition. The bio-dissolution mechanism of magnesium alloys affected by microstructure in a chloride ion containing environment has been investigated in detail. For instance, since AZ91 magnesium alloy after die-casting possessed finer grain size and more homogeneous distribution of intermetallic phases around the boundary in comparison with conventional casting counterpart, excellent corrosion resistance was observed [Zucchi et al., 2006]. On the contrary, the investigation of AZ91 Mg alloys fabricated by different processes [Bobby, 2010] demonstrated different consequences. The Nyquist graphs (a plot between real and imaginary components of impedance) of die-cast, as-cast AZ91 Mg alloy samples and pure magnesium as a reference, shown in Fig. 2.1, indicated that the two alloys had much better corrosion properties than pure magnesium due to reduced corrosion by the addition of aluminium. Nevertheless, the polarization impedance of a sand-cast sample was marginally higher than that of the die-cast sample. The corrosion rate of the die-cast sample obtained from the polarization curve was a little lower than that of the as-cast sample, but no dramatic discrepancy between the two samples was found.

Depending on the morphological analysis of post-degradable samples, the magnesium matrix surrounded by the continuous second phase experienced severe dissolution as pitting corrosion of the die-cast sample, and eventually a configuration like honeycomb was observed because of the insolubility of β-precipitates ($Mg_{17}Al_{12}$) in the vicinity of the matrix. As a result, the implant *in vivo* revealed an obvious tendency to lose its mechanical integrity, which has attributed to the relative rapid degradation of grains in the as-cast sample and the embrittlement of the second phase. In addition, the high volume of insoluble β-precipitate that exists in the die-cast sample may cause negative impact on health in the physiological condition. Therefore, we should deeply and explicitly understand the corrosion behaviour of samples during dissolution, rather than make a conclusion to assess these bio-materials judged solely by corrosion rate, resistance and so on.

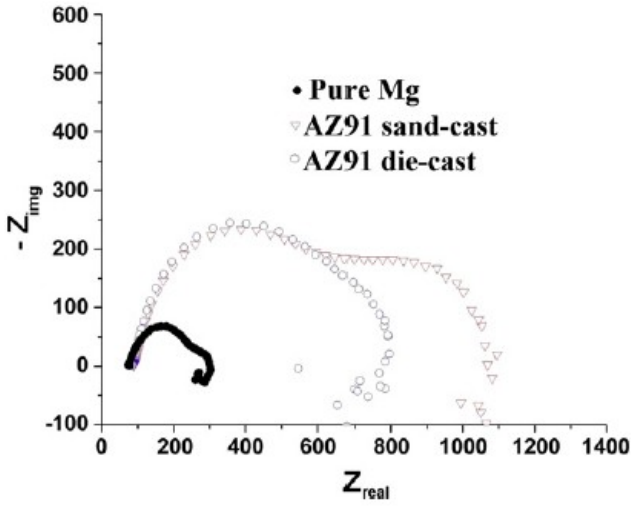

Fig. 2.1 Nyquist plots of the samples in simulated body fluid.

2.1.7 Corrosion properties of Mg alloys

2.1.7.1 Ca-addition

Some researchers have reported that the corrosion resistance against NaCl solution could be enhanced by addition of moderate Ca content.

The corrosion resistance of Mg-xCa (x=1-3 wt.%) alloy samples were explored

systematically through immersion tests and electrochemical measurements by Li et al. [Li et al., 2008]. The results demonstrated that the anti-corrosion properties decreased and the hydrogen evolution increased with increasing calcium content (Fig. 2.2).

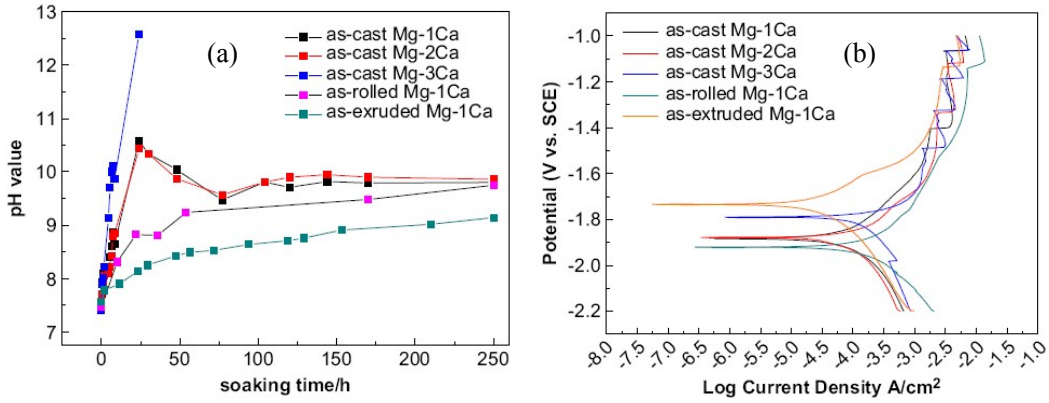

Fig. 2.2 (a) The pH variation of Mg-Ca alloys immersed in SBF as a function of time. (b) Potentiodynamic polarization curves of Mg-Ca alloys in SBF.

Zhang et al [Zhang et al., 2009 a] have also reported corrosion results of Mg-0.6%Si alloy by adding different low Ca content as shown in Table 2.1. The result showed that the addition of 0.18% Ca shifted the corrosion potential remarkably towards a more noble position, but anti-corrosion behaviour has not improved because of high corrosion density. However, the corrosion resistance significantly increased with 0.44% Ca content.

In addition, the electrochemical tests of as-cast Mg-Zn-Mn-Ca alloys containing different Ca content [Zhang and Yang, 2008] showed that the corrosion resistance slightly increased from 192 Ω/cm^2 to 266 Ω/cm^2 when the additive amount of calcium increased from 0.3 wt. % to 0.5 wt.%. However, the corrosion resistance improved significantly and the corrosion density decreased dramatically when the content of Ca increased from 0.5 wt. % to 1.0 wt. %. The tendency of the anti-corrosion property with increasing addition of calcium is quite similar to previous work [Zhang et al., 2009 a].

Table 2.1 Corrosion property of magnesium alloys. (○-**unavailable**)

Measured alloys	reference	Electrolyte composition	Test method	E_{corr} (V)	I_{corr} (μA)	R_{corr} (mmyear^{-})
99.9% Mg	Wang et al., 2008 b	SBF	Immersion test	○	○	3.0
AZ91D	Witte et al., 2005	Borax-phosphate buffer pH 7	OCP SCE	○	○	2.8
LAE442	Witte et al., 2006			○	p	6.9
AZ91	Kannan and Raman, 2008	mSBF-HEPES pH 7.4	OCP SCE	-1.73	65.7	1.1
AZ91+1%Ca				-1.57	17.8	0.3
AZ61+0.4%Ca				-1.71	36.5	0.6
Mg-Mn	Xu et al., 2007	SBF	OCP SCE	-1.85	57	○
Mg-Mn-Zn				-1.51	79	○
WE43				-1.70	16	○
AZ31(SC)	Wang et al., 2008 a	Hanks solution	Immersion test	○	○	0.7
AZ31 (ECAP)				○	○	0.54
AZ31 (HR)				○	○	0.48
AZ31	Wen et al., 2009	SBF	OCP SCE	-1.6	25.1	○
AZ31 (HA coating)				-1.42	0.03	○
AZ91-HA	Witte et al., 2007	artificial sea water	EIS	○	○	1.25±0.16
AZ91	Hu et al., 2010	SBF	EIS	-1.49	70	○
DCPD coated AZ91				-1.52	2.6	○
AZ91 (T4)	Zhou et al., 2009	SBF	EIS	-1.24	0.028 (mA)	0.61
AZ91 (T6-8h)				-1.29	0.066 (mA)	1.44
AZ91 (T4-16h)				-1.19	0.027 (mA)	0.59
AZ91 (T4-24h)				-1.29	0.074 (mA)	1.62
Mg-Ce	Ng et al. 2010	Hanks solution	EIS	-1.92	343	○
Mg-Ce (Heat treatment)				-1.85	4.0	○
Mg-0.6Si	Zhang et al., 2009 a	Hanks solution	OCP SCE	-1.727	30.6	0.38
Mg-0.6Si-0.2Ca				-1.547	36.3	0.39
Mg-0.6Si-0.4Ca				-1.536	14.3	0.15
Mg-0.6Si-1.5Zn				-1.630	12.6	0.14

The electrochemical polarization measurements of AZ91 magnesium alloy with 1 wt.% calcium and AZ61 with 0.4 wt.% calcium in modified simulated body fluid indicated that the corrosion potential obviously shifted towards positive tendency and corrosion current density decreased remarkably in comparison with those of AZ91 alloy despite the presence of similar break down potential for all alloys. This could be related to the accelerated precipitation of calcium phosphate on the surface which retards the corrosion [Kannan and Raman, 2008].

The result of degradation experiment of Mg/Ca composite prepared by powder metallurgy method in Dulbecco's modified Eagle's medium (DMEM) [Zheng et al., 2009] indicated that the corrosion resistance reduced with increasing amount of Ca particulate. It could be explained that the Ca particulate as the anodic member causes severe galvanic corrosion on the surface immersed in electrolyte with Mg matrix as the cathodic member. Therefore, increasing the amount of Ca particulate led to a growing surface area ratio of anodic Ca particulate to Mg so that it resulted in a gradually increasing corrosion rate. However, the corrosion resistance of all composite samples (Mg/1Ca, Mg/5Ca and Mg/10Ca) increased remarkably at the initial stage and kept approximately constant thereafter due to the formation of the protective film on the surface.

In addition, the compositional analysis of corrosion products for all samples demonstrated that no conspicuous difference was observed except for the first 12 hours immersion period. Improved corrosion resistance is probably due to properly refined grain size by the addition of Ca element. Most importantly, it depends on the different second phases and their distribution. Generally speaking, Mg_2Ca is a common second phase in Ca-containing Mg alloys and always plays an important role in the modification of the corrosion behaviour. Zhang and Yang [Zhang and Yang, 2008] have confirmed the effect of Mg_2Ca on the aspect of anti-corrosion by experimental results. Some other Ca-containing intermetallic phase such as Al_2Ca which forms at the cost of subsequent reduction of $Mg_{17}Al_{12}$ phase in AZ91 and AZ61 magnesium alloys is also associated with the enhancement of corrosion resistance

[Kannan and Raman, 2008]. Furthermore, it was discovered that $Mg(OH)_2$ and hydroxyapatite phases also protect alloy samples from further corrosion to some degree.

2.1.7.2 Zn-addition

Zinc can improve the corrosion resistance by increasing its mass fraction in magnesium. The addition of 1.5% Zn to Mg-0.6%Si alloy dramatically increased the anti-corrosion performance in comparison with the alloy without zinc as shown in Table 2.1 [Zhang et al., 2009 a]. Compared to the corrosion resistance of pure magnesium, an extruded Mg-6Zn alloy with the absence of second phase (γ-MgZn) possessed an excellent corrosion property [Zhang et al., 2009 b].

Yin et al [Yin et al., 2008], concluded from Fig. 2.3 that when a Mg-Zn-Mn alloy contains low Zn content (1%-2% Zn), the anti-corrosion behaviour is improved remarkably compared to higher Zn content. The corrosion test of extruded Mg-xZn-1Mn (x=1, 2, 3) in SBF also indicated that the corrosion resistance decreased with the increasing content of Zn element as shown in Table 2.2.

The existence of a Zn-rich layer on the surface of Zn-containing magnesium alloy could protect alloys from further corrosion under aggressive environment [Fan et al., 2004]. But, if the content of Zn element exceeds its maximum solubility in the magnesium matrix, the presence of a massive fraction of second phase (MgZn) accelerates the rate of corrosion and deteriorates the property of anti-corrosion. Zn forms zinc containing phosphate on the surface of magnesium alloys, which is an effective protective film. In addition, it has been extensively accepted that Zn can diminish the effects of Fe and Ni on corrosion property and then improve the anti-corrosion property of Mg-alloy [Li et al., 2006]. The corrosion products of Mg alloys when immersed in SBF, detected by XRD, includes $Mg(OH)_2$, hydroxyapatite (HA) and a kind of magnesium-substituted apatite (amorphous $(Ca_{0.86}Mg_{0.14})_{10}(PO4)_6$) which was pointed out by Kuwahara et al. [Kuwahara et al., 2001].

Table 2.2 Electrochemical parameters of extruded Mg-Zn-Mn alloys. [Yin et al., 2008]

Alloys	E_{corr}, V	R_p, KΩ	E_b, V	E_b-E_{corr}, V
Mg-1Zn-Mn	-1.47	12.35	-1.42	0.05
Mg-2Zn-Mn	-1.46	7.54	-1.38	0.08
Mg-3Zn-Mn	-1.54	4.54	-1.41	0.13

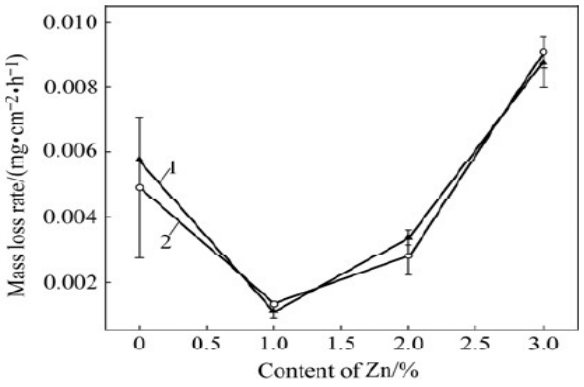

Fig. 2.3 Mass loss rate of extruded Mg-Zn-Mn alloys: 1 cross section sample;

2 longitudinal sample [Yin et al., 2008].

2.1.7.3 RE-addition

RE element was regarded as an effective potential candidate to optimize anti-corrosion property. He et al. [He et al., 2010] have investigated the bio-corrosion of extruded Mg-Zn-Mn with and without yttrium addition. The result demonstrated that the corrosion resistance can be improved remarkably due to the formation of a protective Y_2O_3 film on the surface of magnesium alloy after addition of Y element. Moreover, Zhang et al. [Zhang et al., 2008 a] indicated that the anti-corrosion properties of Mg-Zn-xY (x=0.36%, 0.82%, 1.54%) alloys with low zinc content as shown in Fig. 2.4a are better than those of AZ91E and AZ31 alloys, although an Al-rich protective film formed on the surface of AZ91E and AZ31 alloys which could decrease the rate of degradation.

In addition, the corrosion performance of Gd-containing magnesium alloys was explored by Hort et al. [Hort et al., 2009]. The results shown in Fig. 2.4b demonstrate that the anti-corrosion behaviour could be improved with the additive amount of Gd

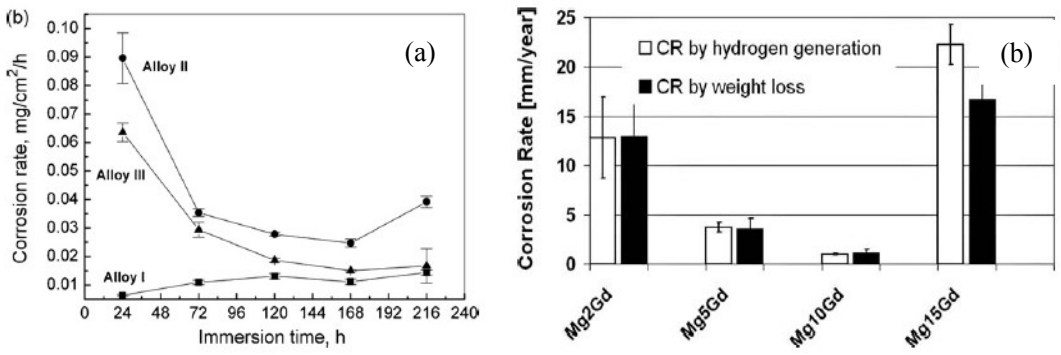

Fig. 2.4 (a) The corrosion rate of Alloy I (Mg-1.98Zn-0.36Y), Alloy II (Mg-1.84Zn-0.82Y) and Alloy III (Mg-1.73Zn-1.54Y) [Zhang et al., 2008 a]. (b) Corrosion rate determined by hydrogen evolution and weight loss for Mg-Gd alloys [Hort et al., 2009].

up to 10wt%. However, the significant increasing trend of corrosion rate was found when the Gd content is 15%. The highest content of Ni was discovered in the 15wt% Gd-containing Mg alloy as an impurity, which deteriorated the corrosion property.

2.1.8 Mechanical properties of Mg alloys & human bone

To completely meet the requirements of adequate clinical implants, the maintenance of mechanical integrity is widely regarded as a crucial parameter accompanied with corrosion resistance. Therefore, the bio-degradable material under *in vivo* service should possess appropriate strength in sync with the process of bone healing, although it can experience corrosion reaction. Mechanical properties of various bone types, biometallic materials, polymers and Mg alloys are summarized in Table 2.3.

2.1.8.1 Ca-addition

Ca has a low density (1.55g/cm^3), which provides the alloy system with the advantage of a similar density to bone. Li et al [Li et al., 2008] have reported mechanical properties of Mg-Ca alloy with different content of Ca and different processes. The result of the research reveals that yield strength (YS), ultimate tensile strength (UTS), and elongation for as-cast Mg-xCa alloy samples decreased with increase Ca content. When the content of Ca reaches ≥ 5%, the alloys are seen to be extremely

Table 2.3 Mechanical properties of natural bones and alloys. (○ **- unavailable)**

Tissue/ material	Comp. Strength (MPa)	Tensiles Strength (MPa)	E-mod. Tensile (GPa)	Yield Strength (MPa)	Elongation at break (%)	Impact strength (J/m^{-2})
Cortical bone	164-240	35-283	5-23	○	1.07-2.10	4-70
Cancellous bone	○	1.5-38	10-1570 (MPa)	○	○	○
Titanium (TiAl6V4, cast)	○	830-1025	114	760-880	12	19
Titanium (TiAl6V4,wrought)	○	896-1172	114	827-1103	10-15	○
cobalt chromium alloys	○	672-1039	○	422-649	9-36	○
Stainless steel 316L	○	480-620	193	170-310	30-40	○
Synthetic Hydroxiapatite	100-900	40-200	70-120	○	○	○
Bioactive glass	○	40-60	35	○	○	○
DL-PLA	○	29-35	1.9-2.4	○	5-6	○
AZ91E-F sand cast	97	165	45	97	2.5	2.7
AZ91E-F HPDC	165	230	45	150	3	○
AZ61A-F	125	295	○	180	12	○
AZ61A-F extruded	110-130	285-305	○	165-205	14-16	○
AZ31 extruded	83-97	241-260	○	165-200	12-16	1.78
AZ31 sheet	110-180	255-290	○	150-220	15-21	1.78
LAE442	○	247	○	148	18	○
WE43 extruded	○	277	○	198	17	○
AM50A-F	113	210	○	○	10	○
AM60B-F	130	225	○	○	8	2.8
AJ62	○	234	45	140	7	13.3

brittle at room temperature and can be broken with bare hands easily. However, the YS, UTS, and elongation increased dramatically after hot rolling and hot extrusion for as-cast alloy as shown in Fig. 2.5a, particularly for Mg-1Ca alloy. Nevertheless, the tensile strength and the elongation of binary Mg-Ca alloy could not absolutely satisfy the requirement of a load-bearing implant application [Li et al., 2008].

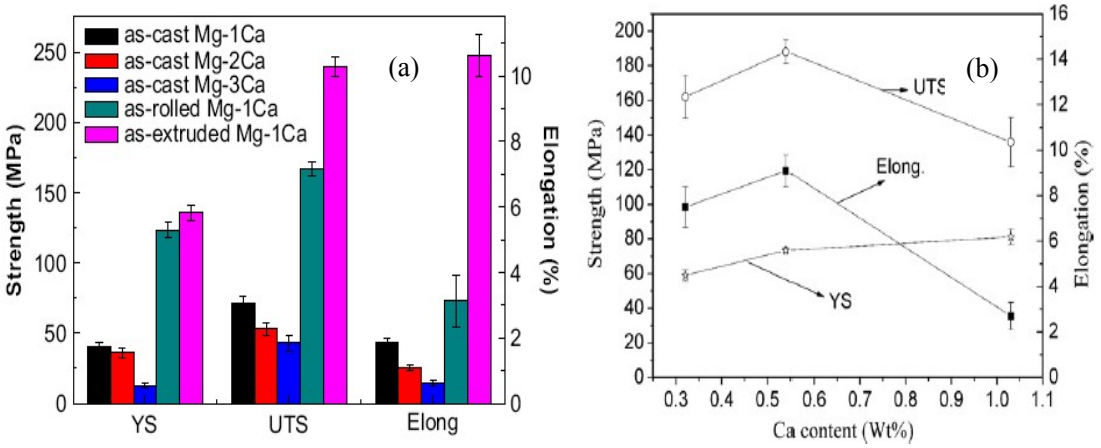

Fig. 2.5 (a) Tensile properties of as-cast Mg-1Ca alloy, as-cast Mg-2Ca alloy, as-cast Mg-3Ca alloy, as-rolled Mg-1Ca alloy and as-extruded Mg-1Ca alloy samples at room temperature [Li et al., 2008]. (b) Mechanical properties of as-cast Mg–Zn–Mn–Ca alloys [Zhang and Yang, 2008].

In addition, the influence of Ca addition to Mg-Zn-Mn-Ca alloys on the mechanical property conducted by Zhang and Yang [Zhang and Yang, 2008] demonstrated that the yield strength slightly enhanced with the increasing amount of Ca element in the alloy due to refined grain size and increased volume fraction of second phase, as shown in Fig. 2.5b. The ultimate tensile strength and the elongation of the alloy increased obviously when the additive fraction of Ca was from 0.3 wt.% to 0.5 wt.% and then dramatically decreased with further Ca addition to 1 wt.%. It could be explained that the second phase ($Ca_2Mg_6Mn_3$) in Mg-Zn-Mn-Ca alloys with 0.3 wt.% and 0.5 wt.% Ca addition transformed into new intermetallics ($Ca_2Mg_6Mn_3$ and Mg_2Ca) when the content of Ca element reached near or above 1 wt.%. Similar microhardness values for binary Mg_2Ca phase and ternary $Ca_2Mg_6Mn_3$ (125-128kg/mm^2) indicates that the two phases should possess approximately identical strengthening efficiency [Larionova et al., 2001]. However, the size difference between these two phases plays a significant role in strengthening. The ductility of Mg-0.9Ca alloy decreases due to the presence of the lamellar Mg_2Ca at the grain boundary which acts as a crack source [Chino et al., 2002]. Hassel et al. have confirmed that the mechanical properties of magnesium alloy could be slightly increased because of the appropriate Ca-addition [Hassel et al., 2006].

However, the mechanical properties of Mg-0.6Si alloy without and with Ca (the content of Ca up to 0.44%) seemed to deviate from the expectation that the mechanical property should get appropriate improvement, although the grain size and shape of second phase were refined because of the existence of relatively low Ca content [Zhang et al.,2009 a].

Zheng et al. [Zheng et al., 2009] have performed the investigation of Mg/Ca composites with different amount of calcium synthesized by PM (powder metallurgy) method. Ultimate tensile strength slightly decreased with the content of Ca element (up to 10%wt), while the tendency of the elongation to decrease was observed with increasing the fraction of Ca (up to 10%wt). Compared with as-extruded Mg-1Ca alloy, it is interesting to note that the yield strength and elongation of Mg/1Ca composite is obviously better but not the ultimate tensile strength. The positive results could be explained by the following reasons: First, the grain size is remarkably refined by PM method so that the yield strength increases in comparison with cast counterparts according to Hall-Petch law. Second, the better elongation might be attributed to the softening effect of the Mg matrix, as the similar phenomenon reported previously by [Lim and Gupta, 2001]. Third, Mg oxide layered on magnesium powder broke into particulates and distributed to the grain boundary which contributes to a mechanical reinforcement by the Orowan mechanism during extrusion [Pérez et al., 2007]. Last but not least, the positive crystallographic texture produced by extrusion resulted in the enhancement of tensile strength [Pérez et al., 2007].

Depending on those consequences of exploration of Mg alloys with the addition of Ca element, the content of calcium must be controlled within a proper range, to improve mechanical properties. Thus, further work has to be conducted.

2.1.8.2 Zn-addition

Zinc was found to be next to aluminium in strengthening effectiveness as an alloying

element in magnesium alloys through the solid solution hardening mechanism. Zhang et al. [Zhang et al, 2009 b] have measured mechanical properties of Mg-6Zn alloys after solid solution treatment and hot working. Moreover, the comparison between the obtained results and the reported properties of Mg-Ca [Li et al., 2008] and Mg-Mn-Zn [Zhang et al., 2008 b] are conducted in this work. It could be seen that the Mg-6Zn alloy demonstrated higher ultimate strength in tension and compression and higher elongation than the extruded Mg-Ca alloy. Meanwhile, it was also interesting to find that the Mg-6Zn alloy showed comparable mechanical properties, although the grain size of the Mg-6Zn alloy is much coarser than that of the Mg-Mn-Zn alloy (>20 μm for the former and <9 μm for the latter).

The mechanical properties of extruded Mg-xZn-Mn (x=1, 2, 3) alloys with different zinc content investigated by Yin et al [Yin et al., 2008] demonstrated that when zinc content is increased from 0% to 3%, both the tensile strength and the yield strength increases remarkably. On the contrary, the elongation decreases with increasing content of Zn. However, the alloy still shows 10% elongation at 3% Zn as shown in Table 2.4. Yuan et al [Yuan et al, 2003] have confirmed the similar conclusion as Yin et al in Mg-xZn-1Si(x=4, 6, 8) alloy and reported that YS and UTS increased while elongation decreased gradually with growing fraction of zinc, which is shown in Fig. 2.6. Moreover, besides the exploration for the effect of different Zn content on the mechanical properties of Mg-xZn-1Mn (x=1, 2, 3) alloys, Zhang et al [Zhang et al., 2008 b] have also studied the impact of the extrusion process. The results of mechanical tests revealed that the yield strength and the ultimate tensile strength of both as-cast and extruded samples slightly improved with increasing amount of zinc element and enhanced second phases (Al-Mn and Mg_7Zn_3; detected by XRD). The extrusion process resulted in the significant increment in the elongation except for the magnesium alloy with 3 wt.% Zn, whose elongation is decreased and even lower than the value of the as-cast counterpart.

Table 2.4 Mechanical properties of extruded Mg-Zn-Mn alloys. [Yin et al., 2008]

Alloy	Ultimate Tensile strength/MPa	Yield strength/MPa	Elongation/%
Mg-Mn	260 ± 2.3	206.2 ± 14.6	18.7 ± 8.5
Mg-1Zn-Mn	280 ± 0.9	246 ± 4.5	21.8 ± 0.6
Mg-2Zn-Mn	283 ± 1.0	248.8 ± 0.8	20.9 ± 0.7
Mg-3Zn-Mn	315 ± 4.3	275.9 ± 0.2	10.5 ± 1.2

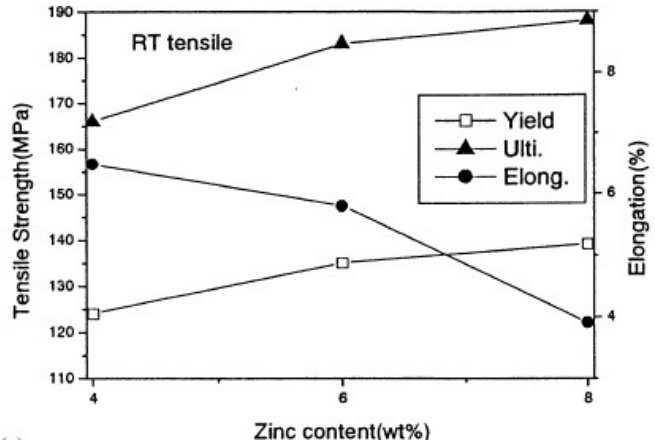

Fig. 2.6 Mechanical properties of the Mg-xZn-1Si alloys at room temperature [Yuan et al, 2003].

The addition of 1.5% Zn to Mg-0.6%Si alloy significantly enhanced the mechanical properties, which indicated the positive effect of the proper Zn content on the mechanical properties [Zhang et al., 2009 a].

During the solidification process Zn element will be rejected by the α-Mg growth front and the segregated Zn restricts grain growth. With increasing Zn content, grain size of the alloy decreases and the yield strength increases with diminishing grain size according to the Hall-Path formula. When the content of zinc is low (1%-2%Zn), zinc element dissolves into primary magnesium and improves the strength of alloys by solid-solution strengthening. When Zn content is above 3% in the alloy, MgZn second phase forms and enhances the strength through a dispersion strengthening mechanism [Boehlert and Knittel, 2006].

2.1.8.3 RE-addition

Since some RE elements possess relatively high solubility in the Mg matrix such as Y

and Gd, they could improve the mechanical properties by the mechanism of solid solution strengthening and are widely considered as promising alloying candidates. Zhang et al. [Zhang et al., 2008 a] have reported the influence of the addition of different Y content to Mg-Zn-Y alloys on the mechanical properties. The yield

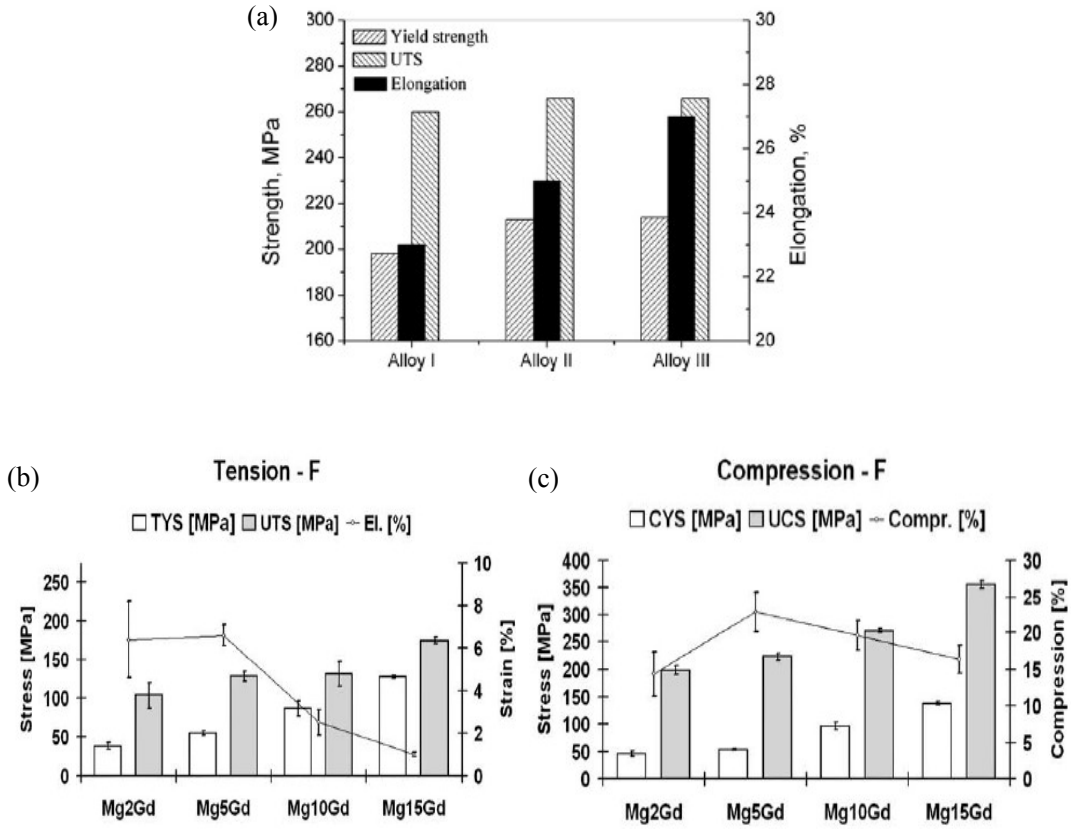

Fig. 2.7 (a) Mechanical properties of Alloy I (Mg-1.98Zn-0.36Y), Alloy II (Mg-1.84Zn-0.82Y) and Alloy III (Mg-1.73Zn-1.54Y) [Zhang et al., 2008]. (b) Tensile properties of Mg-Gd alloys in as-cast condition [Hort et al., 2009]. (c) Compressive properties of Mg-Gd alloys in as-cast condition [Hort et al., 2009].

strength and elongation had a substantial enhancement while ultimate tensile strength slightly improved with increasing the content of Y (up to 1.54% Y) as shown in Fig. 2.7a. The mechanical property measurements for Mg-Gd alloys after different heat treatment were performed by Hort et al [Hort et al., 2009]. The consequences of the tensile tests shown in Fig. 2.7b are that the ultimate tensile strength as well as the tensile yield strength improves with increasing the amount of Gd element, while the

elongation to fracture decreases. The results of compression tests obtained from Fig. 2.7c confirmed to be a similar trend in comparison with that of tensile tests.

2.1.9 Use of chemical additions to Mg alloys and its relevance to biomaterial properties

2.1.9.1 Ca –addition

In the present work, calcium is regarded as a favourable bio-alloying element for the following considerations. (1) It is well known that calcium is a major component in human bone and calcium is also essential in chemical signaling with cells [Ilich and Kerstetter, 2000], so it is regarded as a safe potential element for a bio-medical alloy. The cytotoxicity of Mg-1Ca alloy was investigated by Li et al. [Li et al., 2008]. It could be seen that the morphologies of L-929 cell cultured in the extraction media for a period within 7 days exhibited a healthy flattened spindle shape. (2) Magnesium is necessary for the calcium incorporation into the bone [Serre et al., 1998], which might be expected to be beneficial to bone healing with the co-release of Mg and Ca ions. *In vivo*, biocompatibility [Li et al., 2008] studies discovered newly formed bone. It is characterized by high activity and good alignment of osteocytes around the Mg-1Ca alloy pins.

2.1.9.2 Zn –addition

Zinc is one of the most abundant nutritionally essential elements in the human body, and has basic safety for biomedical applications. The consequence of cytotoxicity assessment confirmed that the in vitro cytotoxicity of Mg-6Zn alloy was found to be Grade 0-1 according to ISO 10993-5: 1999. In addition, although a gap between the implant and surrounding bone tissue occurred during animal implant experiments due to a rapid degradation, the newly formed trabeculae and osteoblasts were still observed. Meanwhile, no disorders of the heart, kidney, liver and spleen existed because of the release of Zn ions [Zhang et al., 2009 b]. Therefore, it indicates that Zn

element is safe as an important potential bio-medical candidate.

The results of hemolysis tests showed that the hemolysis rate of extruded Mg-6wt%Zn alloy was 3.4% which was lower than 5% due to a more favourable corrosion rate of the alloy. As a result, it could be deduced that Mg-Zn alloy will not generate damage of red blood cells according to ISO 10993-4:2002. Moreover, the healthy adhesion of MC3T3-E1 cells on the surface of Mg-Zn alloy was observed despite the fluctuation of pH value [Zhang et al., 2009 b]. Nevertheless, the hemolysis rate of extruded Mg-1Zn-1Mn alloy (65.75%) was much more than the safe standard (below 5%) for biomaterials despite the exhibition of non-toxicity to L-929 fibroblast line because of high cell viability by MMT testing [Zhang et al., 2008 b].

2.1.9.3 RE-addition

Excessive yttrium ions (Y^{3+}) have been shown to change the expression of some rat genes and have adverse effects on DNA transcription factors [Yang, 2006], while many authors stated that gadolinium is highly toxic. Nevertheless, if we successfully manipulate and control the concentration of Y or Gd ions released by Y or Gd containing Mg alloys in the physiological condition below the harmful level through specific and efficient post-treatment method, they are employable for bio-medical applications.

2.1.9.4 Bio-active coating

There are numerous factors that affect bone growth. These are bone morphogenetic protein (BMP) [Derynck and Zhang, 1996], transforming growth factor—β (TGF-β) [Noda, 1989] and platelet-derived growth factor (PDGF) [Helm et al., 1997] used to assess osteogenesis at the implant-bone interface.

Immunohistochemical study demonstrated that a coated sample with bio-active coating has brilliant osteoconductivity in contrast to a sample without coating, since the coated sample showed a much higher BMP-2, TGF-β1 and PDGF expression than

the counterpart. This conclusion was consistent with the consequence of the investigation *in vivo*. The reasons contributing to the observed result could be related to the surface physical properties and the surface chemical properties. Due to the presence of micro-scale or nano-scale pores on the surface of the coated magnesium alloy, the cell adhesion and viability significantly improved, which devoted to the favourable bioactive bone response. In addition, the composition of the surface, including Ca^{2+}, Mg^{2+} and Zn^{2+}, played an important role in accelerating the formation of bone in the vicinity of the Mg alloy with the coating.

As an effective bio-active coating, calcium phosphate (Ca-P) coating has been reported in the past [Cui et al., 2008]. Xu et al. [Xu et al., 2009] have also investigated the properties of Mg-1.2wt%Mn-1wt%Zn alloy after phosphate treatment. The composition of the porous and netlike surface layer after the treatment is $CaHPO_4 \cdot 2H_2O$ with negligible quantity of Zn and/or Mg containing phosphate compounds. Cell experiments *in vitro* (L-929) of pure Ti and Mg alloys with and without a Ca-P coating indicated that the healthy flattened (acicular) morphology and significant enhancement of cell proliferation is observed on pure titanium samples and Ca-P coated magnesium alloy in comparison to the naked Mg alloy. Moreover, there are no remarkable differences in cytocompatibility between pure Ti and Mg alloy with a Ca-P coating.

In vivo, more compact and homogeneous new bone is detected in the vicinity of the coated Mg alloy implant than around the naked one, whereas no negative response from surrounding tissue adjacent to the coated sample is observed. The result demonstrated that the magnesium alloy with a Ca-P coating possessed much better biocompatibility as a potential biomedical implant.

2.1.10 Novel approaches to process Mg alloys

2.1.10.1 Powder Metallurgy route

Due to the benefit of low manufacturing temperature and more uniform distribution of

grains which is hardly obtained by the conventional stir-casting route, a large number of researchers concentrate on the powder metallurgy technique. On the basis of previous work [Li et al., 2008], it is expected that the PM method can be employed to prepare Mg/Ca composites with high content of calcium which also possess favourable mechanical properties, corrosion resistance and good compatibility of as-cast Mg-Ca alloy with low Ca content.

2.1.10.2 Metal matrix composites

Although magnesium and its alloys are regarded as a category of potential effective biodegradable materials, the rapid corrosion rate retards their clinical application. The major frustration to improve the corrosion properties which we always confront is at the cost of mechanical properties. The synthesis of metal matrix composites (MMC) made of magnesium or its alloys as a matrix and hydroxyapatite (HA), which possesses natural bone composition with a low solubility in the body environment [Fulmer et al., 2002], as reinforcements may be a novel feasible method to achieve the excellent combination of good corrosion behaviour and suitable mechanical properties. Therefore, Witte et al. [Witte, 2007] have assessed the properties of extruded magnesium alloy AZ91-20wt%HA metal matrix composite as a biomedical implant. The different Vickers hardness values at different locations were measured depending on the size and distribution of HA conglomerates. Large and inhomogeneously dispersed clusters of HA reveal relative low hardness in contrast to fine and uniform distribution of clusters. The most important aspect is that the average hardness of the sample ($Hv_{0.1}$ = 73 ≈ 730 MPa) is similar to that of natural bone ($Hv_{0.1}$ = 49.8 ≈ 498 MPa). Moreover, the tensile yield strength of the MMC with uniform HA particle distribution was twice that of natural bone, which demonstrates that the MMC-HA could be considered as longer biodegradable implants for load-bearing application.

Compared with AZ91D Mg alloy, the corrosion behaviour of the MMC-HA sample improved in artificial sea water and cell solution by addition, while MMC-HA composites in cell solution containing and without protein exhibited more

homogeneous corrosion than that in sea water. Moreover, the uniform and proper corrosion morphology of the MMC-HA sample is consistent with the results of immersion tests, electrochemical tests and volume loss.

The cytocompatibility assessment indicates that the good adhesion and conspicuous proliferation of human bone derived cells, osteoblasts and macrophages on the surface of the MMC-HA sample were exhibited. This could be attributed to good corrosion resistance which results in the low-level hydrogen evolution and proper pH value in comparison with AZ91D sample.

2.1.10.3 Porous scaffolds

Porous scaffolds configured similarly to natural bone, promote proliferation of osteoblasts and bone formation in the vicinity of hard tissues on the scaffolds. The eminent obstacle of porous scaffolds made of HA, natural polymer for adequate application as degradable implants is their relative poor mechanical properties and rapid corrosion rate [Ma et al., 2001]. Therefore, the excellent combination of proper mechanical properties and satisfactory corrosion behaviour is desirable. Magnesium scaffolds with controlled porosity and pore size may become a promising candidate for clinical bone surgery, since magnesium possesses good mechanical properties and brilliant degradable and bioresorbable characteristics [Witte et al., 2006 and 2005]. Hence, Zhuang et al. [Zhuang et al., 2008] have investigated the property of porous magnesium scaffolds synthesized with 0, 30 and 50 vol% $CO(NH_2)_2$ particles. They found that porosity formed as a result of droplets of low melting point $CO(NH_2)_2$. The porosity of the three samples was 7, 36 and 55% respectively analyzed by the equation:

Total porosity $= (1- \rho/\rho_s) \times 100\%$.

where ρ_s is the density of magnesium and ρ is the apparent density of the porous magnesium specimen which can be measured by the weight divided by the volume of the porous magnesium specimen.

The compressive strength, flexure strength and Young's modulus presented a dramatic descending tendency within a range of the increasing porosity from 7% to 55%, which could be associated with the negative influence of high porosity on the mechanical integrity of the scaffold. It is important to note that the problem of currently serviced implants is either too high Young's modulus of the metallic material or too low mechanical property of ceramics and polymers. Therefore, a porous scaffold provides a feasible way to design the porous magnesium structure that can satisfy different mechanical property requirements as bone substitute.

The corrosion resistance of magnesium scaffolds immersed in physiological saline solution exhibited the similar tendency to mechanical properties, in which the sample with 36% porosity showed better corrosion behaviour in comparison to the 55% porosity one since a greater quantity of aggressive solution would effortlessly penetrate into the sample with high porosity resulting in serious corrosion. However, the corrosion resistance still needs to be further enhanced.

2.1.11 Effect of post-treatments on the properties of bio-degradable materials

2.1.11.1 Heat treatment

Since a homogeneous structure can be obtained by a hybrid solution and aging process, Liu et al. [Liu et al., 2007] have investigated the influence of heat treatment of die-cast AZ63 magnesium alloy on corrosion resistance in simulated body fluid. The solution treatment of all alloy samples, whose surface was protected by carbon powders, were executed at 413 ^{o}C for 24 hours (T4) in air, and then the samples experienced different period of time for ageing treatment (1 h, 5.5 h and 12 h). Compared with the untreated sample, the corrosion properties *in vitro* of its counterparts improved with increasing ageing time due to more homogeneous and continuous precipitation of second phase ($Mg_{17}Al_{12}$). The precipitation of β-$Mg_{17}Al_{12}$ generated by aging significantly optimized the micro-galvanic corrosion in the

vicinity of α-Mg phase [Zhao et al., 2008].

Additionally, the influence of heat treatment of AZ91 magnesium alloy on corrosion performance in the simulated body fluid was investigated by Zhou et al [Zhou wt al., 2009]. A solution treatment (T4) was carried out at 445 ^{o}C for 24 hours in argon atmosphere and water quenched at 25 ^{o}C. An alternative solution treatment (T6) was performed followed by aging treatment at 200 ^{o}C for 8 h, 16 h and 24 h. The results of immersion tests have been listed in Table 2.1. Significant improvement in corrosion resistance was observed after T4 treatment in the initial 8 h immersion in SBF as shown in Fig. 2.8a, and then severe corrosion rate was observed after 168 h immersion in comparison with other heat-treatments as shown in Fig. 2.8b. On the contrary, the corrosion resistance of T6 samples was worse than those of the as-cast and T4 samples when they were immersed in SBF for 8 h. However, the corrosion rate for T6 samples was significantly lower than that of the T4 treated sample for longer immersion (168 h). The different distribution, configuration and size of the β-$Mg_{17}Al_{12}$ phase after heat treatment resulted in the distinguished corrosion behaviour.

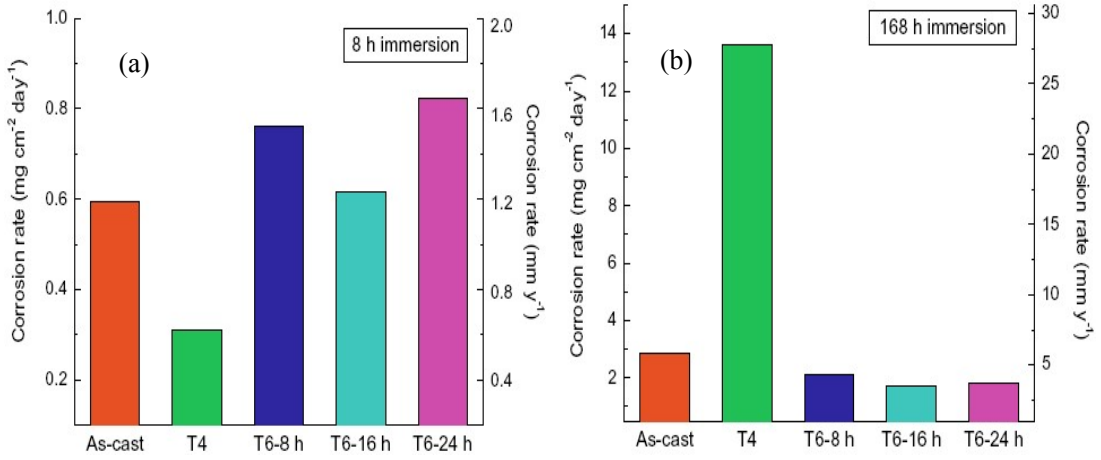

Fig. 2.8 Corrosion rate for as-cast and heat-treated samples in SBF; (a) after 8 hours and (b) after 168 hours. [Zhou et al., 2009]

In order to understand the corrosion behaviour of Mg alloys, the alloy system can be considered as a micro-galvanic corrosion system where β-$Mg_{17}Al_{12}$ phase as a cathode

and α-Mg phase as an anode. On the basis of previous research, the variable percentage of aluminium contained in the primary α-Mg phase influenced the corrosion property. Preferential corrosion tendency is observed in regions with less than 8% Al [Ambat et al., 2000]. Therefore, it causes the phenomenon of localized corrosion initially within the area with less than 8% aluminium. Furthermore, it should also be noted that second phase in aluminium-containing magnesium alloy played a dual role on the anti-corrosion behaviour depending on their fraction and distribution [Scharf et al., 2005]. Finer and homogeneous distribution of second phase acts as a corrosion barrier and the corrosion resistance dramatically improves. Otherwise, the presence of β-phase ($Mg_{17}Al_{12}$) as an effective galvanic cathode led to deterioration of the corrosion properties.

2.1.11.2 Mechanical process

The bio-degradation of magnesium alloy was widely considered as a benefit for the application of absorbable implant, but the fast corrosion severely limited its use in the field of clinical application. Besides the alloy and surface treatment, the mechanical process was regarded as an alternative method to influence the corrosion resistance of the alloy.

The anti-corrosion behaviour of AZ31 magnesium alloy with different processing histories in Hank's solution was investigated [Wang et al., 2008 a]. The three kinds of samples produced using squeeze cast (SC), hot roll (HR) and equal channel angular pressing (ECAP) of the HR material and the corresponding corrosion rates were shown in Table 2.1. Due to the refinement of the grain size, it is noted that the corrosion resistance of the sample after HR improved corrosion resistance remarkably in comparison with that after SC which revealed an aggravated localized pitting mode. However, although the grain size of the sample after HR with further ECAP decreased, the anticipated improvement of corrosion resistance was not observed.

2.1.11.3 Surface treatment

Magnesium alloy is extremely susceptible to the physiological pH (7.4-7.6) and environments including high concentration of chloride ions. Negative effects such as loss of mechanical integrity before the tissue has sufficiently healed and a relatively large amount of hydrogen release over the tolerance limit of physiology, hinder the application as a favourable bio-degradable implant. Although the advanced technology for synthesis of magnesium alloys with a minimal amount of impurities was regarded as a favourable and efficient method to improve the corrosion properties, it is also noted that the application of surface coating is paid more attention due to the ability to protect the alloy surface from its surroundings or contact with corrosion chemicals. Some researchers have pointed that corrosion resistance of pure Mg may be achieved eventually by the proper surface modification [Yamamoto et al., 2008]. Ti coating [Zhang et al., 2005] and heat treatment [Liu et al., 2007] have been adopted to optimize the corrosion behaviour of magnesium alloys. Therefore, the elemental composition and processing history is not the only way to manipulate the rate of corrosion *in vivo*. In addition, the biocompatibility of the surface also plays an important role in the clinical application of implants. Thus, it is necessary to employ an appropriate coating to achieve dual functions (corrosion and biocompatiblity). To be effective, the protective coating must be uniform, adherent and pore-free. Unfortunately, magnesium alloys have a strong tendency to react with surrounding air or water because of high chemical activity, which forms an oxide/hydroxide layer on the surface which has an adverse effect on adhesion and uniformity.

Fluoride treatment Fluoride treatment, as one useful way to inhibit the corrosion of magnesium and its alloys [Yamamoto et al., 2008] and granted for medical purpose due to the advantages of economy, non-toxicity, convenience and easy processibility [Chiu et al., 2007]. The bio-material after fluoride treatment showed an extreme cytocompatibility [Lamolle et al., 2009]. Moreover, it is widely accepted that magnesium is regarded as the most resistant metal to hydrofluoric acid

because of the formation of a protective film of MgF_2 on the surface which retards the corrosion.

Pereda et al. [Pereda et al., 2010] have investigated the influence of fluoride surface treatment on corrosion behaviour. Electrochemical tests indicated that the corrosion behaviour of magnesium obviously improved by fluoride treatment with KF, while the obtained corrosion resistance of Mg (PM) after 0.1 M KF treatment is much better than that after 1M KF treatment. Since the fluorine ion possesses a relatively high electronegativity, it has an obvious tendency to react with hydrogen released from KF-treated magnesium soaked in the F^--containing solution and form HF_2^-, $H_2F_3^-$ and $H_3F_4^-$ surface layer with strong binding energy. The deposited layer may retard the corrosion phenomenon. However, if fluoride treated Mg is immersed in an F^--free solution like PBS, Cl ions substitute for F^- and form the protective layer on the surface as a result of strongly absorbable ability of Cl^-. The layer gradually loses its corrosion barrier.

Witte et al. [Witte et al., 2009] have investigated the corrosion behaviour of extruded LAE442 magnesium alloy with and without fluoride treatment as a bio-medical degradable implant in rabbits, and assessed the biocompatibility and cytotoxicity. A favourable corrosion resistance of LAE442 Mg alloy *in vivo* was observed. Moreover, the corrosion resistance improved further by fluoride treatment. Depending on low corrosion rate of both cases, the evolution of hydrogen gas was remarkably restricted under the tolerated limit of hydrogen adjacent to the bio-degradable implant, which effectively prevented the occurrence of a gas cavity by fluid (blood) flow in the rabbit model [Witte et al., 2008]. Adverse effects on health like infection and negative reactions were not clinically discovered during the period of post-operation *in vivo* except in liver tissue which was closely related to the rare earth element released from both alloys. However, the protective MgF_2 coating may retard the corrosion temporarily in the initial 4 weeks after operation, the dissolution of MgF_2 coating caused by corrosion brought the symptom of irritation in the vicinity of the local synovial tissue.

Thermal oxidation The corrosion behaviour of AZ91 magnesium alloy after the treatment of thermal oxidation was executed by Majumadar et al [Majumadar et al., 2008]. Isothermal oxidation was carried out at 200 ℃ and 300 ℃ for 4 h to 25h (under each temperature) in air. The data from the electrochemical test suggested that the corrosion potential of the samples after oxidation obviously shifted towards the noble direction due to formation of magnesium oxide on the surface in comparison with samples without post-treatment. Therefore, better corrosion resistance was attributed to the presence of stable magnesium oxide as an effective corrosion barrier. Among the thermally oxidized alloy (AZ91), the best retarded corrosion behaviour was achieved when oxidized at 200 ℃ for 25 h. Nevertheless, the corrosion rate of samples after oxidation at 300 ℃ relatively increased compared with the samples oxidized at 200 ℃ due to existence of micro-defects in the oxidation film.

The contact angle between metal and SBF slightly reduced with increasing in temperature and time of the post-oxidation due to modification of the composition and morphology of the alloy surface.

The cytocompatibility test was also conducted for samples modified at 200 ℃ for 25 h. Compared with the original alloy, the percentage of adhered cells and their proliferation on the surface increased remarkably, which was possibly due to the oxide film. Hence, the consequence of the experiment implied that the cell adhesion and proliferation may be influenced by surface characteristics like wettability, surface charge, surface free energy and topography. In addition, the wear resistance of the AZ91 alloy after oxidation at 200 ℃ for 25 h enhanced dramatically in comparison with the alloy without treatment because of the presence of uniform oxide film on the surface.

HA coat Hydroxyapatite (HA) has been widely considered as a bio-medical material due to brilliant biocompatibility and bioactivity, while the composition and structure of HA were exactly identical to natural bone. Moreover, HA can optimize the corrosion resistance of magnesium alloys, which was responsible for possession of

high thermodynamic stability. Therefore, a titanium alloy substrate with HA coating as a bio-implant has been studied [Dumelie et al., 2008]. Nevertheless, HA coating on magnesium alloy substrates and their corrosion behaviour in simulated body fluid have hardly been performed. Since it possesses low melting point and inferior heat resistance, many methods to deposit HA on the Mg alloy substrate at high working temperature such as physical vapour deposition are unavailable. Electro-deposition can provide uniform coating at room temperature by changing the electrochemical potential and electrolyte concentration [Kuo and Yen, 2002]. HA coating on magnesium alloy by electrodeposition method [Song et al, 2008], resulted in a layer consisting of dicalcium phosphate dehydrate (DCPD) and β-tricalcium phosphate (β-TCP). They could convert into hydroxyapatite after immersion in alkali solution. Therefore, this study indicates that DCPD and β-TCP are the precursors for the formation of HA.

Wen et al [Wen et al., 2009] have coated HA onto extruded AZ31 Mg alloy and studied the corrosion performance in alkali environment. The as-deposited coating consisted of DCPD and HA, while a partial amount of DCPD immersed in NaOH solution converted into HA, as previously reported by Song et al. [Song et al., 2008]. The coated layer is a kind of Ca-deficient HA and is speculated by the measured average Ca/P atom ratio in comparison with the theoretical value of HA.

The analysis of the data from electrochemical testing indicated that the corrosion resistance of the magnesium alloy improved significantly due to the formation of the coating as an effective protective barrier. When the as-deposited alloy experienced alkali treatment, the anti-corrosion behaviour slightly improved. It is believed that the coating becomes more stable after alkali treatment. Hence, besides the characteristic of the chemical of coating, the stability also plays an important role in affecting the corrosion behaviour. Furthermore, the result of immersion testing in SBF suggested that as-deposited alloy and alloy post-treated in alkali environment possessed an excellent anti-corrosion behaviour due to the presence of Ca-P-Mg apatite as an efficient corrosion barrier in the Mg-rich interface in the initial 10 days.

Due to the low working temperature, the biomimetic method was extensively regarded as a feasible and effective vehicle to deposit coating on magnesium and its alloy with low heat resistance [Boanini and Bigi, 2006]. On the basis of favourable benefits, Hu et al. [Hu et al., 2010] investigated the corrosion behaviour of AZ91D magnesium alloy modified by DCPD coating on the surface through a biomimetic method by immersion in simulated body fluid. The Mg alloy after solution treatment at 420 ^{o}C for 24 h was submerged in a $Ca(NO_3)_2$ solution, while a K_2HPO_4 solution was gradually dribbled into the former solution. The formation of DCPD on the magnesium substrate was observed. The data from electrochemical measurement demonstrated that the corrosion current density of the alloy with DCPD coating decreased dramatically in comparison with that of the alloy without DCPD coating which was more than 33 times the former. Interestingly, it was seen that DCPD was not only transformed into HA but also acted as nuclei sites to induce the precipitation of HA after soaking in SBF.

Part 2: Metallurgical aspects of Mg alloys

2.2.1 Chemical and physical properties of Magnesium

Magnesium is among the alkaline earth metals and its average atomic mass is 24.305 g/mol. The melting temperature is 649 ^{o}C. It possesses excellent thermal and electrical conductivity. The free state of magnesium hardly exists under natural atmosphere due to its high chemical activity, tending to react with water, oxygen, nitrogen, phosphorous and chlorine.

Normally, Magnesium reveals an appearance of a silvery and white shade. It is worth mentioning that Mg is the lightest of all structural metals which are used in building and the automobile industry.

Pure magnesium possesses a hexagonal closed-packed (h.c.p.) crystal structure under atmospheric pressure [Jete and Foote, 1935]. The atomic locations in the magnesium unit cell, and the principal planes as well as directions are illustrated in Fig. 2.9. The lattice parameters of pure Mg at 25 ℃ are a = 0.32092 nm and c = 0.52105 nm within marginal error (± 0.01%) [Stager and Drickamer, 1963]. Since the ideal value of c/a ratio for the ABAB close-packed layers of atoms is 1.633, the h.c.p. structure of pure magnesium is almost perfectly ideal (c/a = 1.6236). If the Mg crystal undergoes plastic deformation, primarily, it happens on the (0001) basal plane and in the close-packed $<11\bar{2}0>$ direction of the plane. Secondary slip occurs in the $<11\bar{2}0>$ direction on the $\{10\bar{1}2\}$ perpendicular face planes. Twinning of pure magnesium can be observed most frequently across the $\{10\bar{1}0\}$ series planes, and the occurrence of secondary twinning is across the $\{30\bar{3}4\}$ planes.

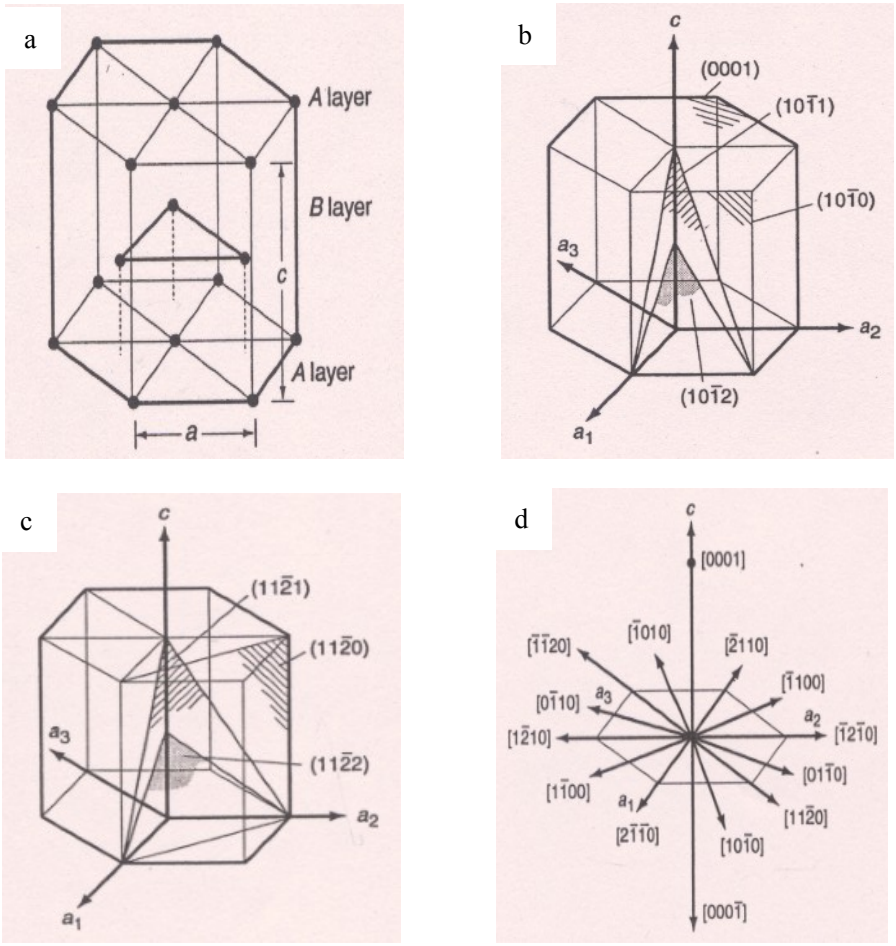

Fig. 2.9 The magnesium unit cell crystal. (a) atomic position. (b) Basal plane, a face plane, and principal planes of the $[1\bar{1}00]$ zones. (c) Principal planes of the $[1\bar{2}10]$ zone. (d) Principal directions. [Roberts, 1960]

2.2.2 Magnesium and its alloys

The mechanical properties of magnesium at 20 ℃ are shown in Table 2.5. In a bid to meet the various requirements for the practical application, different elements such as aluminium, zinc, cerium, silver, yittrium and zirconium are alloyed in commercial magnesium alloys.

Mg as a medical material: For the purpose of clinical application, harmful elements should be avoided for alloying with Mg. As discussed in Part 1 of this chapter, based on corrosion properties, zinc and calcium have been widely regarded as potential alloying candidates for magnesium in the field of bio-degradable materials research.

Here, the metallurgical aspects of Mg-Zn-Ca alloys are reviewed.

Table 2.5 Typical mechanical properties of unalloyed magnesium at 20 ℃. [Avedesian and Baker, 1999]

Form and section	Tensile strength, MPa	0.2% tensile yield strength, MPa	0.2% compressive yield strength, MPa	Elongation in 50 mm (2 in.), %	Hardness	
					HRE	HB(a)
Sand cast, 13mm (1/2 in.) diam	90	21	21	2-6	16	30
Extrusion, 13mm (1/2in.) diam	165-205	69-105	34-55	5-8	26	35
Hard rolled sheet	180-220	115-140	105-115	2-10	48-54	45-47
Anneal sheet	160-195	90-105	69-83	3-15	37-39	40-41
(a) 500 kg load, 10 mm dia ball						

Binary Mg-Zn alloy: The phase diagram of binary Mg-Zn alloy is shown schematically in Fig. 2.10(a). Based on the diagram, the maximum solid solubility of Zn in Mg is approximately 6.2 wt.% (i.e. 2.5 at.%) at 325 ℃, whereas the solubility descends to 1.6 wt.% (i.e. ~0.6 at.%) at room temperature in the equilibrium state [Okamoto, 1994]. If the addition of zinc element exceeds the ultimate concentration, intermetallic particles can spontaneously precipitate from the magnesium matrix. For instance, solidification follows the dashed line as showed in Fig. 2.10(a) starting with the formation of primary α-Mg below the corresponding liquidus temperature. As the temperature decreases, the eutectic phase forms due to eutectic reaction. Eventually, it will co-exist with primary magnesium. Generally, the second phase (MgZn) seen along grain boundaries as shown in Fig. 2.10(b), is extensively accepted as the product of the eutectic reaction. The MgZn phase formation has been confirmed by X-ray diffraction analysis [Zhang et al., 2009 b]. In addition, other kinds of potential intermetallics are also marked in the phase diagram.

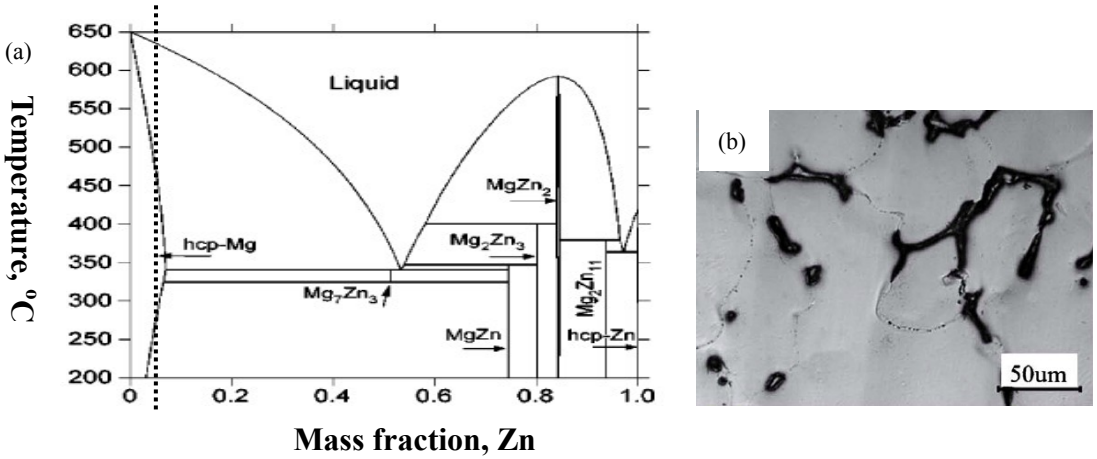

Fig. 2.10 (a) The Mg-Zn phase diagram [Ansara et al., 1998]. (b) Microstructure of conventional-cast Mg-6Zn sample [Zhang et al., 2009 b].

Binary Mg-Ca alloy: The phase diagram of binary Mg-Ca alloy is illustrated in Fig. 2.11(a). Mg_2Ca is the second phase in this system. Mg_2Ca possesses the Laves C14 crystal structure [Aljarrah and Medraj, 2008]. Due to the extremely low solid solubility of Ca in Mg, the Mg_2Ca intermetallics form by adding only a small quantity of calcium. As shown in Fig. 2.11(b), the typical metallographic microstructure of α-(Mg) primary grains with Mg_2Ca phase precipitating interdendritically is observed.

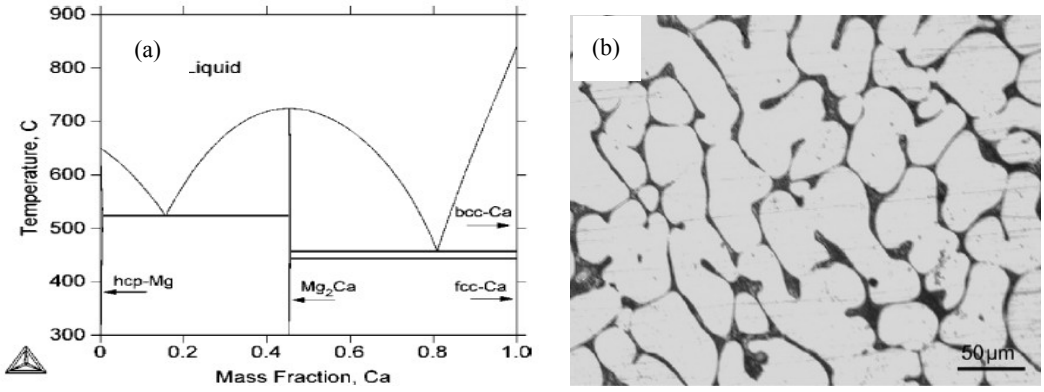

Fig. 2.11 (a) The Mg-Ca phase diagram [Agarwal et al., 1995]. (b) Microstructure of conventional-cast Mg-2Ca sample [Li et al., 2008].

Ternary Mg-Zn-Ca alloy: The Mg-Zn-Ca phase diagram was first plotted by Paris [Paris, 1934] via cooling of 189 different alloys in sixteen different isopleths. The composition of intermetallics of this ternary alloy has been in dispute among a large number of researchers. Eventually, Jardim et al. [Jardim et al., 2002]

successfully investigated the ternary compound by advanced analysis methods, and confirmed it to be $Ca_2Mg_6Zn_3$ in composition. Another second phase of $Ca_2Mg_5Zn_{13}$ has been reported by Clark [Clark, 1961]. However, insufficient and limited evidence is available to verify its presence. The microstructure of conventional-cast Mg-3Zn-1Ca alloy fabricated as a part of this thesis is shown in Fig. 2.12. A large volume of second phase particles, possibly, the $Ca_2Mg_6Zn_3$ phase can be seen.

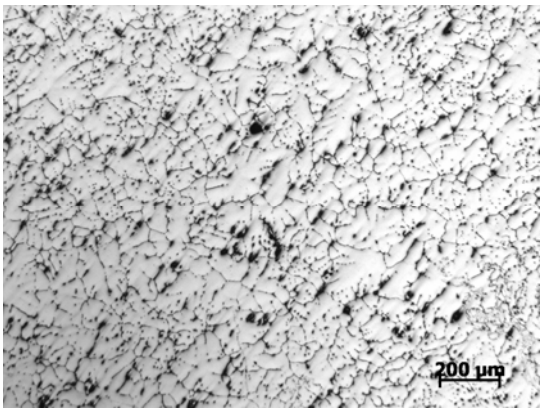

Fig. 2.12 Micrograph of conventional-cast Mg-3Zn-1Ca alloy prepared in this study.

Commercial alloys: Normally, a large quantity of commercial magnesium alloys contain aluminium, to provide strengthening. Mg-Al-Zn alloys are known as AZ series alloys such as AZ31, AZ61 and AZ91, which are commonly used in industrial application. In addition, AJ62 and AM60 as other available Mg alloys, which contain approximately 6.0 wt.% Al, are also widely used in some engineering application. The compositions of these commercial alloys are illustrated in Table 2.6.

Table 2.6 Compositions of commercial magnesium alloys (wt.%). (Note that only the two major alloying elements are shown.)

Al-containing Mg alloys				
AZ91	9Al	1Zn		bal. Mg
AZ31	3Al	1Zn		bal. Mg
AZ61	6Al	1Zn		bal. Mg
AJ62	6Al	2Sr		bal. Mg
AM60	6Al	0.13-0.6 Mn		bal. Mg
LAE442	4Li	4Al	2RE	bal. Mg
Al-free Mg alloys				

WE43	4Y	3RE	bal. Mg
ZE41	4Zn	1RE	bal. Mg
ZK51	5Zn	1Zr	bal. Mg

2.2.3 Solidification process

Phase transformations can be regarded as an atomic vibration issue and the driving force is thermal energy. If a specific motion of an atom contributes to a decrease in the free energy of the system, it is possible that an embryo or cluster can survive and turn into nuclei eventually. According to different nucleation conditions, the type of nucleation process is typically divided into homogeneous nucleation and heterogeneous nucleation. In homogeneous nucleation, a solid generates uniformly in pure liquid, whereas a solid forms on the surface of pre-existing particle or in crevices of the mould wall which accelerate the nucleation event during the heterogeneous nucleation process.

Homogeneous nucleation The process of homogeneous nucleation is shown schematically in Fig. 2.13a. If some liquid clusters assemble to form a small sphere of solid, the corresponding variation of the systematic free energy from G_1 to G_2 will occur spontaneously. As a result, the free energy change caused by the formation of solid $\triangle G = G_2 - G_1$ is given as following:

$$\triangle G = -Vs\ \triangle G_v + A_{SL}\gamma_{SL}$$

where $\triangle G_v = G_V^L - G_V^S$, V_s stands for the volume of the solid sphere, A_{SL} is the solid/liquid interfacial area, and γ_{SL} represents the solid/liquid interfacial free energy. Below the equilibrium melting temperature, the ΔG_v has a positive value.

If the solid possesses an optimized sphere shape and γ_{SL} is isotropic, $\triangle G$ could further be related to the radius of the solid as follows:

$$\triangle G_r = -4/3\pi\, r^3 \triangle G_v + 4\pi r^2 \gamma_{SL}$$

According to Fig. 2.13b, it is obviously observed that the volume free energy decreases as r^3, while the interfacial energy increases with r^2. For a given

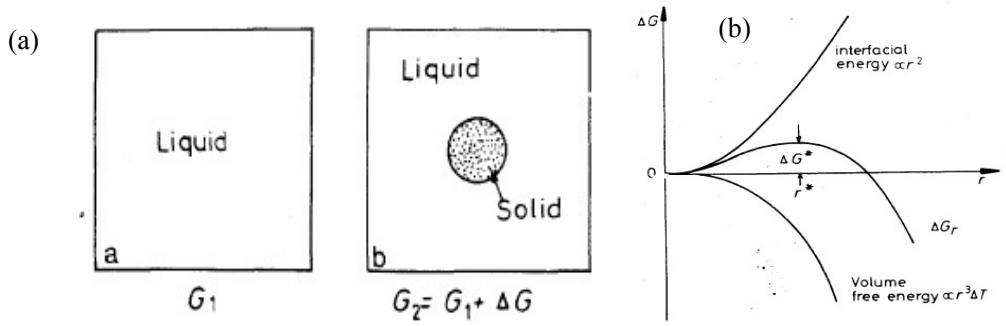

Fig. 2.13 (a) The process of homogeneous nucleation. (b) The schematic diagram of the relationship between the free energy change and the solid sphere of radius r. [Porter and Easterling, 1992]

undercooling, a certain radius r* shown in Fig. 2.13b is connected with a maximum excess free energy. If $r < r^*$, the free energy of the system is decreased via dissolution of the solid, whereas the system could decrease its energy by permitting solid growth under the circumstances of $r > r^*$.

Heterogeneous nucleation Reduction of the interfacial energy term is a favourable method to achieve nucleation at small undercooling under a given volume free energy. As shown in Fig. 2.14, the heterogeneous nucleus forms on the mould wall or in mould-wall cracks. If we assume that γ_{SL} is isotropic, it will be easily seen

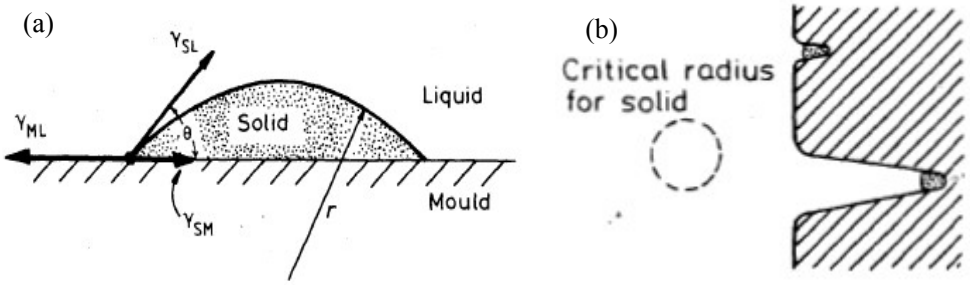

Fig. 2.14 Heterogeneous nucleation of spherical cap (a) on a flat mould wall and (b) in mould-wall crevices. [Porter and Easterling, 1992]

that for a given volume of solid, the interfacial energy is decreased by the spherical cap shape of the embryo with a 'wetting' angle θ. Therefore, the equation of free

energy of heterogeneous nucleation will be combined with the term of 'wetting' angle as follows:

$$\Delta G_{het} = \{-4/3\pi\, r^3 \Delta G_v + 4\pi r^2 \gamma_{SL}\} S(\theta)$$

where

$$S(\theta) = (2 + \cos\theta)(1-\cos\theta)^2/4$$

From the equation of S(θ), we can estimate that its numerical value will be lower or equivalent to 1 which only depends on θ. As a result, it can be concluded that the activation energy barrier of heterogeneous nucleation is much smaller than that of homogeneous nucleation as illustrated in Fig. 2.15(a). In addition, the requirement of undercooling for heterogeneous nucleation is apparently lower than that necessary for homogeneous nucleation as shown in Fig. 2.15(a) and 2.15(b).

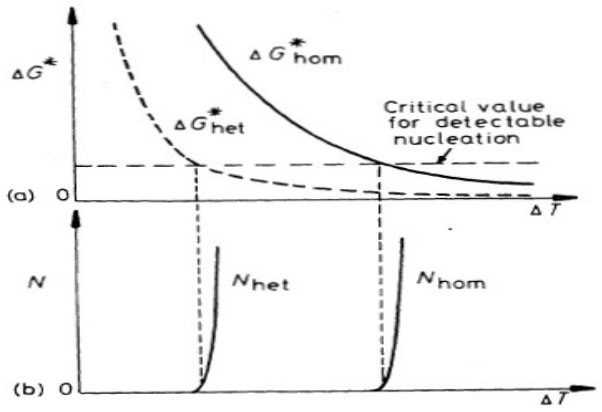

Fig. 2.15 (a) Variation of ΔG* with ΔT for homogeneous and heterogeneous nucleation. (b) The corresponding nucleation rates assuming the same critical value of ΔG*. [Porter and Easterling, 1992]

Normally, heterogeneous nucleation always happens during the solidification of a liquid. Moreover, due to its effect on refinement of fine grain size, heterogeneous nucleation is also reinforced by adding an appropriate amount of inoculant in commercial practice. However, it needs to be mentioned that the effectiveness of the inoculant is associated with the wetting angle and the surface roughness to a great degree. In addition, lattice match between the inoculant phase and the alloy phase which is to be nucleated/solidified is the most important characteristic to be

considered.

2.2.4 Refinement of grain size for magnesium alloys

Since the possession of a finer grain size for magnesium alloys always results in favourable mechanical properties and structural homogeneity, a large number of researchers are filled with enthusiasm and passion to investigate efficient approaches. Normally, due to the rapid solidification rate, the grain size refinement of Mg alloys can be achieved by high-pressure die casting (HPDC) process with the absence of a grain refiner. However, lower cooling rate casting methods cannot produce samples with a uniform and optimized microstructure unless a refiner agent is employed prior to casting.

Generally, we are accustomed to classify magnesium alloys into two typical groups according to whether aluminium element is included in the alloy or not. Al-free Mg alloys are ZE43, ZK60 as well as WE43 and Al-containing Mg alloys are AZ91, AM60 AZ61, AZ31 etc.. Zirconium has been widely accepted as an effective grain refiner for Al-free Mg alloys [Qian et al., 2004]. Nevertheless, due to the undesirable reaction between Zr and Al, stable intermetallic phases form, which are unfortunately ineffective for nucleants for magnesium alloys. As a result, the anticipated effect of grain refinement for Al-containing Mg alloys is not achieved. For non-HPDC application, especially for AZ31, the discovery of a suitable and functional refiner will be regarded as a meaningful and important work by the manufacturing industry.

In the following, the current technical status for grain size refinement of Mg alloys is introduced:

1. Grain refinement for Al-containing Mg alloys

Superheating Superheating liquid metal is known to reduce the grain size significantly when compared to samples with low superheat [Cao et al., 2007]. The function of superheating on grain refinement depends on alloy composition and process variables.

Carbon inoculation Carbon inoculation is extensively considered as another effective approach to improve grain sizes of Mg-Al based alloys [Qian and Cao, 2005]. It is worth mentioning that calcium carbide and hexachloroethane seem to function more efficiently than other carbon inoculation methods. The reduced grain size is related to the presence of carbon inoculation as functional nucleants for Al-containing Mg alloys.

The Elfinal Process The addition of 0.4 to 0.5 pct of iron particles in the form of $FeCl_3$ at 740℃ and 780℃ can contribute to the grain size refinement of Mg-Al based alloys confirmed by Farbenindustrie [Farbenindustrie, 1942]. Al - and Fe-rich intermetallics are likely to be a reasonable explanation for the observed reduced grain size [Cao et al., 2004], however, Fe is known to increase the corrosion rate of Mg alloys and is not being used effectively. A finer grain size could be observed for high-purity Al-containing magnesium alloy, which was confirmed by the Tamura group [Tamura et al, 2002]. However, the mechanism of native grain size refinement is still waiting for further exploration. It should be noted that this process seems to be consistent with the Elfinal process which improves grain sizes by the existence of Fe in high-purity Mg-Al based alloys [Cao et al., 2004].

Grain size refinement by other additives: Some other refiner agents such as Sr, RE (rare earth elements) and Si have also been used for improving the grain size of Al-containing Mg alloys besides those mentioned.

2. Grain refinement for Al-free Mg alloy

Under normal cooling rate, zirconium has been confirmed as a promising and effective refiner agent for Mg alloys with little or no Al, Mn, Si and Fe [Emley, 1966]. The positive impact on the uniform and finer grain size is not only related to the existence of Zr-rich cores by peritectic solidification which accelerate the nucleation of primary magnesium, but also responsible for insoluble Zr as efficient nucleants due to same crystal structure and identical lattice parameters between α-Zr and magnesium [Qian et al., 2004].

2.2.5 Processes and treatments of magnesium alloys

2.2.5.1 Gravity and low-pressure casting:

Normally, magnesium alloy castings can be obtained by almost every conventional casting method. However, according to specific service demand for the component, we need to carefully weigh options in order to make a correct choice. In the following, some typical methods to cast Mg alloys are introduced.

Sand Casting: When liquid metal is poured into a mould of sand, it is referred to as sand casting. As a traditional method, it is still widely accepted for the manufacturing applications, especially for the aircraft industry, because it is economical and can produce component in a large range from a few ounces to as large as 1400 kg. However, to successfully complete the casting process, some inhibitors such as sulfur and boric acid, which aim to prevent mould-metal reactions, are necessary. The quantity of inhibitor is influenced by the moisture content of the sand, pouring temperature and parameters of the casting alloy.

Investment Casting: Investment casting is a casting method designed to achieve high dimensional accuracy for small castings by making a mould of refractory slurry, which sets at room temperature, surrounding a wax pattern which is then melted out to leave a mould without joints. Generally speaking, it is difficult to distinguish the difference between modern sand casting and investment casting. However, compared with the process of sand casting, investment casting can produce tighter tolerances and thinner wall section samples, but it should be pointed out that the cost per casting is relatively high and the limitation of the casting size also confines its extensive application.

Permanent-Mould Casting: According to whether metal cores or destructible sand cores as usual, the permanent-mould castings are classified into two typical types: permanent-mould and semi-permanent mould respectively. The castings produced by this process possess relatively good surface finish and precise dimensions, while the

mechanical properties are also superior to those of sand castings due to faster solidification. However, the inflexible mould shape is hardly modified once it is constructed, and complex castings are not practical by this process. In addition, some structural defects can easily be formed.

Low-Pressure Die-Casting Process: The die employed in this process is almost identical to those for permanent-mould casting. The main discrepancy between these two processes is that the metal flows into the mould from underneath under a little pressure. Currently, this technology is carried out to manufacture high-quality automobile wheels.

Other casting methods: Relied on its benefits, squeeze casting can successfully produce high-quality components for magnesium alloys which can't be achieved by other casting methods. Additionally, semisolid process, as another economical casting method, which leads to more uniform and finer grain size for Mg alloy products, is widely applied in industry.

2.2.5.2 High Pressure Die casting:

In high-pressure die casting (HPDC), the two halves of the mould are clamped together by hydraulic force. Liquid metal rapidly flows through a narrow entrance under pressure and guarantees complete filling of the mould. A high cooling rate also results in a material with finer grain size. Moreover, it should be mentioned that HPDC is a favourable method to produce high-volume components.

At the moment, the HPDC process is used for most magnesium alloys due to their advantages for die casting. In the following, these advantages are listed:

1. Depending on good fluidity for most Mg alloys, complex and thin-wall components are produced by this method.

2. Compared with aluminium and zinc, lower volumetric specific heat of Mg alloys allows them to cool more quickly, which means that it can shorten cycle time and

reduce die wear.

3. Low density as a physical characteristic of magnesium can make high gate pressures achieved under modest pressures.

4. Low solubility of iron in magnesium liquid can effectively decrease the probability of die sticking phenomenon that happens to aluminium. If this effect combines with the low specific heat per volume for Mg alloys, the die will last much longer than aluminium application.

2.2.5.3 Solution heat treatment:

Heat treatments are always carried out for improving the mechanical properties of magnesium alloys. According to alloy composition (cast or wrought) and expected condition in-service, we need to choose appropriate type of heat treatment. Normally, solution heat treatment enhances strength and contributes to improve toughness as well as shock resistance. Subsequently, artificial aging improves hardness and yield strength, whereas the toughness is deteriorated instead. As a result, the desirable property combination can be achieved through changing parameters (time and temperature).

2.2.5.4 Melt conditioning by advanced shear technology (MCAST)

The melt conditioning by advanced shear technology (MCAST) was exclusively developed and patented by the research group led by Prof. Fan at BCAST, *Brunel University, UK*. The mechanism of the melt conditioning machine relies on perfect-intermeshing screws, which are self-wiping and co-rotating during the process. A high shear rate and a high intensity of turbulence are the two important characteristics of the MCAST unit, and guarantee that the melt experiences strong and efficient distributive mixing at an excellent level. In addition, due to intensive shearing, a uniform temperature, chemical composition as well as uniform dispersive

nucleation sites in the melt can also be achieved [Fan, 2002]. Cast components fabricated with melt conditioned liquid metal have shown to have superior microstructures and mechanical properties.

Chapter 3
Experimental Techniques & Procedure

3.1 Introduction

In this chapter, the specific procedures for preparation of samples, the process methods, advanced characterisation analysis and mechanical property measurements employed in this research are introduced.

3.2 Material preparation

In this study, different alloys and composites were investigated to understand the effect of HA particles on the metallurgical structure, mechanical properties and for future bio-corrosion behaviour. The preparation procedures for alloys and composites are schematically shown in Fig. 3.1. All the alloys were heated in an electrical resistance furnace, and melted in steel crucibles under protective gas (99.6% N_2 + 0.4% SF_6). The flow rates for N_2 and SF_6 are 6 litres/minute and 0.0025 litres/minute, respectively. To improve the distribution of HA particles, the impeller was designed according to the crucible dimension. Mixing process was carried for three times, at 20 minute intervals. Each time the mixing time is between 3 and 4 minutes. Subsequently, conventional cast (670 ℃~680 ℃), HPDC and TP1 (TP1 660 ℃) samples were produced. The compositions and the casting processes of all the samples are listed in Table 3.1.

Table 3.1 List of chemical compositions and casting process.

Composition	Conventional cast		MC-cast	HPDC	MC-TP1	TP1
	12 mm	31 mm				
Mg-1Zn-1Ca	●	●	○	○	○	●
+ 1HA	●	●	○	○	○	○
+ 3HA	●	●	○	○	○	●
+5HA	●	●	○	○	○	○
Mg-3Zn-1Ca	●	●	○	●	○	●
+1HA	●	●	○	●	○	○
+3HA	●	●	○	○	○	●
+5HA	●	●	○	○	○	○
+10HA	○	●	○	○	○	○
+15HA	○	●	○	○	○	○
Mg-5Zn-1Ca	●	●	●	●	●	●
+1HA	●	●	○	●	○	○
+3HA	●	●	●	●	●	●
+5HA	●	●	○	●	○	○
+10HA	○	●	○	○	○	○
AZ91D	○	○	○	○	○	●
+0.1HA	○	○	○	○	○	●

+0.2HA	○	○	○	○	○	●
+0.5HA	○	○	○	○	○	●
+1HA	○	○	○	○	○	●
+3HA	○	○	○	○	○	●
AM60	○	○	○	○	○	●
+3HA	○	○	○	○	○	●
AJ62	○	○	○	○	○	●
+3HA	○	○	○	○	○	●
Mg-1Ca	●	●	○	○	○	○
Mg-5Zn	○	●	○	○	○	●

●— Done ○— Not done

(a)

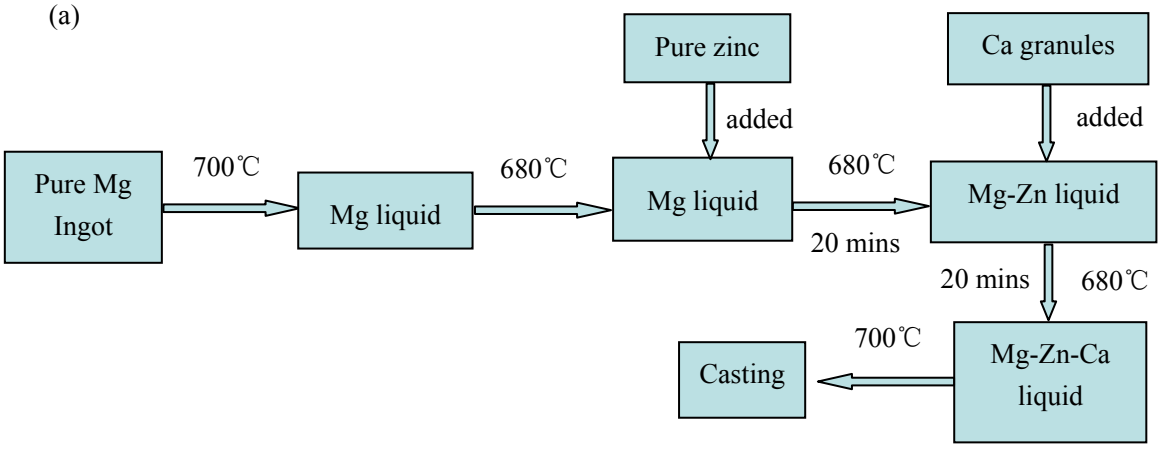

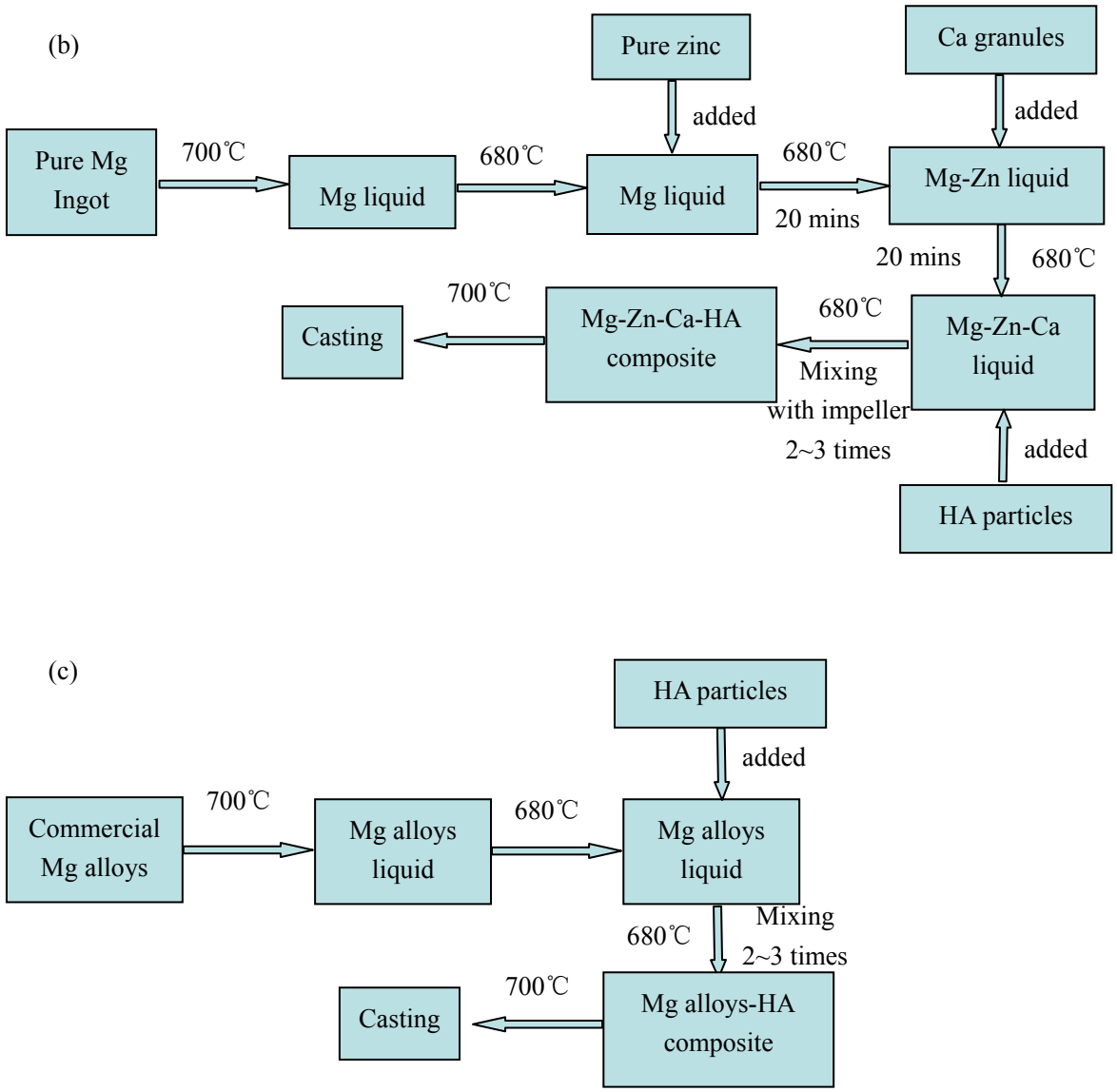

Fig. 3.1 Procedures of preparations for (a) Mg-Zn-Ca alloy samples, (b) Mg-Zn-Ca-HA composite samples and (c) commercial Mg alloys-HA composite samples.

3.3 Melt conditioning by advanced shear technology (MCAST)

To achieve homogeneous distribution of HA particles and low porosity in the microstructure, the melt conditioning by advanced shear technology (MCAST) was employed. This technology was exclusively developed and patented by the research group lead by Prof. Fan at BCAST, *Brunel University, UK*. The mechanism of the

melt conditioning machine mainly relies on the perfect-intermeshing screws, which are self-wiping and co-rotating during the process as indicated in Fig. 3.2. A high shear rate and a high intensity of turbulence as an important characteristic of the MCAST unit guaranteed that the melt experienced strong and efficient distributive mixing at high level. In addition, due to the highly intensive shear, a uniform temperature, chemical composition as well as uniform dispersive nucleation sites in the melt also achieved. The shear rate $\dot{\gamma}$ formed in the gap between the head of the screw flight and barrel surface was calculated according to the equation as following:

$$\dot{\gamma} = N\pi\left(\frac{D}{G} - 2\right)$$

where N stands for the rotation speed of the screw, D stands for the outer diameter of the screw, and G stands for the gap between the screw flight and barrel surface.

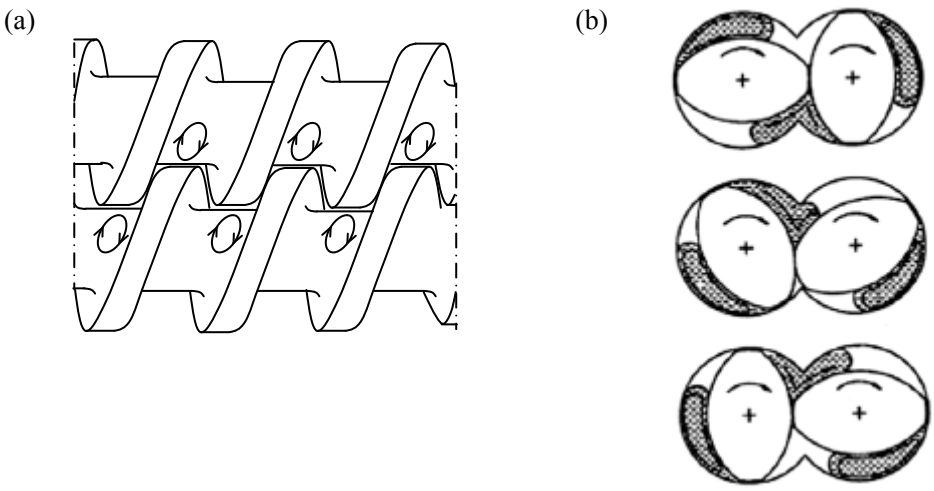

Fig. 3.2 Schematics illustration the fluid flow of twin-screw process.

(a) longitudinal view and (b) transverse view. [Ji et al., 2001]

The procedure for the MCAST experiment:

a) Materials were synthesized in several small steel crucibles placed in a resistance furnace covered protective gas (SF_6 and N_2) at 700 ℃. When

the melt is ready, a crucible containing an appropriate quantity of fluid was taken and manually stirred to make sure homogeneity, and then the melt was poured into the inlet of the MCAST unit (Fig. 3.3) at the specific pouring temperature measured by a thermocouple.

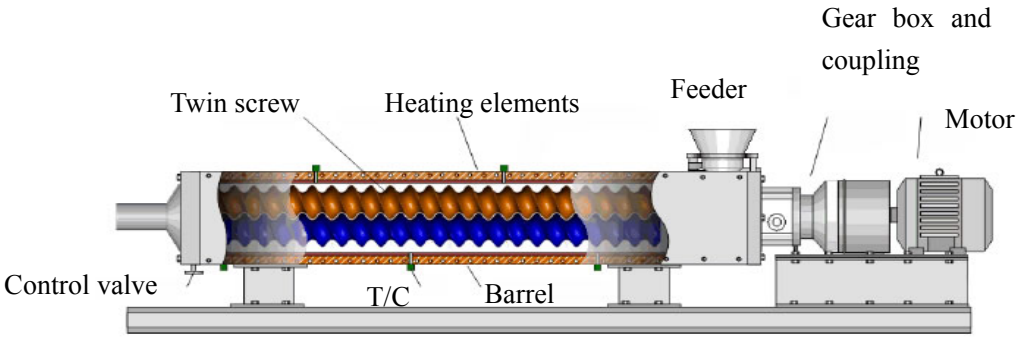

Fig. 3.3 Schematic illustration of the MCAST machine

b) The MCAST machine was operated to process the fluid according to the set parameters (500 rpm, 60 sec, 650 ℃).

c) For a while, when the shear process finished, the control valve was opened and the processed melt was fed into TP1 mould or casting mould.

3.4 Casting process

3.4.1 Moulds for conventional casting

In this work, we have used two types of steel cylindrical moulds. Mould inner diameters were 33 mm and 13 mm. The wall thickness was approximately 30 mm and the height was 127 mm for the former one. For the latter one, the wall thickness was 12 mm and the height was 127 mm. It is necessary to mention that these moulds were pre-heated at 350 ℃ in resistance furnace for sufficient time prior to casting procedure. The samples for microstructural investigations were taken at the middle of each cast. The small bars were cut into standard tensile samples for tensile strength measurements.

3.4.2 High Pressure Die-Casting (HPDC)

As a high-speed manufacturing method, the high pressure die casting (HPDC) process has been widely accepted and practiced, especially for the automotive industries. The HPDC machine employed in this research was made by *L.K. Machinery Co. Ltd., Hong Kong*. The major components of the HPDC machine are illustrated in the Fig. 3.4. The plunger in the machine was 60 mm in diameter, which possesses a maximum accelerated shot speed of 6.22 ms^{-1}. The 280 tons load can be applied to clamp the die. In order to maintain a uniform temperature across the die-cavity during pre-heating, 8 cartridge heaters were equipped symmetrically into the two halves of the die block. In addition, for the purpose of precise temperature control, a thermocouple was also located inside the die block along the heating manipulator unit. In addition, an external thermocouple was applied to test the temperature of the die-cavity surface before any casting operations. The die temperature was 180 ℃. The molten alloys or composites for the die casting have been prepared at the specific temperature according to the requirement of the investigation.

The procedure for die casting operation in detail was as following:

a) To diminish the negative effect of impurity remained from previous casting on the consequence, we have cleaned the surface of the die.

b) Using tangs, the steel crucible containing a sufficient amount of melt was taken from the resistance furnace and poured into the shot sleeve at the designated temperature measured by an external thermocouple. It's worth mentioning that the dross was removed from the liquid metal with a small spoon before pouring into the shot sleeve.

c) Plunger speed, position and pressure were set to required level, and then the machine automatically completed the casting steps: injection, intensifying, dwell (while the casting fully solidifies), and finally ejects the cast component.

The intensifier was set to trigger at a pressure drop of 65% with an intensifying pressure of 70 bar and with a 30-45 s dwell time until ejection. The casting produced is shown in Fig. 3.5 which consists of two tensile samples and two fatigue samples along with the runner system.

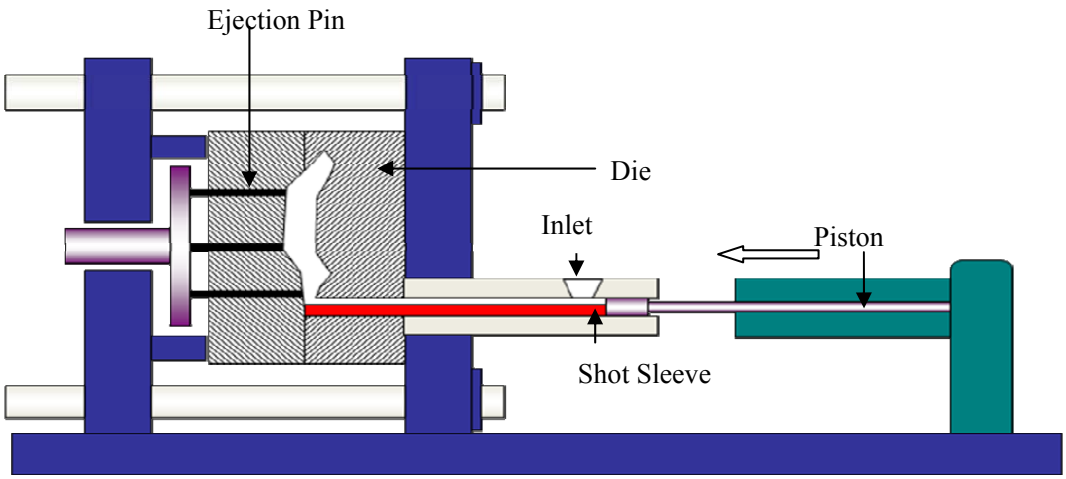

Fig.3.4 The structural sketch of the 'high pressure die-casting' (HPDC) machine.

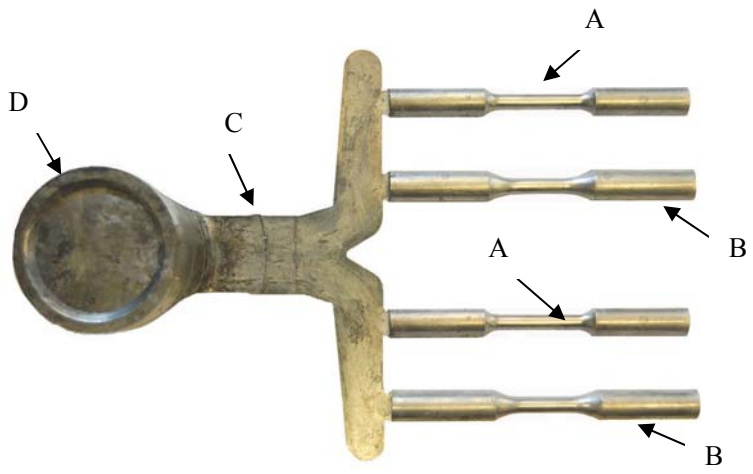

Fig. 3.5 Schematic illustration of a die-casting sample produced by the HPDC machine (A) Tensile sample (diameter 6.4 mm), (B) Fatigue sample (diameter 6.3 mm), (C) Runner, and (D) Biscuit.

3.4.3 Test Procedure -1 (TP-1) mould

The cooling rate plays an important role in influencing the grain size of the alloy. In a bid to investigate the effect of different processing parameters on the grain size for the

specific alloy, a constant cooling rate is definitely desirable. Therefore, as a favourable and common method the standard test procedure-1 (TP-1) [Aluminium Association, 1987] mould technique is employed across the research labs both at academic institutes and industries, which is illustrated in Fig. 3.6. The procedures of the experiments are as followings:

a) The steel crucible containing the alloy was heated in the electrical resistance furnace at 700 °C until the material completely transformed to liquid and stirred the melt with or without HA reinforcement.

b) Prior to the experiment, TP-1 mould was pre-heated to 350 °C. In addition, the water to a quench reservoir was supplied beforehand, and water flow rate was adjusted to 3.8 l/min which resulted in 25 mm immersion from the bottom of ladle.

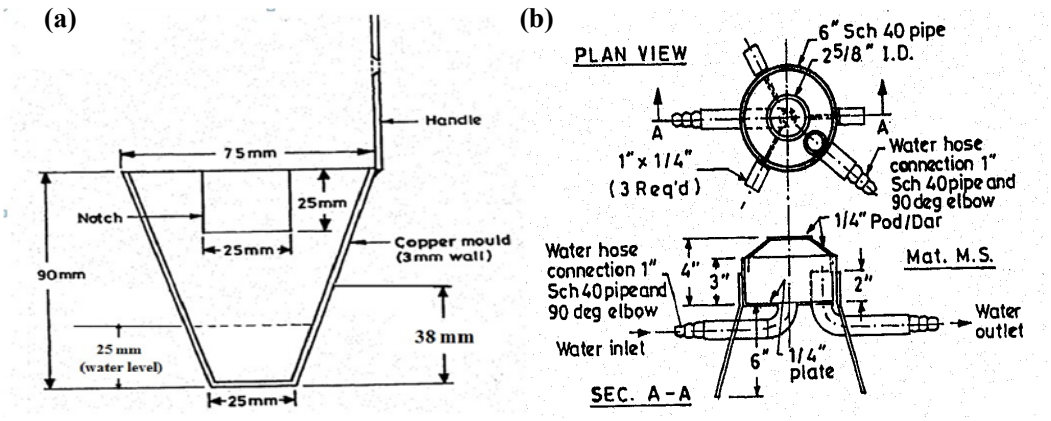

Fig. 3.6 Schematic illustration of the TP-1 moulds (a) ladle (b) plan and side view of mould design. [Aluminium Association, 1987]

c) To maintain the same pouring temperature (660 ℃) for various experiments, the temperature of the melt was monitored using a thermocouple. When the prepared melt reached the expected temperature, it was poured into the TP-1 mould and then located rapidly on a quench tank for a short period.

d) For micro-structural examination, TP-1 mould cast sample was cut at 38 mm above the base as showed in Fig. 3.6a. The cooling rate at this position corresponds to 3.5 Ks^{-1}.

3.5 Microstructural Characterization

For microstructural analysis of all cast samples, thin sections were cut from the centre of the conventional cast cylinder and embedded in Bakelite by mounting equipment (Buehler-*met phenolic Powder*) using a Buehler, Simplimet 1000 automatic mounting press, which included 90 seconds of heating at 150 ℃ at a pressure of 290 bar followed by 180 seconds of water cooling. After that, the embedded samples were ground using SiC abrasive papers with various grits (600, 1200, 2500 and 4000), and then polished using a 0.04 μm colloidal silica suspension until the microstructures were clearly observed under optical microscopy.

3.5.1 Etching surface treatment

After grinding and polishing the samples as described above, the sample surface was cleaned several times by ethanol and cotton wool to eliminate residue completely, and then dried by hot air blower. The sample surface was etched with acetic-picral colour etchant *(4.2g picric acid (conc.), 70mL ethanol, 15mL distilled water and 15 mL acetic acid (conc.))* for approximately 2 seconds, and immediately washed by ethanol and dried.

When the etching treatment was completed, the phenomenon of brightness variation across the surface of the sample is apparently observed due to abrupt changes in the sample surface topography. Using the plane polarised light mode of the optical microscope, the presence of various colours on the sample surface indicated different grain orientation.

3.5.2 Optical microscopy (OM)

The Zeiss Optical Microscope (OM) combined with a digital camera and a computer was employed for the micro-structural observation and grain size measurement. In addition, to obtain images from the camera and execute relevant analysis, the software Axiovision was also installed in the computer. Depending on experimental demands,

we could adjust settings of the microscope to take desirable pictures of samples either with or without etched surfaces.

The light contrast between the bright matrix and the dark unevenness such as grain boundaries or intermetallics could be apparently seen in the bright field (BF) mode. The reason to cause this phenomenon is related to the weakened intensity of the reflected light due to light dispersion from grain boundaries and the interfaces between second phases and matrix.

The measurement of the grain size of the cast sample is carried out by exposing it to the plane polarized light (PP) mode which relies on a polarizing filter mounted inside the incoming light path. Due to various orientations of different grains, PP light reflects from the samples with strong reflecting waves and generates special wave components. These different components will change according to the favourable direction across the sample.

3.5.3 Grain size measurements

The grain size measurements for the Mg-alloys/composites were carried out on colour etched samples using a mean line-intercept method. The mean intercept length is $\bar{l}$ used as the grain size and is calculated using the following equation:

$$\bar{l} = \frac{L_i}{N_i}$$

where L_i is the total length of the test lines and N_i the total number of grain boundary intersections on each test line. The measured standard deviation from the average grain size measurements is used as the error in grain size measurements.

3.5.4 X-ray diffraction (XRD)

As a versatile, non-destructive research technology, X-ray diffraction (XRD) had been extensively accepted to analyze the information about the chemical composition and

crystallographic structure of natural or manufactured materials in detail. In this work, an XRD machine, located at the Bulk Superconductivity Research Group, Department of Engineering, University of Cambridge, equipped with Cu K_{∞} target (λ = 1.54056 Å) has been used in this study to record XRD patterns in Mg-Zn-Ca/HA composites/alloys.

Normally, any crystal possesses a number of different orientations, and each with different specific distance *d* between parallel planes. As a result, when a monochromatic X-ray beam with wavelength λ projected into a crystalline substance (Phase) at an angle θ, diffraction is generated unless the total distance of the rays traveled from successive planes satisfy an integer value n of wavelengths. Through changing the angle θ, the Bragg's Law conditions:

$$n\lambda = 2d\sin\theta$$

are satisfied by different *d*-spacings in polycrystalline materials. Eventually, the XRD pattern of the sample is plotted, which includes the angular position and intensities of the resultant diffracted peaks of radiation. Nevertheless, if a mixture of substance is investigated, the consequent diffraction graphs consist of the individual patterns combined.

3.6 Mechanical property testing

3.6.1 Hardness tests

To assess the plastic penetration behaviour of a material surface, a Vickers indenter (Vickers hardness H_v) made by *Akashi Corporation* in Japan (Model NO. MICROMET 5101) was employed to measure micro-hardness. Normally, a square base diamond pyramid used as the indenter, which possesses the specific separation angle (l36°) between the opposite faces of the pyramid. The Vickers hardness value can be calculated by the equation:

$$HV = 1.0544\left(\frac{P}{d^2}\right)$$

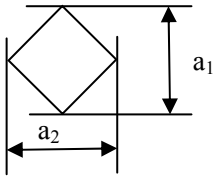

where *P* stands for applied load in kg, and *d* stands for diagonal length in mm. It is worth mentioning that the indention dimensions of two diagonals (a_1 and a_2) which are perpendicular to each other are measured, and then turned into average valued: $d = (a_1+a_2)/2$. According to Vickers hardness chart, the corresponding *Hv* value to each measured *d* is eventually obtained. The average hardness of the sample was obtained by an average of at least six indentions under a load of 0.5 kg.

3.6.2 Tensile tests

Samples for tensile measurements were prepared by HPDC process and conventional casting method. The dimensions of the test samples which were produced by the standard die attached to HPDC machine, were 6.4 mm in gauge diameter, 25 mm in gauge length and 12 mm diameter in the grip section. Due to the cylinder shape of conventional casting samples, they needed to be machined into tensile bar shape according to the standard tensile bar dimensions.

The universal measurement machine (Instron ® 5569) was used to test the stress-strain curves of samples at a cross head speed of 2 mm/min. (strain rate: 1.33×10^{-3} s^{-1}). The machine equipped with a computer could automatically test and record the tensile property results such as Young's modulus, 0.2% proof yield stress, ultimate tensile strength and elongation. To obtain precise elongation, an extensometer with 25 mm in gauge length was manually clipped to every test sample. All samples were measured at room temperature.

3.7 Cooling curve measurement

The schematic illustration of the experimental setup for measuring the cooling curves

is shown in Fig. 3.7. The steel crucible covered with a 13 mm thick layer of thermal insulation and a 0.5 mm diameter thermocouple which connected with computer was used in this work. Prior to measurements, the crucible was pre-heated to 700 ℃ in electric resistance furnace. To make results accurate, we need to make sure that the thermocouple is located in the middle of Mg melt. Moreover, the protective gas is also used during the test, which aims at preventing Mg melt from oxide reaction with air. Eventually, the temperature of the melt as a function time is recorded by a data acquisition software.

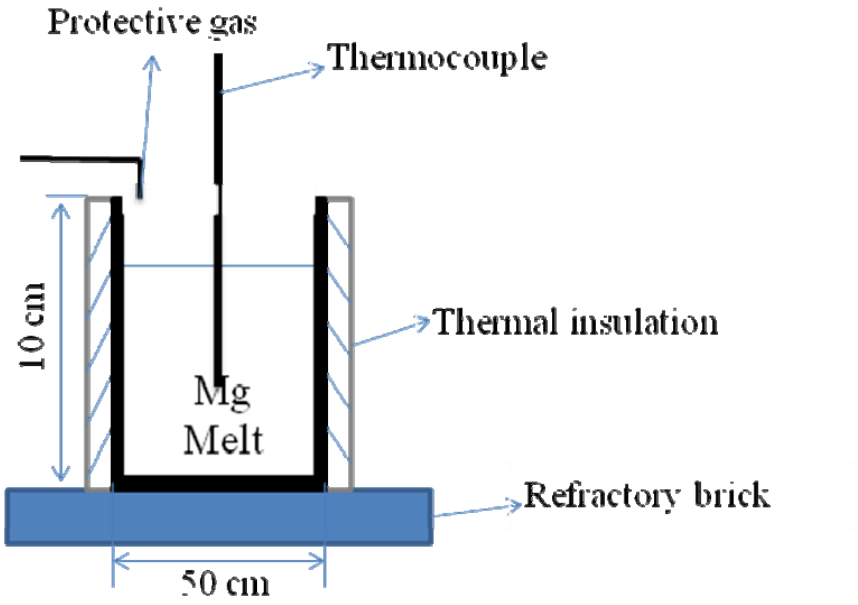

Fig. 3.7 The diagram of experimental setup for measuring the cooling curve.

Chapter 4
Results and Discussion

4.1 Microstructure

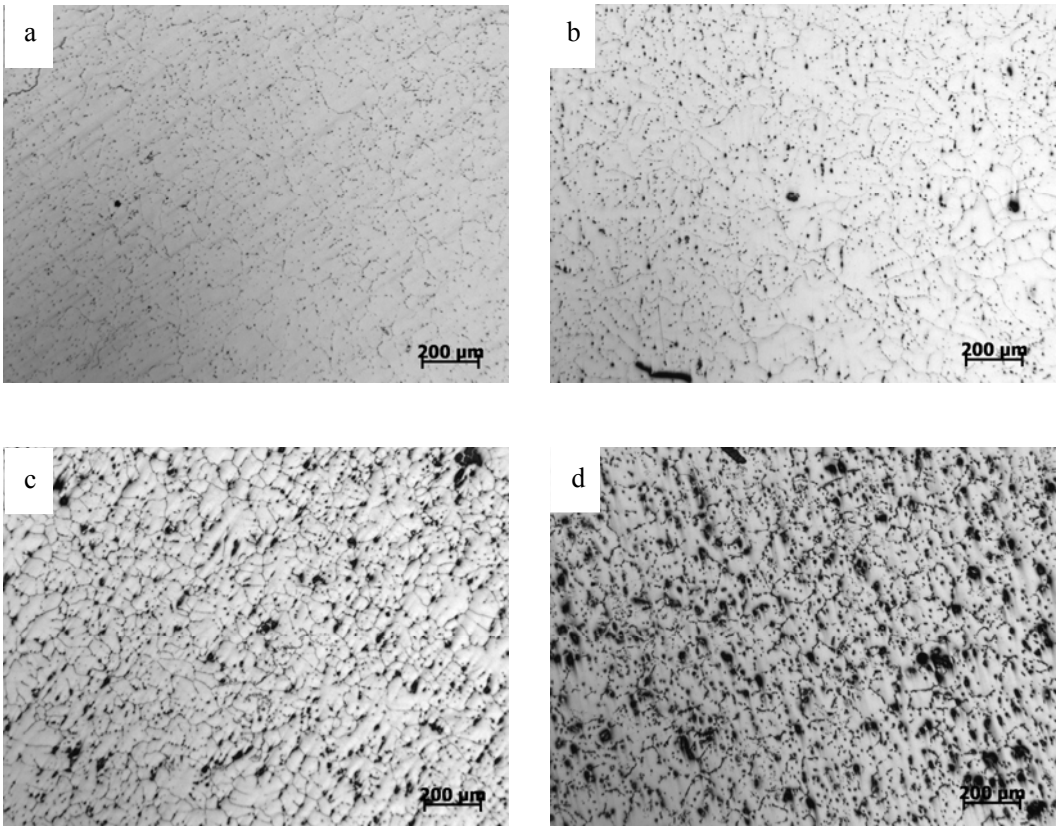

Fig. 4.1 Optical micrographs of conventional cast Mg-xZn-1Ca alloy for (a) x = 0; (b) x = 1; (c) x = 3; (d) x = 5.

Figure 4.1 shows optical micrographs of conventional Mg-xZn-1Ca alloy samples. It is obviously seen that the microstructure of Mg-1Ca alloy is quite similar to that of Mg-1Zn-1Ca alloy. Both possessed a small quantity of second phase. Since the maximum dissolution of Zn in magnesium is approximately 2-3 wt.%, the typical microstructure still consists of Mg_2Ca second phase after adding 1 wt.% Zn. Nevertheless, the amount of intermetallic particles gradually increased with increasing

fraction of zinc element. It may be explained that when the addition of zinc element exceeded the limit of solubility in Mg matrix, an increasing fraction of second phase subsequently formed. It is necessary to mention that Mg_2Ca second phases observed in Fig. 4.1 (a) are replaced by $Ca_2Mg_6Zn_3$ when Zn concentration is high (>3%). This replacement of Mg_2Ca by $Ca_2Mg_6Zn_3$ has been previously reported [Bamberger et al., 2006].

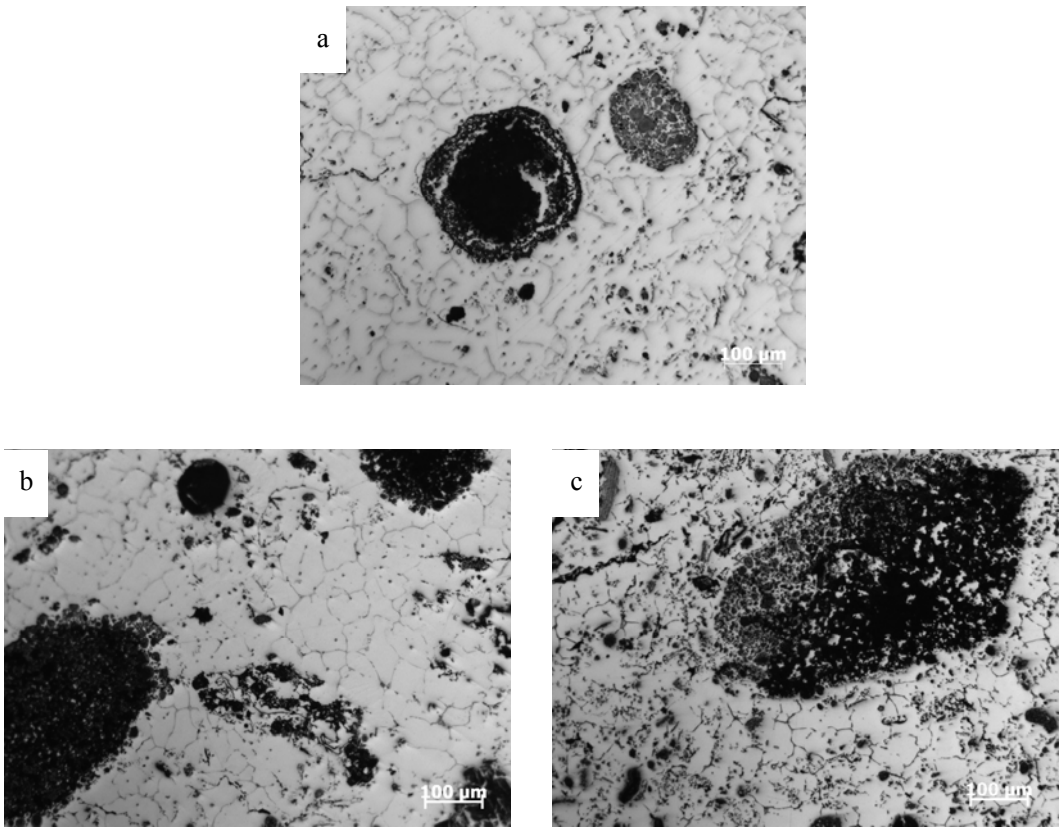

Fig. 4.2 Optical micrographs of conventional cast Mg-1Zn-1Ca-xHA composites for (a) x = 1; (b) x = 3; (c) x = 5.

Figure 4.2 presents the optical micrographs of conventional cast Mg-1Zn-1Ca-xHA composites. Apart from presence of Mg-Ca second phase particles in the magnesium matrix, dark in colour agglomerates of HA particles exist in the microstructure for Mg-1Zn-1Ca/HA composites. Although, large size agglomerates are easily seen in the microstructure, finely dispersed HA particles are also seen in the microstructure. Moreover, the size and number of the clusters gradually increased with increasing

fraction of HA powders. The microstructures for Mg-3Zn-1Ca-xHA and Mg-5Zn-1Ca-xHA composites are shown in Fig. 4.3 and they are hardly different from Mg-1Zn-1Ca-xHA composites shown in Fig. 4.2.

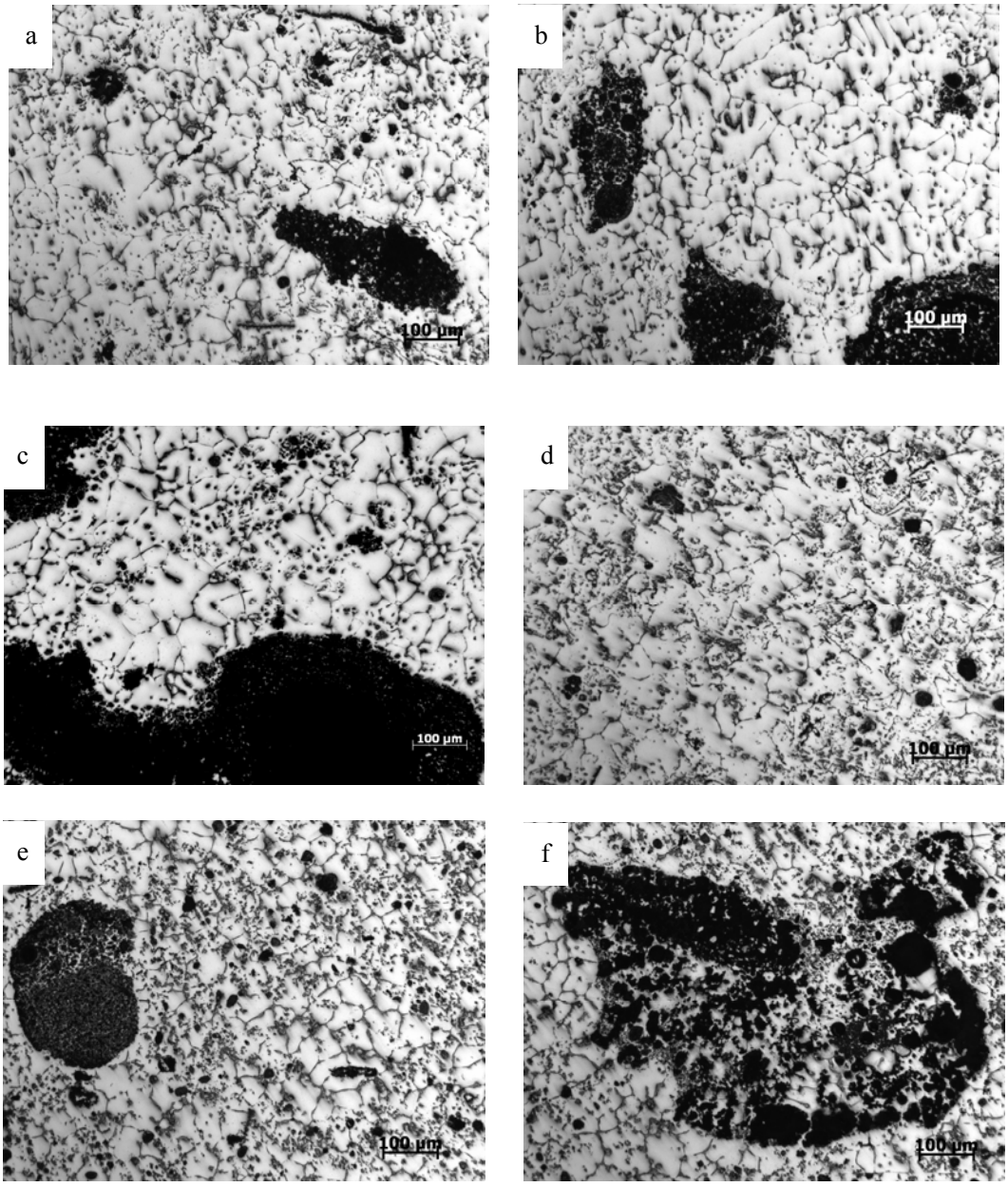

Fig. 4.3 Optical micrographs of conventional cast Mg-3Zn-1Ca-xHA composites for (a) x = 1; (b) x = 3; (c) x = 5 and Mg-5Zn-1Ca-xHA composites for (d) x = 1; (e) x = 3; (f) x = 5.

The optical micrographs of Mg-5Zn-1Ca-xHA alloy/composites processed by high-pressure die-casting (HPDC) unit are shown in Fig. 4.4. The intermetallics are observed along the grain boundary and the agglomerates of HA particles are also

observed in microstructures of Mg-5Zn-1Ca-xHA composites. Therefore, there are no distinctive differences between conventional and HPDC sample microstructure besides the possession of different grain size (see section 4.4).

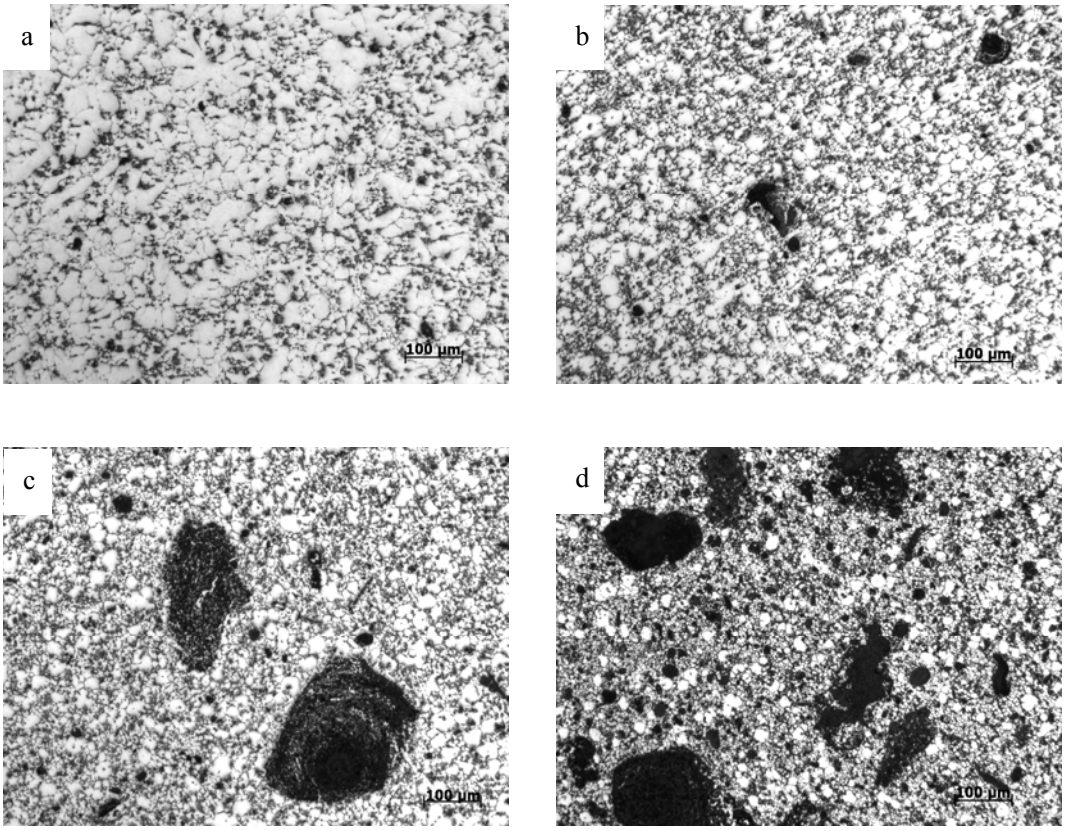

Fig. 4.4 Optical micrographs of Mg-5Zn-1Ca-xHA alloy/composites produced by HPDC for (a) x = 0; (b) x = 1; (c) x = 3; (d) x = 5.

In order to improve the distribution of HA particles, the Mg/HA slurry was sheared intensively using "melt-conditioning by advanced shear technology" (MCAST). The optical micrographs of samples processed by MCAST technology and conventional cast corresponding ones are compared in Fig. 4.5. Compared with the microstructure of conventional Mg-5Zn-1Ca alloy, the distribution of intermetallic particles exhibits much better homogeneity after intensive shearing. The large agglomerates of HA that existed in as-cast composite are almost extinct, and the average size of HA agglomerates is significantly decreased. The HA agglomerate size is compared in Fig. 4.6 for conventional cast and MC-cast samples. It can be seen that the MC-cast

process results in relatively fine dispersion of agglomerates. Unlike in the conventional process, there are no agglomerates above 200 μm in MC-cast processed samples. The observed improved microstructure is as a result of high shear rate, a high intensity of turbulence generated by MC machine. These results are in agreement with an earlier study of Al/SiC composites [Hari Babu et al., 2008; Tzamtzis et al., 2009]. Fine dispersion of HA particles are expected to contribute for much improved corrosion due to increased interface area between Mg matrix and HA inclusion.

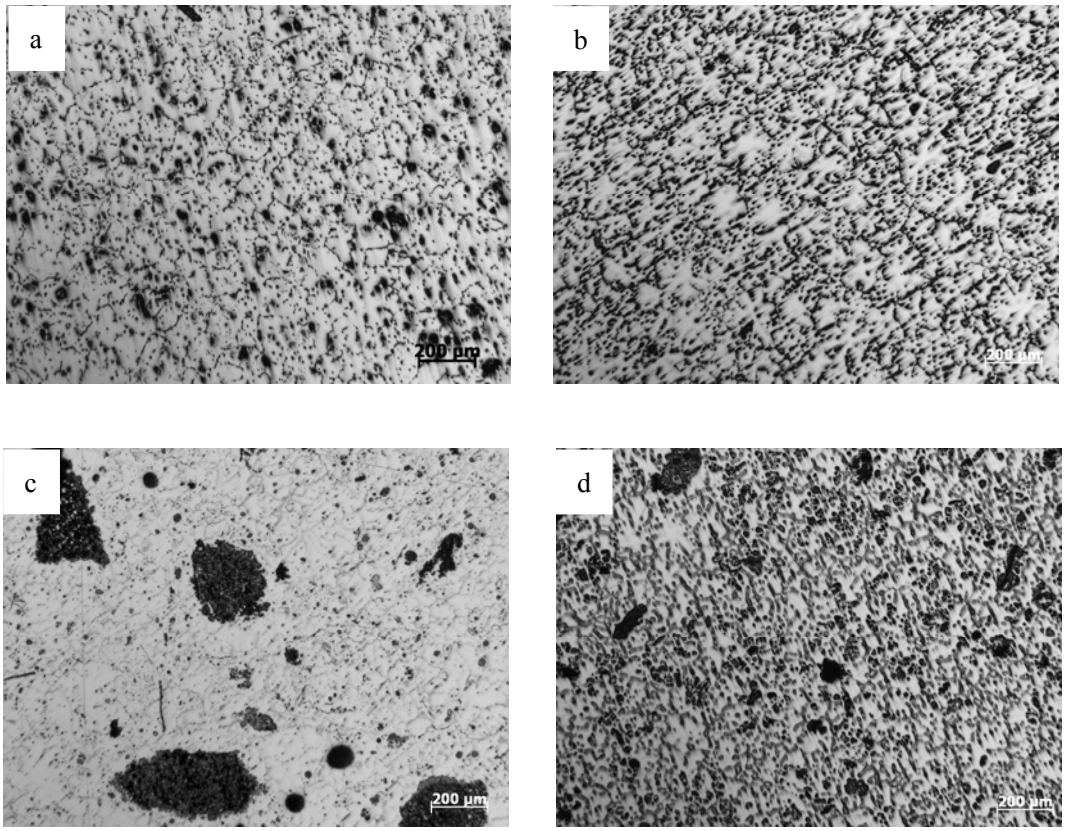

Fig. 4.5 Optical micrographs of Mg-5Zn-1Ca alloy (a) conventional cast (b) MC-cast (casting after shearing intensively the slurry using MCAST). (c) and (d) are for Mg-5Zn-1Ca-3HA composites processed with conventional cast and MCAST, respectively. In both alloys and composites, intensive shearing the liquid/slurry is observed to result in much improved distribution of second phase inclusions and reinforcement particles.

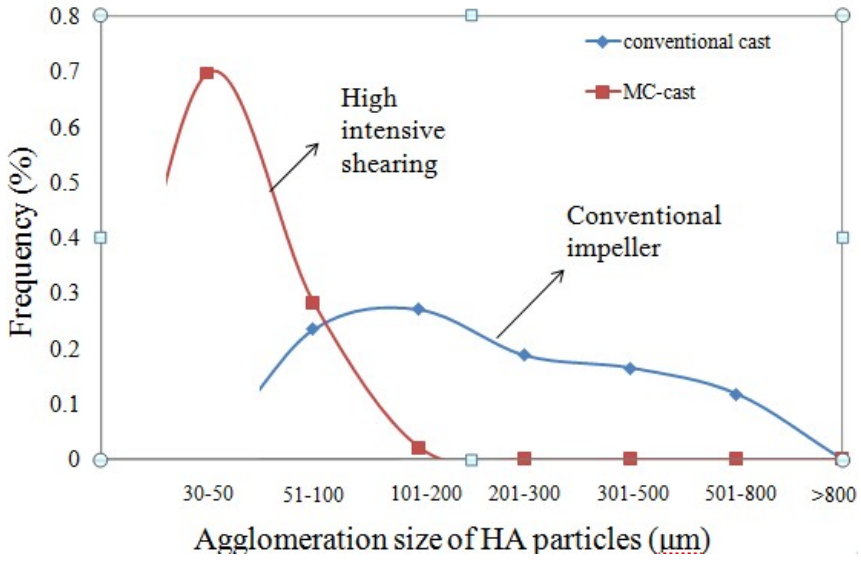

Fig. 4.6 HA agglomerate size disribution for conventional and MC-cast processes.

4.2 XRD analysis

The XRD patterns for as-cast Mg-1Zn-1Ca, Mg-3Zn-1Ca and Mg-5Zn-1Ca alloys are shown in Fig. 4.7. For Mg-1Zn-1Ca alloy, all the observed peaks correspond to α-Mg. Peaks are indexed to h.c.p crystal structure of Mg. No additional peaks related to second phases are observed in both Mg-1Zn-1Ca and Mg-3Zn-1Ca, even though microstructures in Fig. 4.1(b) and 4.1(c) show presence of intermetallics. However, several new peaks (marked with "*") are detected for Mg-5Zn-1Ca samples in comparison with the XRD pattern of pure magnesium. These additional peaks represent second phases, which may be ternary intermetallics ($Ca_2Mg_6Zn_2$) and a very small amount of Ca-rich $CaMg_2$ phase as reported previously [Bamberger et al., 2006]. The intensity of XRD peaks corresponding to these second phases is not strong enough for detection due to their low volume concentration.

It is important to understand whether there is a chemical reaction between HA and Mg liquid metal during the mixing process. To enable us to detect the second phases using XRD, we have fabricated an MMC containing 10 wt.% HA (Mg-5Zn-1Ca-10HA

composite). The XRD patterns for pure HA particles, Mg-3Zn-1Ca cast alloy and Mg-5Zn-1Ca+10%HA samples are compared in Fig. 4.8. The XRD pattern for 10 wt.% HA added Mg-5Zn-1Ca resulted in additional peaks. These peak positions

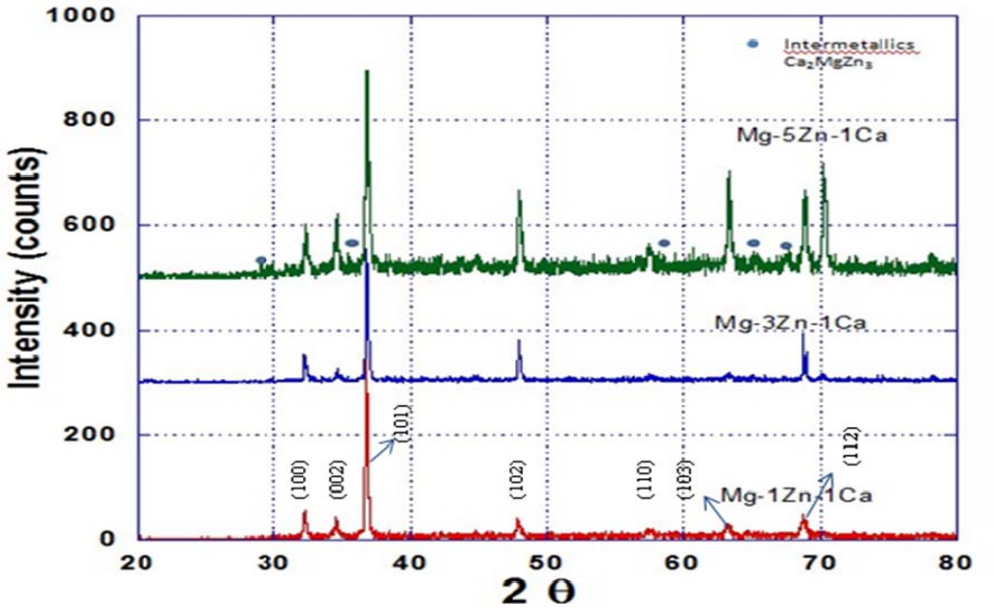

Fig. 4.7 XRD patterns of conventional cast Mg-1Zn-1Ca, Mg-3Zn-1Ca and Mg-5Zn-1Ca alloys.

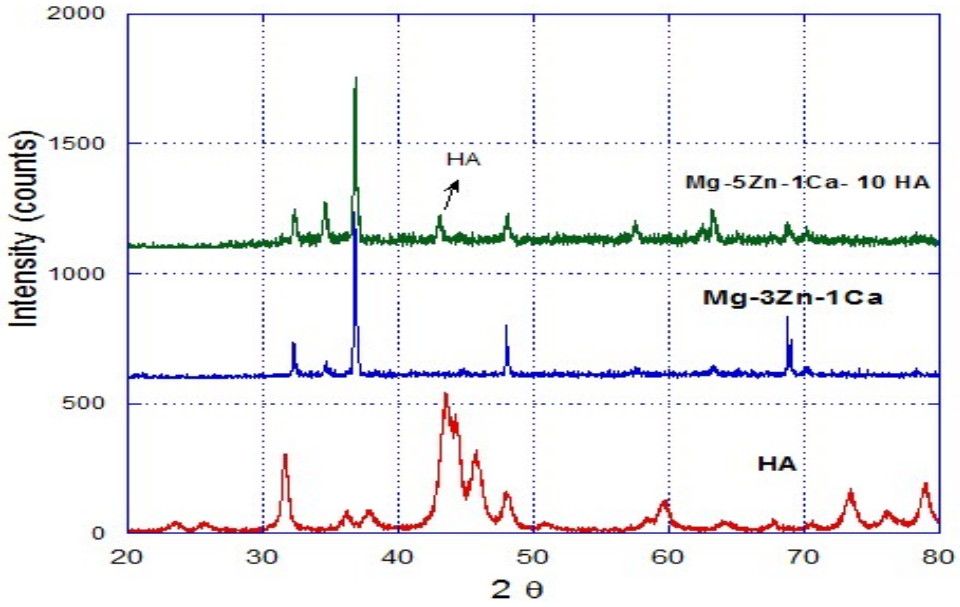

Fig. 4.8 XRD patterns of HA particles, conventional cast Mg-3Zn-1Ca alloy and Mg-5Zn-1Ca-10HA composite.

match with those of the HA phase, suggesting that the HA phase remained chemically

unaffected during mixing with Mg-Zn-Ca liquid metal. It can be concluded that the observed agglomeratess are indeed HA based phase particles. The chemical reaction between HA and Mg, if there is any, is not detected by the XRD. To investigate the interface between Mg and HA, high resolution electron micrograph study may be needed.

4.3 Tensile property

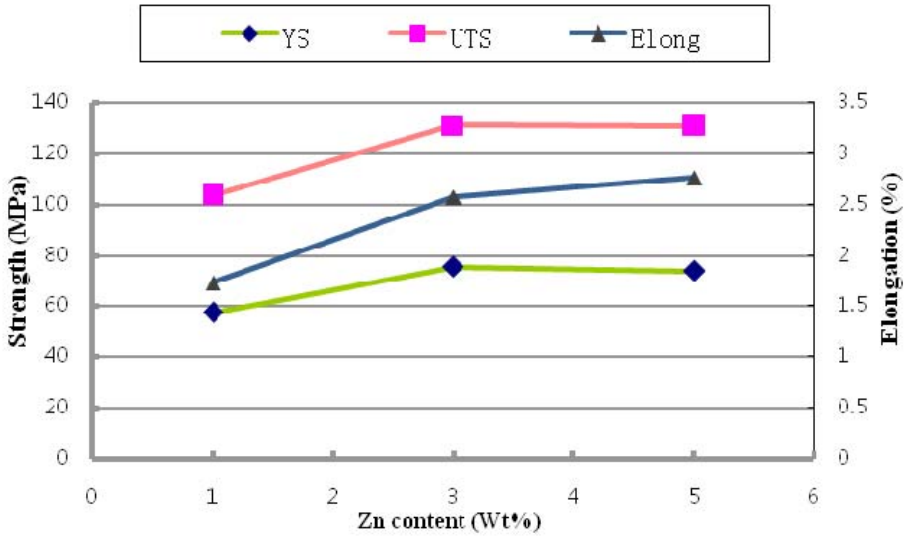

Fig. 4.9 Tensile properties of as-cast Mg-1Zn-1Ca, Mg-3Zn-1Ca alloy and Mg-5Zn-1Ca alloys at room temperature.

The results of tensile strength measurements shown in Fig. 4.9 demonstrate that the yield strength and the ultimate tensile strength obviously increased when the content of Zn element increased from 1 wt.% to 3 wt.%, whereas they were approximately invariable when Zn addition increased to 5 wt.%. It is worth mentioning that the tendency of elongation is completely opposite against previous reports, which indicate that it should gradually drop with increasing the Zn fraction [Yin et al., 2008; Zhang et al., 2009 b].

The observed mechanical behaviour can be clarified by the following reasons. First,

during solidification, Zn solute is ejected by the Mg growth front and can restrict the grain growth. In other words, at a given cooling rate (i.e, the rate at which the heat is extracted from the liquid metal), Zn can contribute to grain growth restriction. Therefore, with increasing content of zinc, the grain size decreases and as a result the yield strength can enhance with reduced grain size according to the Hall-Petch formula. Second, when 3% Zn is included into alloy, the Zn-based second phase will precipitate from the Mg-matrix, which can enhance the strength by a dispersion strengthening mechanism. However, the presence of more intermetallic phase along the grain boundary may have a detrimental effect on the elongation. Third, the unexpected trend of elongation could be related with the defects in the cast structure, such as large voids caused by poor die filling during conventional casting, when Zn concentration is low.

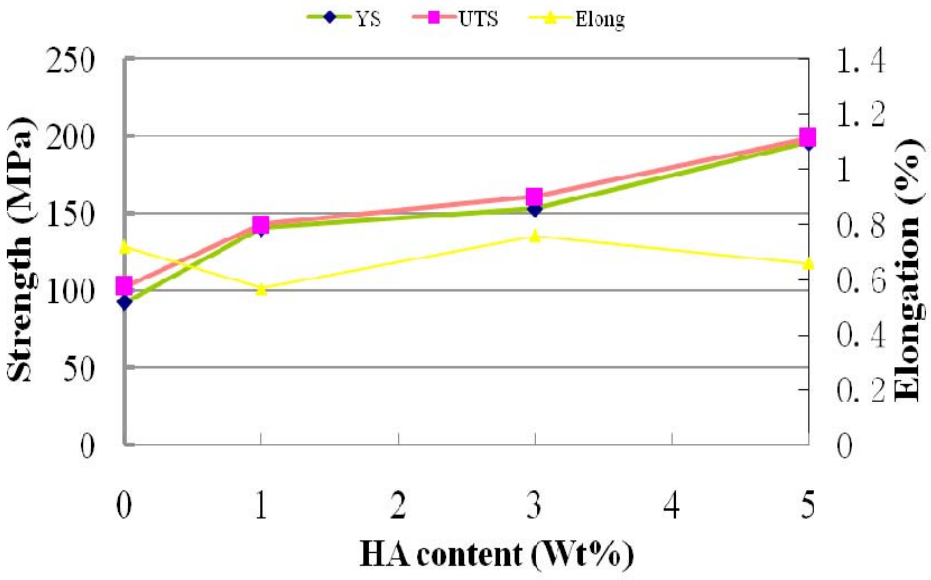

Fig. 4.10 Tensile properties of Mg-5Zn-1Ca-xHA alloy/composites produced by HPDC as a function of HA content.

Tensile properties of Mg-5Zn-1Ca-xHA samples produced with high-pressure die casting (HPDC) method are shown in Fig. 4.10. The yield strength and the ultimate tensile strength have improved by increasing the HA addition, significantly. It could be related to the phenomenon of load transfer that occurs in MMCs. The applied load

can be transferred to the reinforcement (HA) which possesses good load-bearing capability. With the increasing fraction of HA, more reinforcement exists in the structure, which could tolerate more load. However, the elongation almost fluctuated around 0.7%, which deviates from the anticipated results of elongation deterioration with increased HA fraction. The elongation of the non-reinforced alloy is also very low. These results indicate that casting defects dominate elongation in HPDC specimens.

In summary, the tensile properties of Mg-Zn-Ca alloys and composites investigated in this study are similar to that of cortical bone [Staiger et al., 2006]. It is important to note that the mechanical properties of Mg alloys and composites could be altered significantly with the use of Zn as an alloying element and HA as reinforcement.

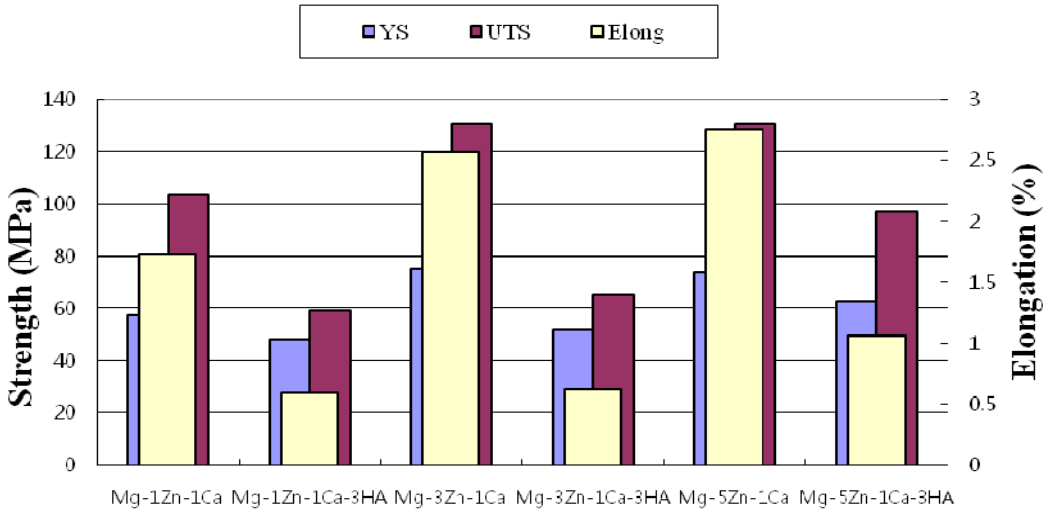

Fig. 4.11 Comparison of tensile properties for conventional cast Mg-xZn-1Ca alloy and with 3 wt.% HA addition for x =1, 2 and 3.

Tensile strength and elongation are compared for Mg-xZn-1Ca alloy and Mg-xZn-1Ca-3HA composite (x=1, 2, 3) in Fig. 4.11. Although HA resulted in the refinement of grain size, the existence of HA powder in the structure seems to reduce the yield strength, the ultimate tensile strength and elongation, when slurry cast into a cylindrical steel mould. As a matter of fact, it could be associated with some

inevitable defects such as large porosity by the gravity-casting method due to the increased viscosity of the liquid metal by the addition of HA. As a result, the presence of defects severely deteriorates the mechanical properties and eventually accelerates the failure of the sample during tensile test. Therefore, the result of conventional cast samples is opposite to that of HPDC samples which are rarely influenced by large structural defects due to effective die filling under high pressure.

4.4 Hardness

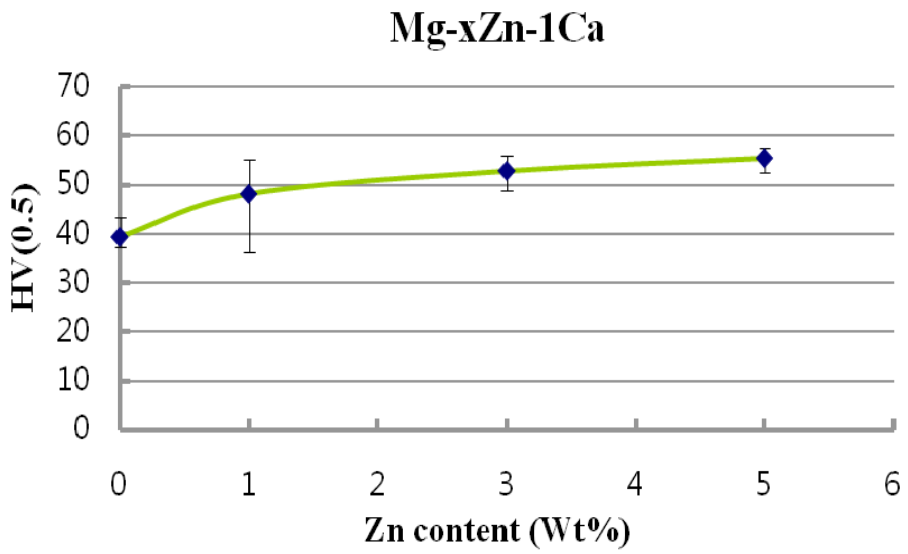

Fig. 4.12 Hardness of conventional cast Mg-xZn-1Ca alloys for x=0, 1, 3, 5 at room temperature.

The hardness of Mg-1Ca alloy is enhanced by the addition of Zn, while the slight improvement of hardness is observed with further increasing content of zinc element up to 5 wt.% as shown in Fig. 4.12. Increased hardness is attributed to the strengthening effectiveness of Zn in magnesium alloys. When the content of Zn is controlled under a relatively low level (1-2 wt.% Zn), zinc element dissolves into magnesium matrix and improves the strength of alloys by solid-solution strengthening mechanism. Nevertheless, when the Zn addition exceeds 3 wt.%, the intermetallic phase (Ca_2MgZn_2) precipitates from the matrix, which contributes to the improvement

of the hardness by dispersion strengthening mechanism [Bamberger et al., 2006].

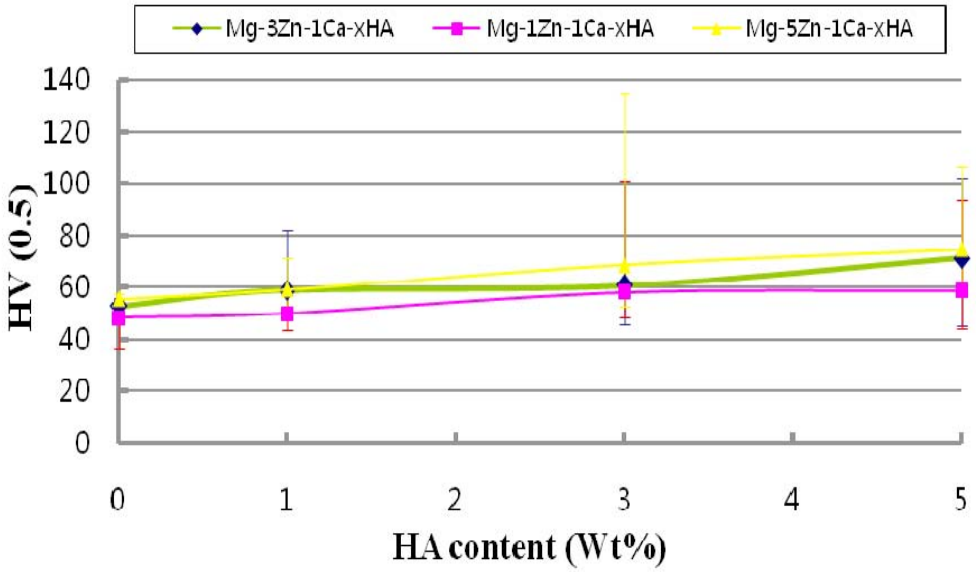

Fig. 4.13 Hardness of conventional cast Mg-xZn-1Ca-yHA alloy or composite samples (x=1, 3, 5; y=0, 1, 3, 5) at room temperature.

Hardnesses of the samples tend to increase with the elevating fraction of HA as shown in Fig. 4.13. Moreover, compared with 1 wt.% and 3 wt.% Zn series composites, the more prominent hardness was observed among Mg-5Zn-1Ca-yHA composites (y=1, 3, 5). Significant variation in local hardness value is observed, depending on the location. Low hardness ($HV_{0.5}$ = 50.3) was observed within metal matrix (Fig. 4.14a), while some regions possessed intermediate hardness ($HV_{0.5}$ = 65.1) due to the presence of small clusters of HA (Fig. 4.14b). Nevertheless, the measurement within big agglomerate of HA (Fig. 4.14c) led to higher hardness ($HV_{0.5}$ = 99.9). This shows that the overall hardness of the composite materials depends on the distribution of the HA particles. However, a limitation of accurate micro-indention measurement in this research is the limited resolution of microscope attached to micro-hardness equipment, which occasionally leads to indentation to takes place within the agglomerate rather than matrix and is the possible source for observed large error.

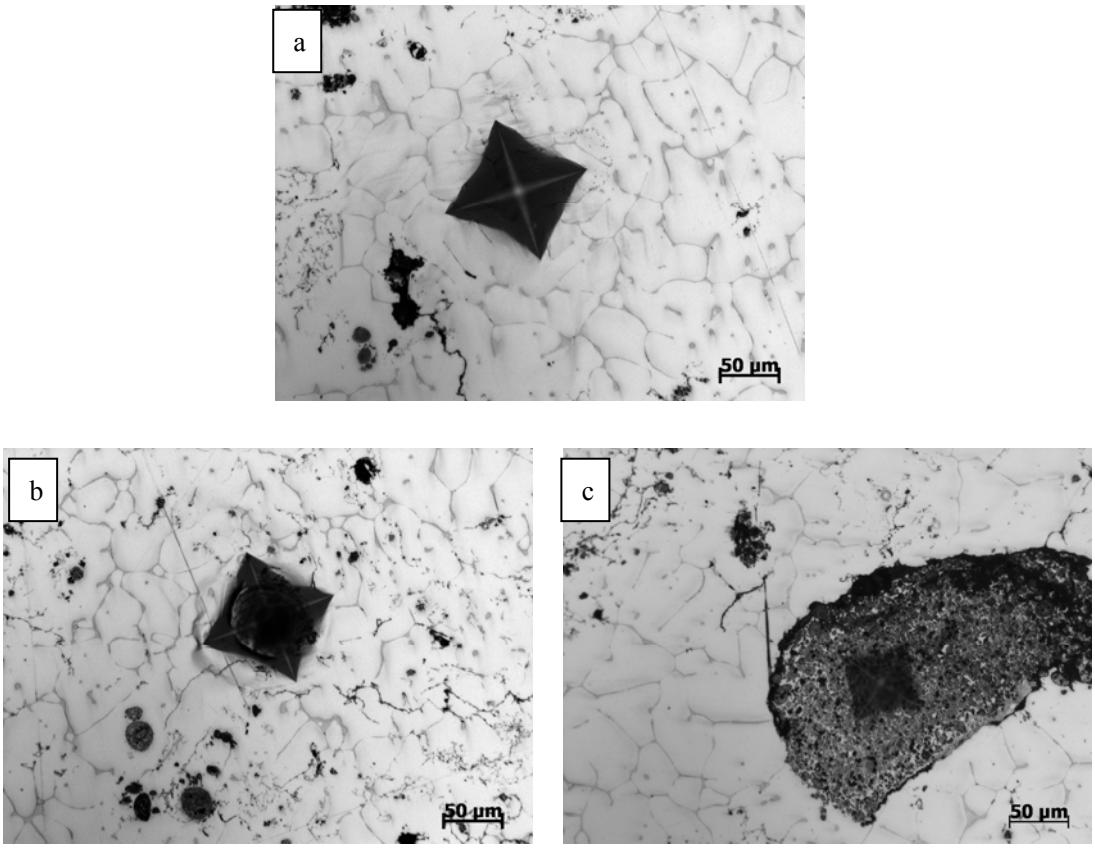

Fig. 4.14 Microstructure of Mg-3Zn-1Ca-3HA showing the Vickers hardness indents in different locations of MMC-HA sample.

On the basis of the micro-hardness of cortical bone (Hv~ 49.8) [Hodgskinson et al., 1989], it is easy to find out that some measured samples in this study seem to approach the characteristic values of natural bone. Moreover, hardness for alloys processed in this study is comparable to that of Al-containing magnesium alloys ($HV_{0.1}$ = 80 and 73) [Witte et al., 2007]. It is important to note that the poisonous negative effect on health by the presence of aluminium element for alloys studied by Caceres et al. and Witte et al. [Caceres et al., 2005; Witte et al., 2007] can be avoided in the alloys proposed here. In addition, the yield strength of Mg-5Zn-1Ca-xHA (x=1, 3, 5) composites samples by HPDC process is about 140-196 MPa, which was similar to the compressive yield strength of natural bone (130-180 MPa). Therefore, these mechanical properties demonstrate that Mg-5Zn-1Ca-xHA (x=1, 3, 5) composites (MMC-HA) are promising candidates as biomedical materials for bone load-bearing application.

4.5 Grain size for various alloys/composites

Fine grain structure is favourable for anti-corrosion property of Mg alloys. Optimization of grain structure by efficient approaches is always considered as an important issue of the solidification process. Chemical inoculation and physically induced grain refinement are two common methods that are commonly used to achieve this tough task.

4.5.1 Ca-addition

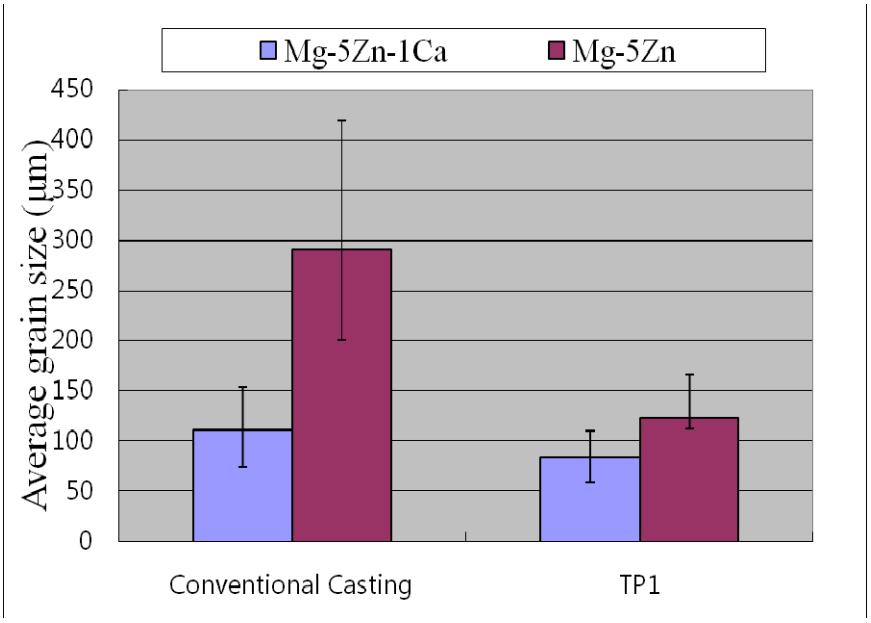

Fig. 4.15 Average grain sizes for conventional cast Mg-5Zn-1Ca and Mg-5Zn alloy. The grain sizes for same alloys under TP1 cast condition are also shown.(cooling rate for conventional and TP1 cast are ~1 K/s and 3.5 K/s, respectively.)

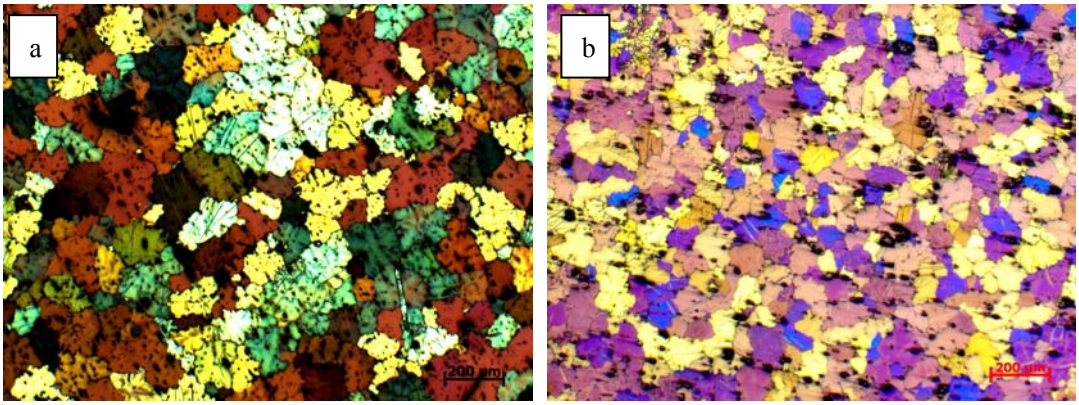

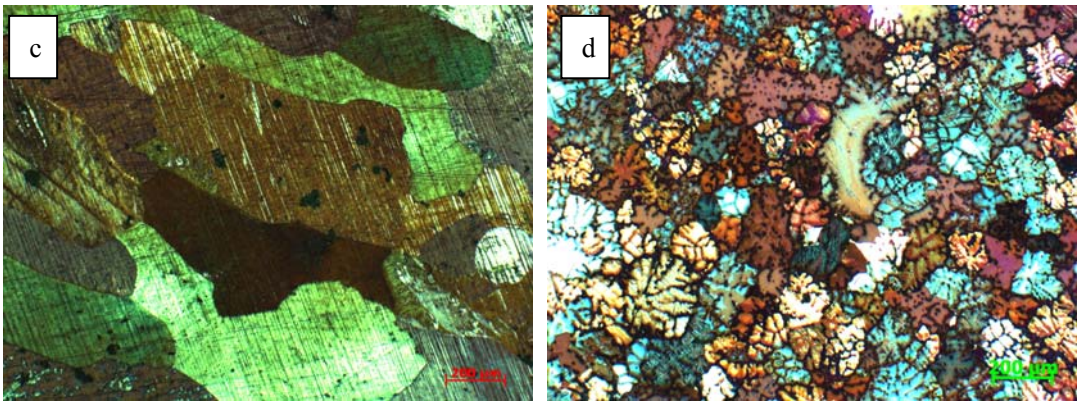

Fig. 4.16 Micrographs of etched samples: (a) conventional cast Mg-5Zn-1Ca alloy; (b) the TP1 sample of Mg-5Zn-1Ca alloy; (c) conventional cast Mg-5Zn alloy; (d) the TP1 sample of Mg-5Zn alloy.

The results from Fig. 4.15 demonstrate that the average grain size is apparently refined by the addition of 1 wt.% Ca for conventional cast and TP1 samples. Moreover, the effect of Ca on the refinement of grain size can be observed by naked eyes according to Fig. 4.16. It could also be related to the precipitation of intermetallic phase $Ca_2Mg_6Zn_3$ and a small quantity of $MgCa_2$ from the Mg matrix [Bamberger, 2006] instead of solely Mg_2Zn when Mg-5Zn was alloyed with calcium. These intermetallics may have contributed to heterogeneous nucleation process as described in Chapter 2 (literature review-part 2). Reduced grain size could be related to the growth restriction of Ca solute by the α-Mg solvent front [Ramirez et al., 2008]

4.5.2 Zn-addition

In Fig. 4.17, the influence of zinc element on the grain size is presented. The plotted line shows that the grain size systematically decreased with increasing content of solute element Zn. The Micrographs of etched samples shown in Fig. 4.18 also confirm the effect of zinc element on grain size refinement.

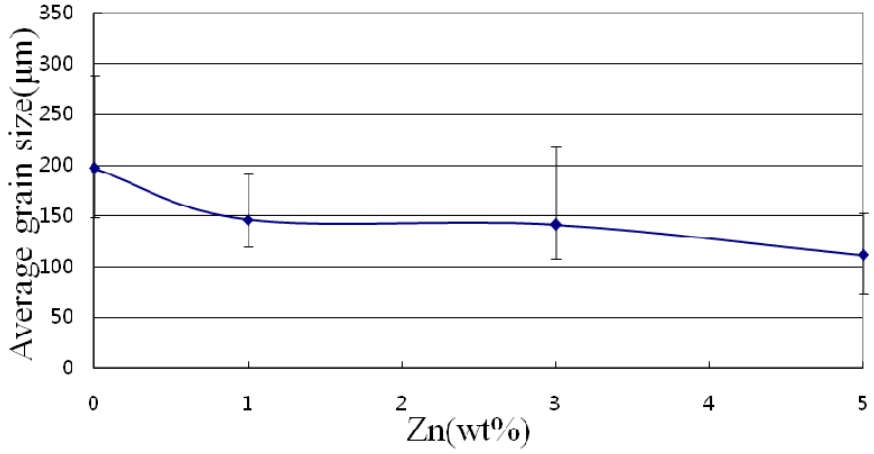

Fig. 4 17 Average grain sizes for conventional cast Mg-1Ca, Mg-1Zn-1Ca, Mg-3Zn-1Ca and Mg-5Zn-1Ca alloys.

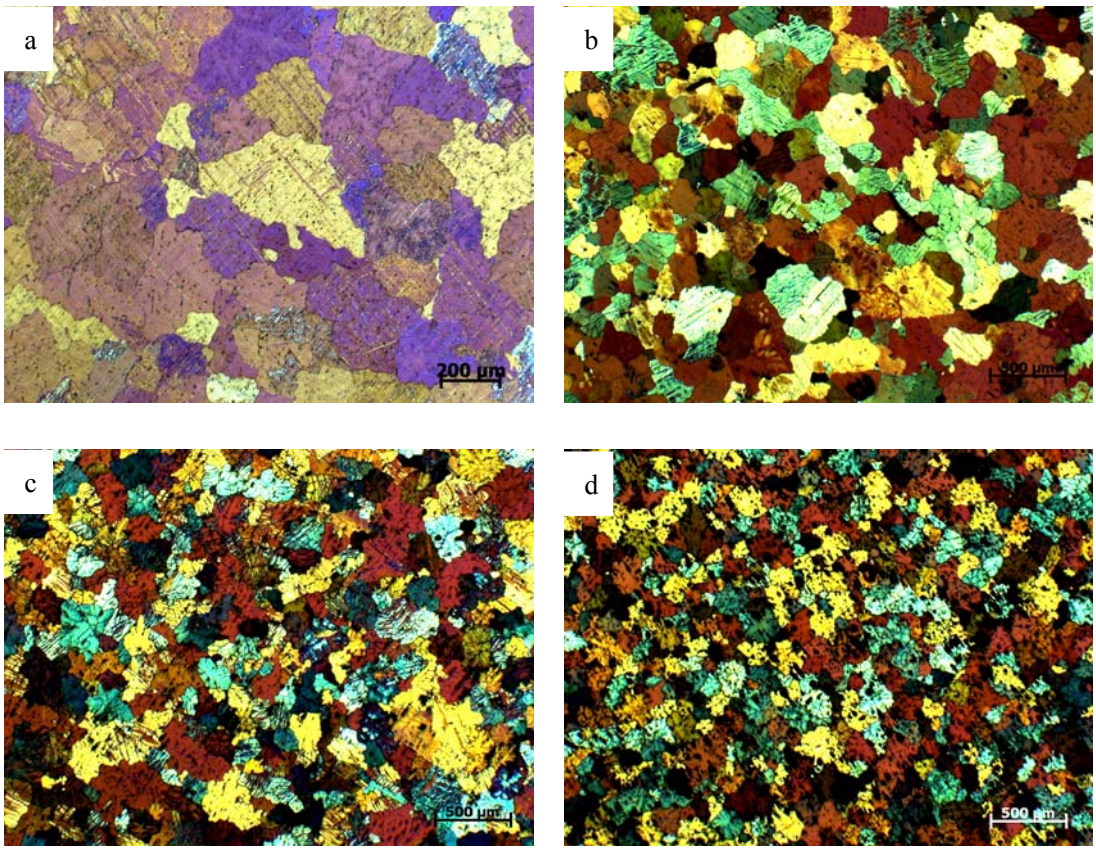

Fig. 4.18 Micrographs of etched samples of conventional cast sample for (a) Mg-1Ca; (b) Mg-1Zn-1Ca; (c) Mg-3Zn-1Ca; (d) Mg-5Zn-1Ca.

4.5.3 HPDC process

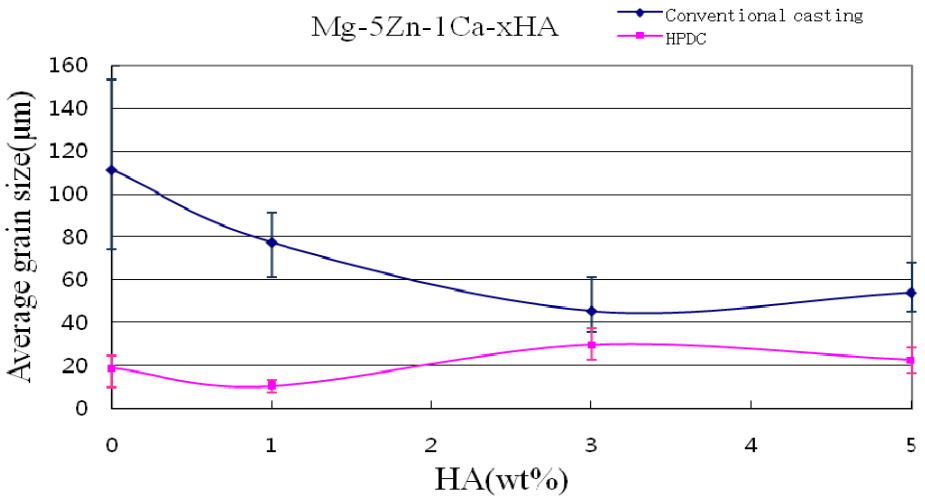

Fig. 4.19 Average grain sizes for Mg-5Zn-1Ca-xHA samples produced by conventional casting method and HPDC process (x=0, 1, 3, 5).

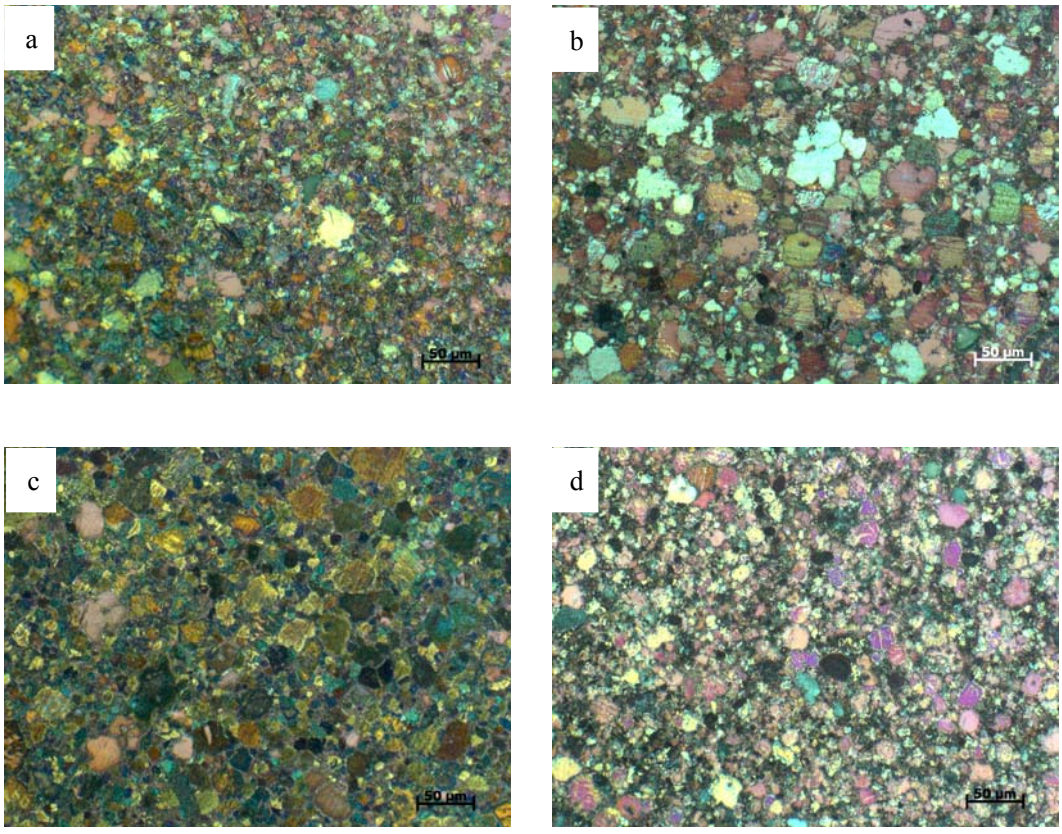

Fig. 4.20 Micrographs of etched samples of Mg-1Zn-1Ca-xHA alloy/composite sample produced by HPDC process for (a) x=0; (b) x=1; (c) x=3; (d) x=5.

As shown in Fig. 4.19, compared with grain sizes of conventional castings in steel cylindrical mould, HPDC process significantly reduces the grain size due to high cooling rate. Microstructures are presented in Fig. 4.20. However, the anticipated tendency that the gradual decrease with increasing the content of HA particles is not observed for HPDC samples. HPDC is expected to provide high cooling rates (10^3-10^4 ℃/s). During solidification under such high cooling rate, due to increased homogenous nucleation rate and limited time for grain growth, fine grain structure is obtained when without HA addition.

4.5.4 HA-addition

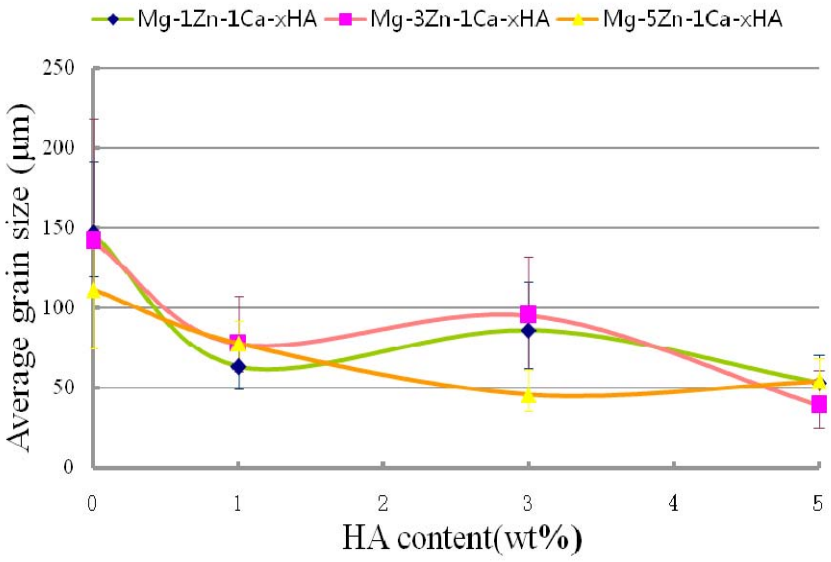

Fig. 4.21 Average grain sizes for conventional cast Mg-1Zn-1Ca-xHA, Mg-3Zn-1Ca-xHA and Mg-5Zn-1Ca-xHA samples for x = 0, 1, 3, 5.

As shown in Fig. 4.21, the grain sizes of the Mg-Zn-Ca alloys have been significantly reduced by the addition of 1 wt.% HA particles. The result firmly demonstrates that the presence of HA particles has a positive influence on the refinement of grain size. However, when the HA content is up to 3 wt.%, the grain sizes of Mg-1Zn-1Ca-3HA composite and Mg-3Zn-1Ca-3HA composite suddenly increases, which is completely opposite to expectation. Eventually, the alloy with 5 wt.% HA possessed similar grain

sizes, and the minimum grain size (~38.9 μm) is obtained from the Mg-3Zn-1Ca-5HA samples. The microstructures are shown in Fig. 4.22, 4.23 and 4.24.

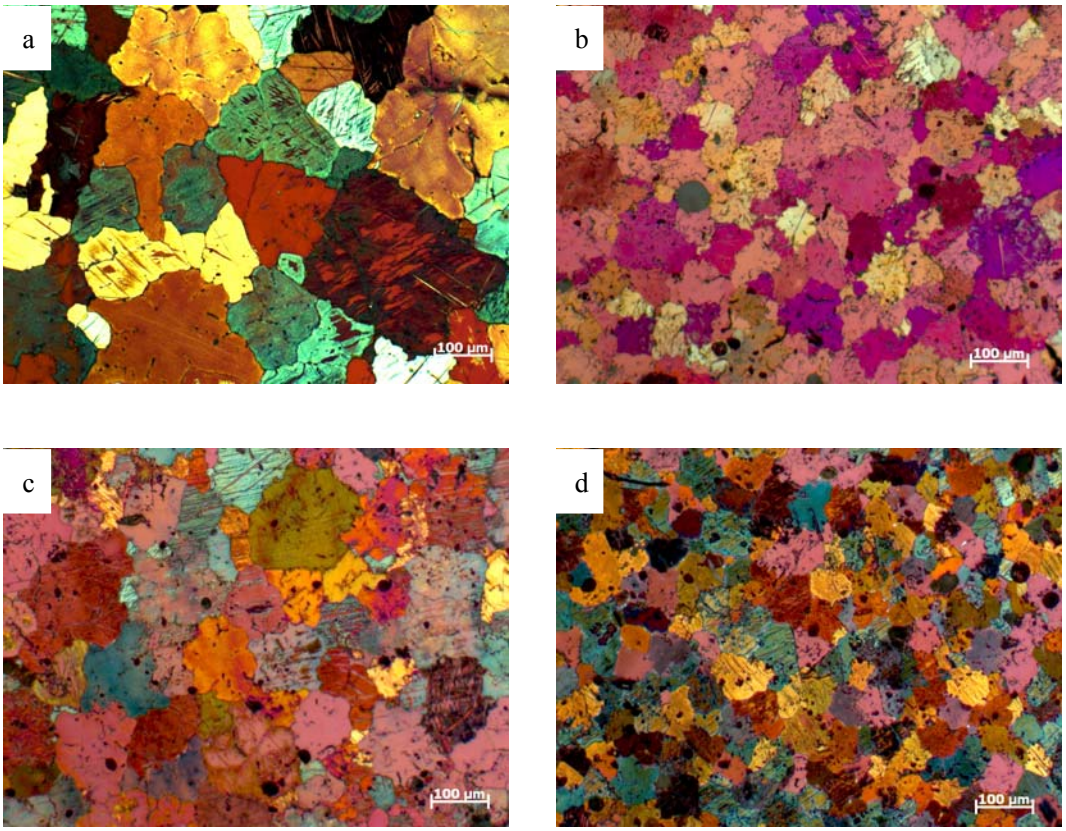

Fig. 4.22 Micrographs of etched samples of conventional cast samples for (a) Mg-1Zn-1Ca alloy; (b) Mg-1Zn-1Ca-1HA composite; (c) Mg-1Zn-1Ca-3HA composite; (d) Mg-1Zn-1Ca-5HA composite.

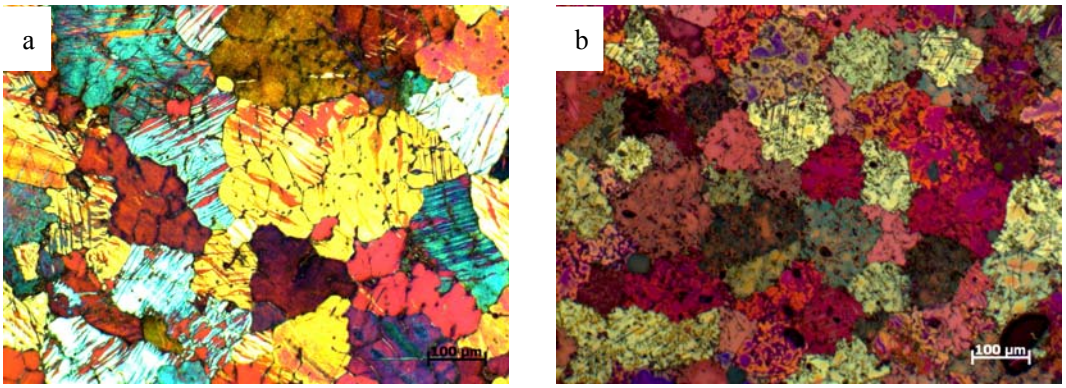

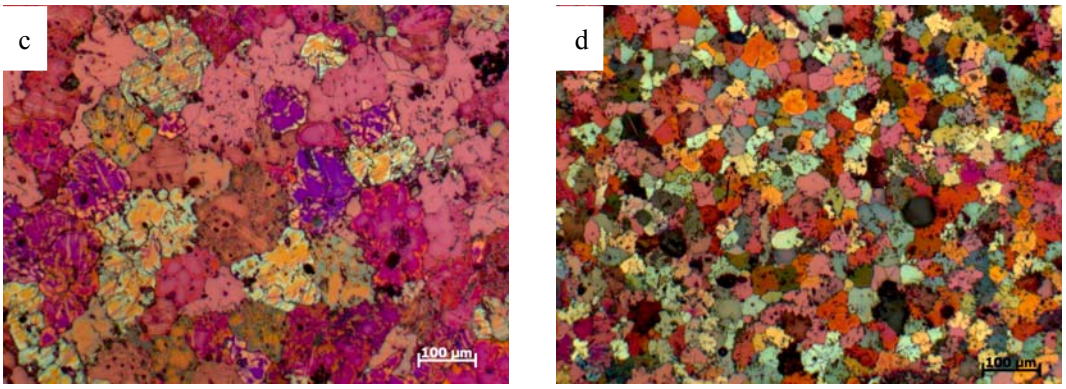

Fig. 4.23 Micrographs of etched samples of conventional cast samples for (a) Mg-3Zn-1Ca alloy; (b) Mg-3Zn-1Ca-1HA composite; (c) Mg-3Zn-1Ca-3HA composite; (d) Mg-3Zn-1Ca-5HA composite.

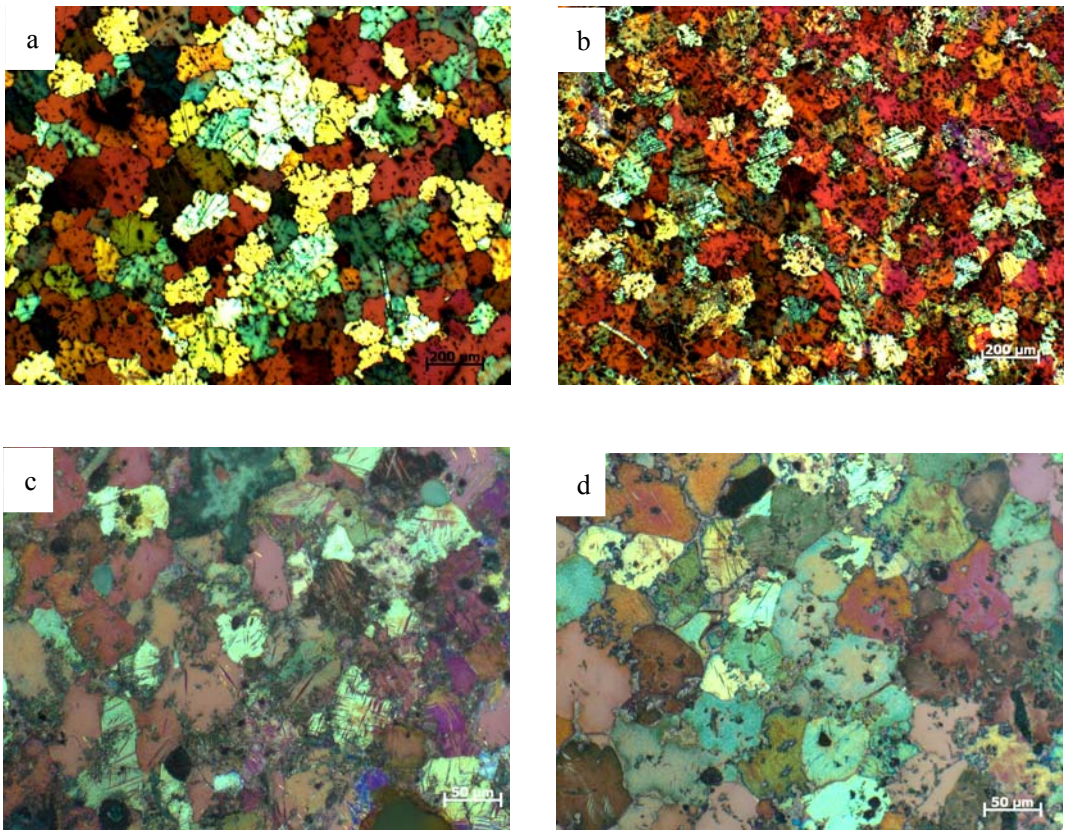

Fig. 4.24 Micrographs of etched samples of conventional cast samples for (a) Mg-3Zn-1Ca alloy; (b) Mg-3Zn-1Ca-1HA composite; (c) Mg-3Zn-1Ca-3HA composite; (d) Mg-3Zn-1Ca-5HA composite.

Referring to the classical theory of heterogeneous nucleation, we can explain the reason for the refinement of grain size by the addition of HA powder. The nucleation embryo could not successfully transform into nuclei unless it overcomes the

activation energy barrier. After adding HA particles, they could reduce the solid/liquid interfacial energy and the embryo turns into the shape of a spherical cap with a 'wetting' angle θ. Therefore, for a given volume of solid, the energy barrier to nucleation is decreased and thereby nuclei can be formed at higher undercooling. In other words, heterogeneous nuclei can form at higher temperature than homogeneous nuclei.

Based on the lattice structures presented in Fig. 4.25, it is noted that lattice parameter *a* of HA is three times as that of pure Mg, which means that there can be a good lattice match between HA and Mg. As a result, there could be a good wetting between HA and Mg. Turnbull [Turnbull, 1953] has defined the potency P of a nucleant, which is related to the contact angle θ between the spherical cap and substrate as $P \propto 1/\theta$. Hence, it is absolutely possible that the addition of HA particles can enhance the heterogeneous nucleation process.

According to the above analysis, we could anticipate that the effect of grain size refinement should be more prominent by increasing the amount of HA particles up to 5%. However, as shown in Fig. 4.21, the increased grain size for Mg-1Zn-1Ca-3HA composite and Mg-3Zn-1Ca-3HA composites when compared to low concentration of

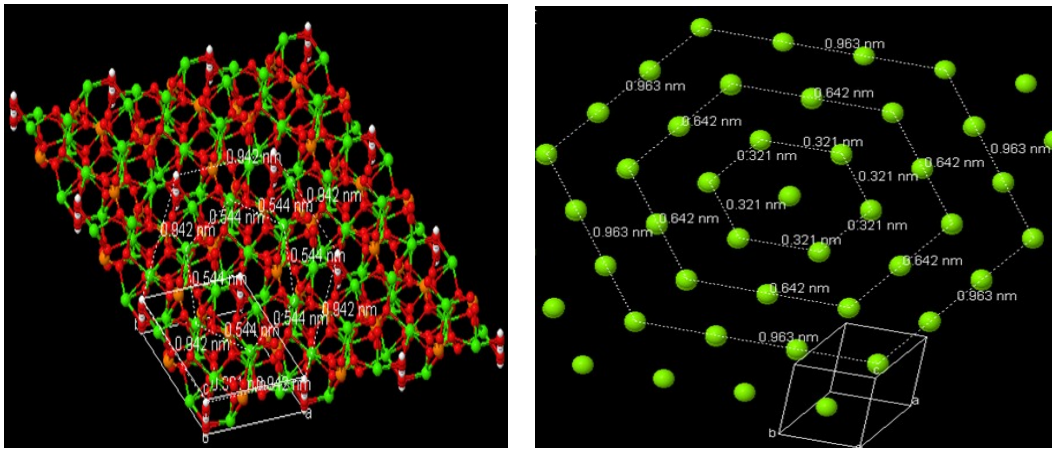

Fig. 4.25 Lattice structures of (a) hydroxyapatite and (b) pure magnesium.

(Their parameters are 9.4 Å and 3.2088 Å, respectively.)

HA addition may be associated with relative inhomogeneous distribution of HA

caused by severe agglomeration and prevented acceleration of heterogeneous nucleation process.

To eliminate the impact of different cooling rate on the grain size and also to simulate cooling rate achieved in industrial practice, the casting is conducted using test procedure-1 (TP1), which is expected to provide cooling rate of 3.5 K/s. The grain sizes of TP1 samples are significantly decreased in comparison with those of conventional samples due to the higher cooling rate (3.5 K/s) as shown in Fig. 4.26. Representative micrographs of etched surfaces are shown in Fig. 4.27. We also could effortlessly make similar conclusion through visible comparison between the alloy and the corresponding composite. The result further confirms that HA particles refine grain size for Mg alloys and is simply due to heterogeneous nucleation process facilitated by HA particles, rather than variation in cooling rate.

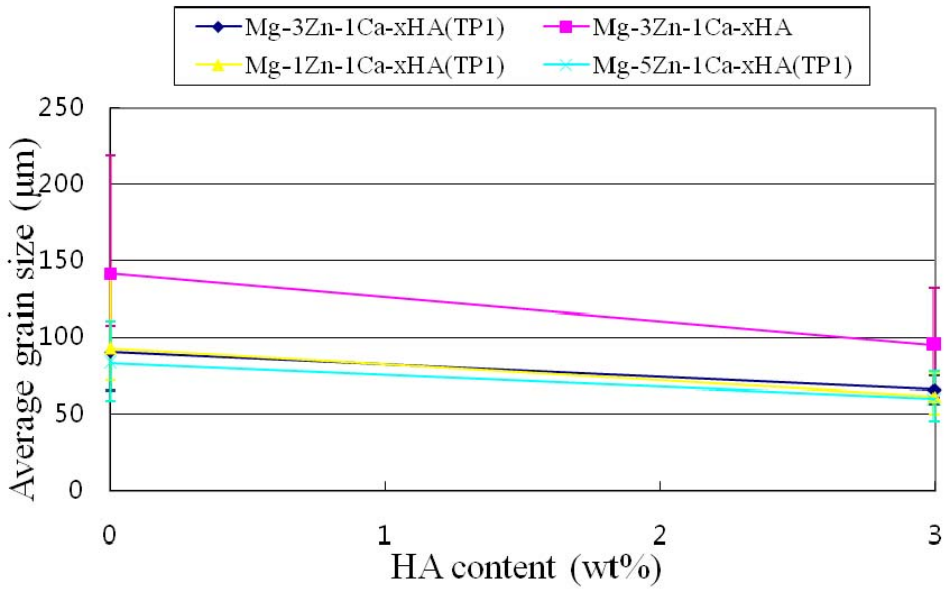

Fig. 4.26 Average grain sizes for conventional cast Mg-3Zn-1Ca-xHA samples, TP1 cast Mg-1Zn-1Ca-xHA, Mg-3Zn-1Ca-xHA and Mg-5Zn-1Ca-xHA (TP1) samples (x = 0,3). The pouring temperature in TP1 mould was 660 ± 1 ℃.

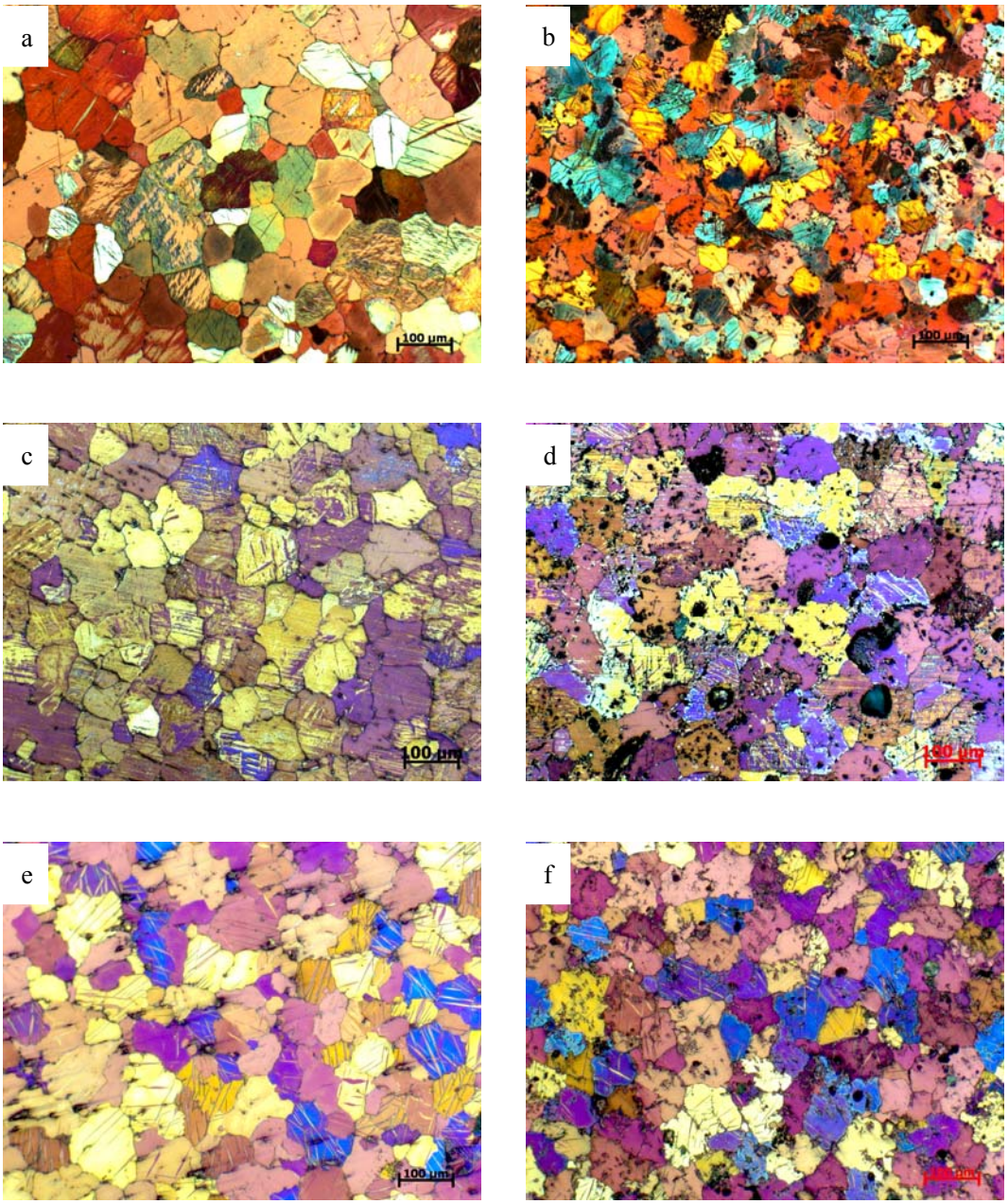

Fig. 4.27 Micrographs of etched samples of TP1 cast samples for (a) Mg-1Zn-1Ca alloy; (b) Mg-1Zn-1Ca-3HA composite; (c) Mg-3Zn-1Ca alloy; (d) Mg-3Zn-1Ca-3HA composite; (e) Mg-5Zn-1Ca alloy; (f) Mg-5Zn-1Ca-3HA composite. (Pouring temperature 660 ± 1 ℃.)

Generally speaking, it is very difficult to refine a commercial Al-containing magnesium alloy by chemical methods. The moderately efficient carbon-based refiner explored in the late 1930s is still employed for refining the grain size currently. Thus, the influence of HA particles on the commercial Mg alloys containing aluminium element is also investigated in this thesis.

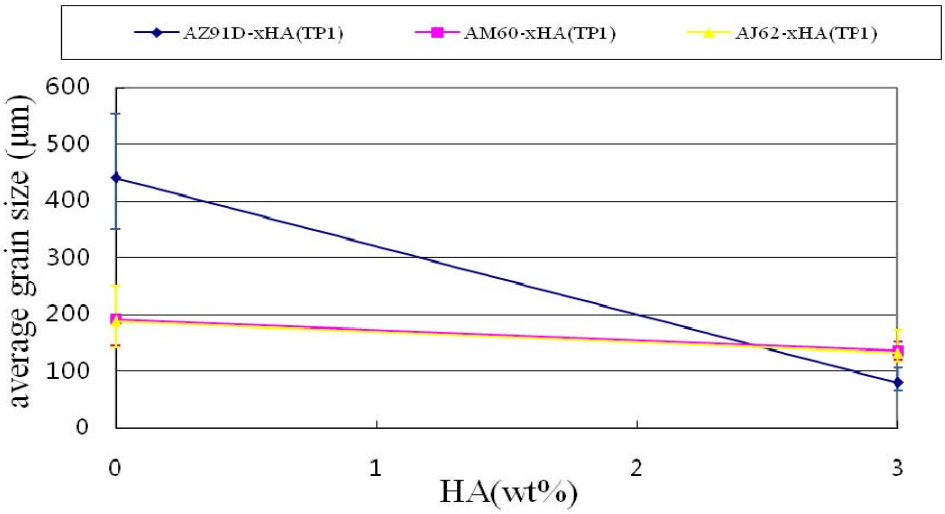

Fig. 4.28 Average grain size for AZ91D alloy, AZ91D-3HA composite, AM60 alloy, AM60-3HA composite, AJ62 alloy and AJ62-3HA composite. (TP1 660 ℃)

The average grain sizes for different samples are shown in Fig. 4.28, which indicate that HA particles possessed significant effect on the grain size refinement for AZ91D alloy. The grain size sharply decreased from 441.5 μm to 80.8 μm by the addition of 3 wt.% HA. However, the grain sizes for AM60 and AJ62 alloys just have slight improvement. The corresponding microstructures are revealed in Fig. 4.29. Based on this investigation, we suggest that the HA is a promising grain refiner for Al-containing magnesium alloys.

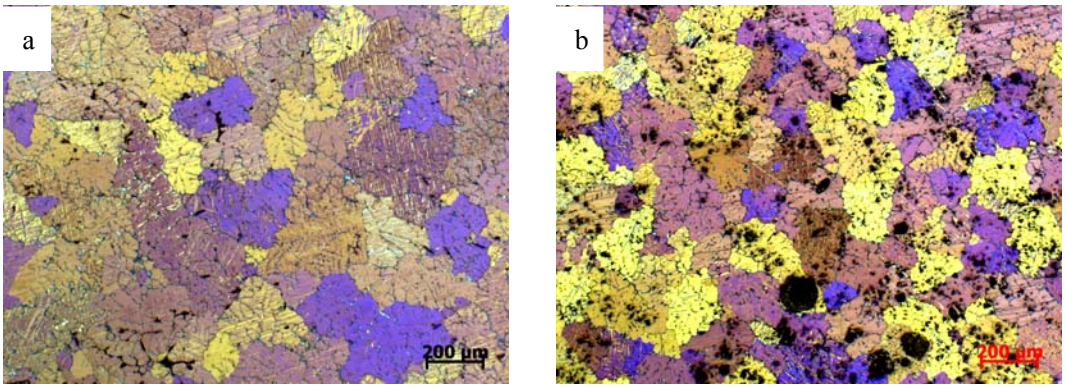

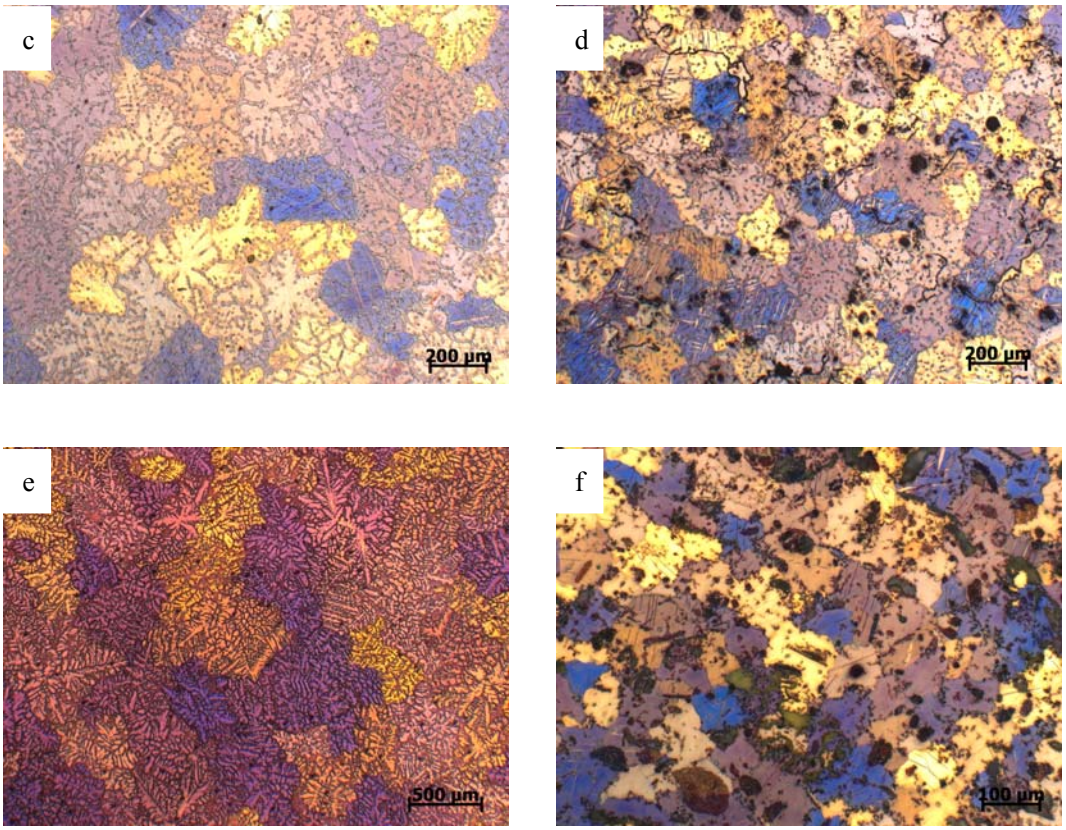

Fig. 4.29 Micrographs of etched samples: (a) AJ62 alloy; (b) AJ62-3HA composite; (c) AM60 alloy; (d) AM60-3HA; (e) AZ91D alloy; (f) AZ91D-3HA composite. (TP1 660 ℃)

On the basis of the remarkable reduction of the grain size by adding 3 wt.% HA to AZ91D, it is worth investigating the influence of various low concentration of HA content on the grain size. Excessive amount of reinforcement particles in the microstructure can reduce the elongation. Therefore, AZ91D-0.1HA, AZ91D-0.2HA, AZ91D-0.5HA and AZ91D-1HA composites have been processed and their grain size measured. The average grain size versus HA content for AZ91D is shown in Fig. 4.30.

It is exciting to note that the grain size of AZ91D alloy sharply decreased from 441.5 μm to 176.9 μm by adding just 0.1 wt.% HA, and then gradually reduce with increasing fraction of HA. The corresponding microstructures are shown in Fig. 4.31. Therefore, it can be concluded that a small quantity of HA particles can strongly influence on the refinement of grain size of AZ91D. Considering that HA addition

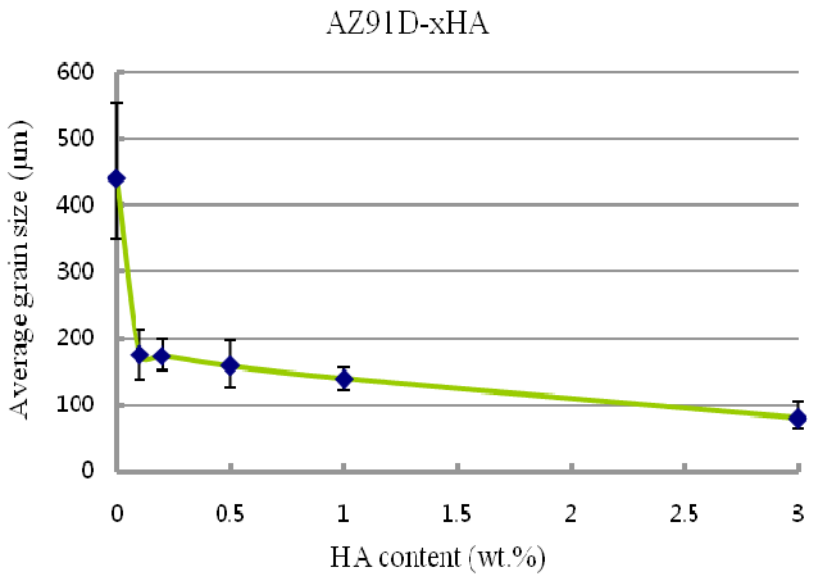

Fig. 4.30 Average grain sizes for AZ91D-xHA (x=0, 0.5, 1, 3) samples. (TP1 660 ℃)

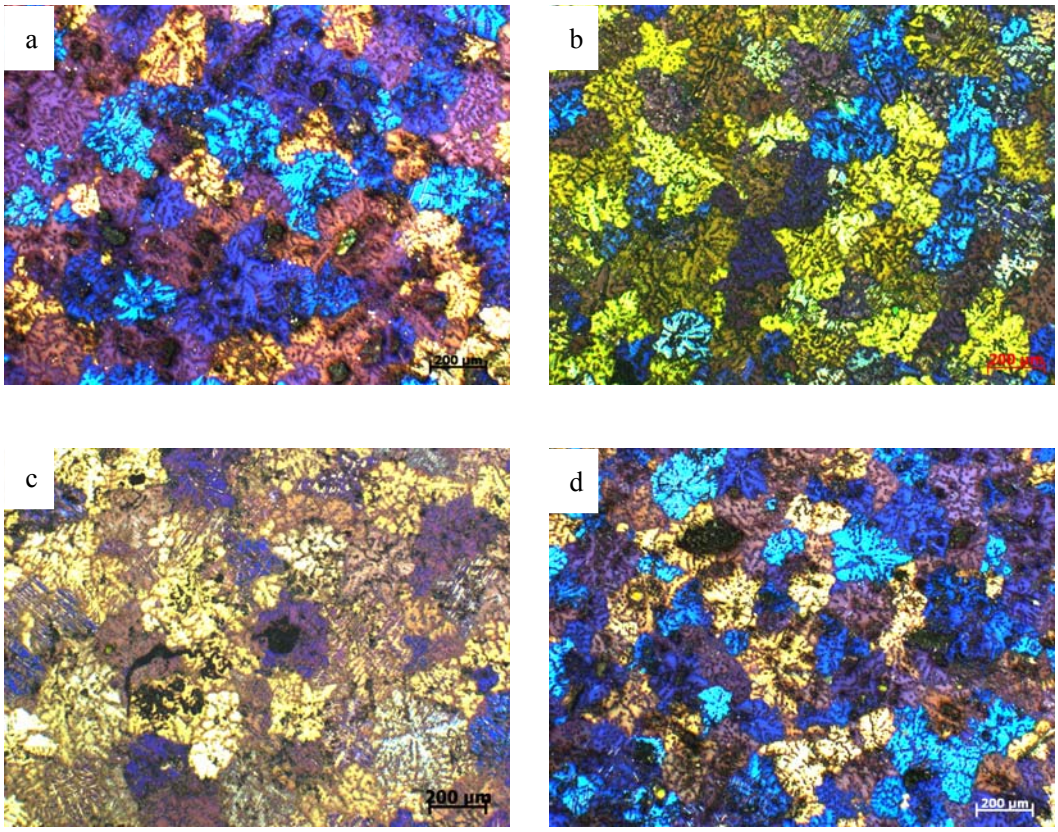

Fig. 31 Micrographs of etched samples of AZ91D-xHA composite for (a) x=0.1; (b) x=0.2; (c) x=0.5; (d) x=1. (TP1 660 ℃)

does not deteriorate mechanical properties (see Fig. 4.10), eventually, it may be

possible to put HA into industrial application as a promising effective refiner for commercial Al-containing magnesium alloys.

4.5.5 Effect of mixing process on the AZ91D grain size

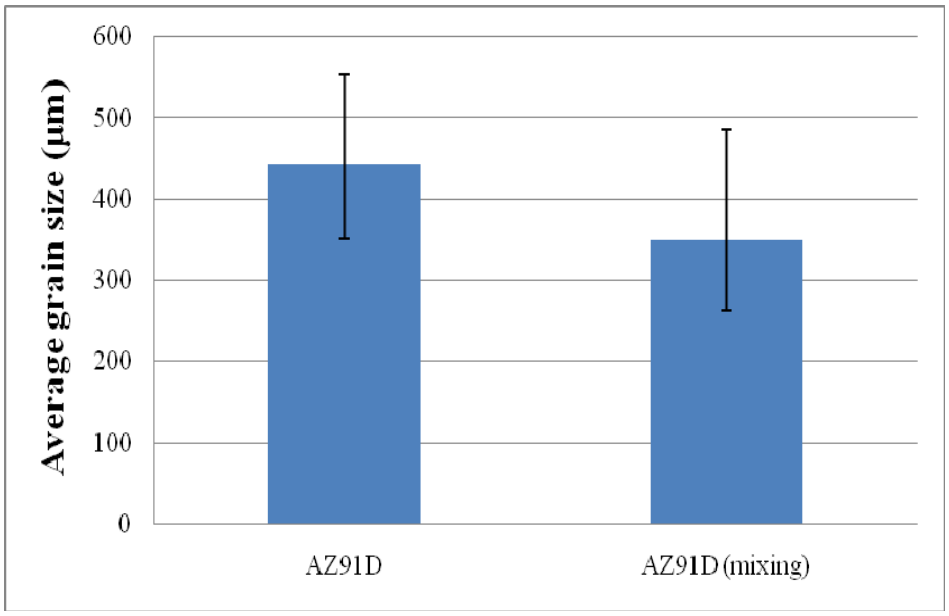

Fig. 4.32 Average grain sizes for AZ91D and AZ91D (mixing) samples (TP1 660 ℃).

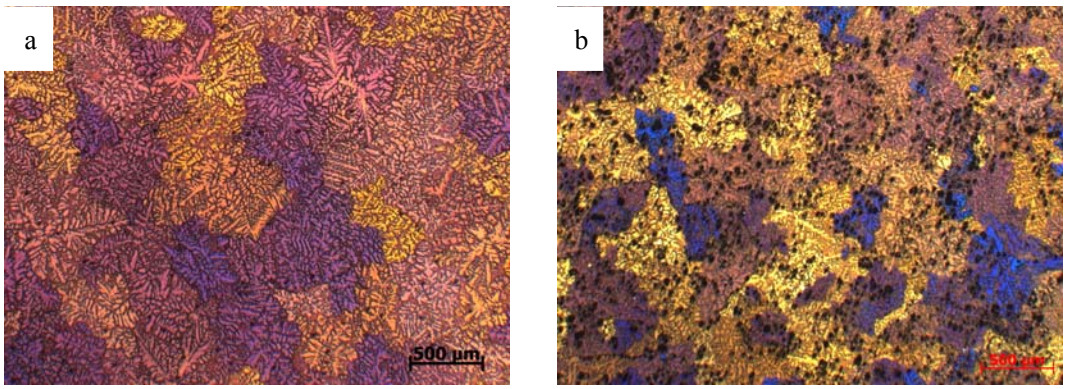

Fig. 4.33 Micrographs of etched samples of (a) AZ91D alloy and (b) mixing-AZ91D alloy (TP1 660 ℃).

In order to investigate the effect of mixing on the grain size of AZ91D alloy, liquid metal was stirred with impeller and cast into TP1 mould. Results shown in Fig. 4.32 and 4.33 confirm that mixing procedure is also effective on the grain size of AZ91D. The reason may be explained that the inevitable existence of Mg oxides or

intermetallics tend to be dispersed homogeneously due to mixing, which could accelerate the heterogeneous nucleation as an effective nucleant sites [Fan et al., 2009]. Although stirring liquid metal at high speed with impeller resulted in reduction of grain size, the addition of HA to liquid metal dramatically decreases the grain size.

4.5.6 Cooling curve measurements

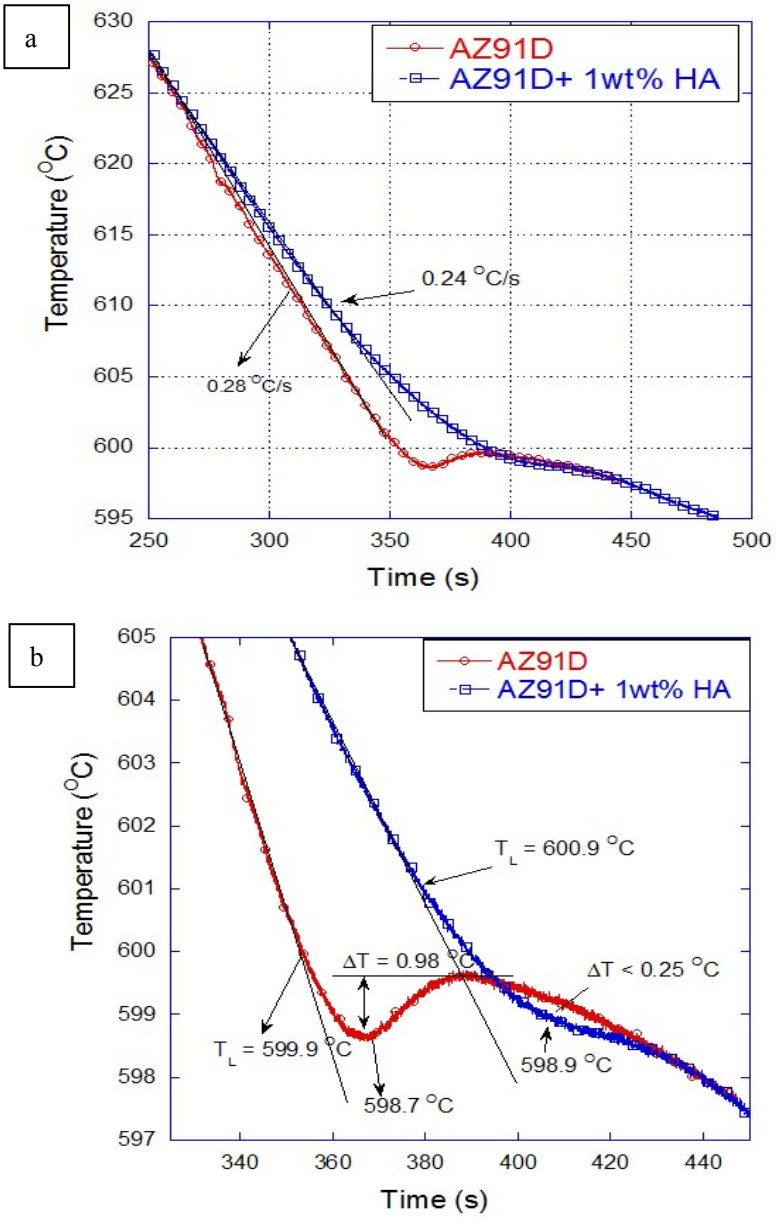

Fig. 4.34 Cooling curves for AZ91D and AZ91D-1HA.

To understand the effect of HA particles on grain size refinement for AZ91D, we

have measured cooling curves for AZ91D and AZ91D added with 1 wt.% HA. It needs to be mentioned that insulation material is wrapped around the steel crucible to prevent the temperature of melt decreasing too rapidly during solidification process. The measured cooling curves are presented in Fig. 4.34. Based on Fig. 34 a, it is noted that the cooling rate of AZ91D is approximately 0.28 ℃/s, which is quite similar to that of AZ91D-1HA (0.24 ℃/s). Measured data close to the liquidus line is shown in Fig. 34(b). The undercooling for AZ91D is measured to be 0.98 ^{O}C, whereas the addition of 1 wt.% HA particles dramatically decreased the undercooling ($\Delta T <$ 0.25 ℃). The observed results clearly demonstrate that the existence of HA inclusions in the Mg-liquid metal can enhance heterogeneous nucleation process and as a result reduces the grain size of castings, which is consistent with the measured grain size in this study.

Chapter 5
Conclusion

The main purpose of the work performed in this thesis is to design magnesium-based alloys and metal matrix composite materials as potential bio-medical materials. On the basis of bio-degradable and bio-compatible nature, Mg is chosen as a matrix and Hydroxyapatite as a reinforcement phase. The Mg alloys are fabricated by commercial pure magnesium ingot, pure zinc and pure calcium granules according to different weight proportion. The following is the summary of extensive research work on Mg-Zn-Ca/HA alloys and composites.

- *Extensive literature survey* conducted in this thesis suggests that Zn and Ca are bio-compatible alloying metals in Mg alloys which not only improves mechanical properties, but also improves corrosion properties. In this study we have manufactured various Mg-Zn-Ca alloys and found out that the fraction of intermetallic particles gradually increased with increasing the content of zinc element. Presence of $Ca_2Mg_6Zn_3$ intermetallic phase is confirmed with X-ray diffraction study.
- When Hydroxyapatite (HA) powder added into the liquid metal, after solidification, HA particles are observed to agglomerate in composites due to inadequate mixing efficiency of conventional impeller, and the degree of agglomeration became higher with increasing the percentage of the reinforcements. Although a little progress could be achieved by HPDC process in comparison with conventional casting method, the relatively large cluster of reinforcements still exist in the microstructure. However, due to high intensive shear and turbulent force generated by MCAST process, the dispersion of HA particles and second phase significantly improved.
- Tensile tests indicate that yield strength and ultimate tensile strength increased with increasing the fraction of Zn in Mg-Zn-Ca alloys. These properties are

further improved by the HA addition when processed with HPDC process. However, since microstructural defects such as porosity, as a result poor die filling due to viscous nature of slurry, resulted in inconsistent elongation.

- Vickers micro-hardness is also increased with increasing the content of zinc. HA particle addition also increased the average hardness of Mg-Zn-Ca/Ha composites in comparison with alloys. The improving tendency of micro-hardness by increasing the HA reinforcement concentration is clearly observed. However, it is noted that local micro-hardness varied significantly due to inhomogeneous distribution of HA particles.
- Zn addition could refine the grain size of the alloys, which is in agreement with the well established concept of grain restriction due to ejected Zn solute by the Mg grain growth front. Similarly, Ca is also observed to refine grain size significantly. Fine grain structures are expected to contribute for improved corrosion resistance.
- Grain size refinement is remarkable when HA is added to the Mg-Zn-Ca alloy. Grain size is also decreased for commercial Al-contained Magnesium alloys such as AZ91D, AJ62 and AM60 with the addition of HA. It is absolutely worth mentioning that grain size of commercial AZ91D alloys which is normally quite difficult to be refined by the chemical method, was significantly reduced from 441.5 μm to 176.9 μm by the addition of a little quantity of 0.1 wt.% HA. The results strongly suggest that HA as effective nucleant sites accelerated the process of heterogeneous nucleation and is confirmed by the reduced undercooling for HA added AZ91D alloy. Therefore, we believe that hydroxyapatite (HA) as a promising efficient refiner and should be paid more attention for structural applications and medical applications of Mg/HA composites.

Chapter 6
Future work

Metallurgical aspect of Mg/HA aspects: The research performed in this work has confirmed that Mg-Zn-Ca/Ha MMCs produced by HPDC process can be potential materials for bio-medical application, since their mechanical properties including, modulus, tensile strength and Vickers hardness values are quite close to that of natural bone. Nevertheless, the elongation of all the samples is definitely unfavourable due to structural defects and big agglomerates of HA particles existed in microstructure by insufficient mixing. However, depending on the observed effect of improved homogeneous distribution of HA particles with intensive shearing, we anticipate that the mechanical properties of these samples produced by intensive shearing combined with HPDC can be obviously improved, especially for elongation. In addition, based on observation of grain refinement with HA addition for Al-containing commercial magnesium alloys, implementation MCAST and MC-HPDC process should be carried out in future. The corresponding composite samples are expected to exhibit finer microstructure and improved mechanical properties.

6.2 Biomedical properties of Mg/HA: As bio-degradable medical materials, the assessments of bio-corrosion resistance and bio-compatibility in physiological condition are absolutely necessary for these novel designed Mg-Zn-Ca/HA alloys and composites. Due to the absence of bio-related facilities at BCAST, these measurements will be conducted in TJUT, China. The electrochemical method and immersion tests will be employed to test the corrosion resistance of samples in SBF (simulated body solution). In order to evaluate the effect of metal ions released by corrosion on cell viability, the measurements of cytotoxicity should be performed according to ISO 10993-5: 1999.

References

[Agarwal et al., 1995], R. Agarwal, J.J. Lee et al., Calorimetric Measurements and Thermodynamic Optimization of the Ca-Mg System, Z. Metallkd, 86 (1995) 103.

[Aljarrah and Medraj, 2008], M. Aljarrah, M. Medraj, Thermodynamic modeling of the Mg–Ca, Mg–Sr, Ca–Sr and Mg–Ca–Sr systems using the modified quasichemical model, CALPHAD 2008;32(2):240–51.

[Aluminium Association, 1987], Aluminium Association, (1987): Standard Test Procedure for Aluminium Alloy Grain Refiners: TP-1, (The Aluminium Association, Washington DC).

[Ambat et al., 2000], R. Ambat, N.N. Aung, W. Zhou, Evaluation of microstructural effects on corrosion behaviour of AZ91D magnesium alloy, Corros. Sci. 42 (2000) 1433–1455.

[Ansara et al., 1998], I. Ansara, A.T. Dinsdale, M.H. Rand (Eds.), COST 507: Thermochemical Database for Light Metal Alloys, vol. 2, European Commission, 1998.

[Avedesian and Baker, 1999], M.M. Avedesian, H. Baker, 'Magnesium and Magnesium Alloys', ASM International, Materials Parks, OH, USA, 1990, pp. 10.

[Bamberger et al., 2006], M. Bamberger, G. Levi et al., Precipitation hardening in Mg-Ca-Zn alloys, Metallurgical and materials transaction A, volume 37A, Feb 2006-481.

[Boanini and Bigi, 2006], E. Boanini, A. Bigi, Biomimetic synthesis of carbonated hydroxyapatite thin films, Thin Solid Films, (2006) 497, 53-57.

[Bobby, 2010], M. Bobby Kannan, Influence of microstructure on the in-vitro degradation behaviour of magnesium alloys, Materials Letters, 64 (2010) 739–742.

[Boehlert and Knittel, 2006], C.J. Boehlert and K. Knittel, The microstructure, tensile properties, and creep behaviour of Mg–Zn alloys containing 0–4.4 wt.% Zn, Mater Sci Eng A 417 (2006), pp. 315–331.

[Caceres et al., 2005], Caceres C, Poole W, Bowles A, Davidson C. ection thickness, macrohardness and yield strength in hp dc magnesium alloy AZ91. Mater Sci Eng A 2005; 402:269–77.

[Cao et al., 2004], P. Cao, M. Qian et al., Effect of iron on grain refinement of high-purity Mg–Al alloys, Scripta Mater., 2004, vol. 51, pp. 125-29.

[Cao et al., 2007], P. Cao, M. Qian and D.H. StJohn, Mechanism for grain refinement of magnesium alloys by superheating, Scripta Materialia 56 (2007) 633–636.

[Chino et al., 2002], Y. Chino, M. Kobata, H. Iwasaki and M. Mabuchi, Tensile Properties from Room Temperature to 673 K of Mg-0.9mass%Ca Alloy Containing Lamella Mg_2Ca, Mater. Trans., 43 (2002) 2643–2646.

[Chiu et al., 2007], K.Y. Chiu, M.H. Wong, F.T. Cheng, H.C. Man, Characterization

and corrosion studies of fluoride conversion coating on degradable Mg implants, Surf Coat Tech 2007;202:590–8.

[Clark, 1961], J.B. Clark, JCPDS Card 12-266, 1961.

[Clyne, 2000], T.W. Clyne, Comprehensive composite materials, Oxford: Pergamon; 2000.

[Cui et al., 2008], F. Cui, J. Yang, Y. Jiao, Q. Yin, Y. Zhang, I.S. Lee, Calcium phosphate coating on magnesium alloy for modification of degradation behaviour, Fron Mater Sci China 2008; 2(2):143–8.

[Derynck and Zhang, 1996], R. Derynck, Y. Zhang, Intracellular signalling: the mad way to do it, Curr Biol. 1996; 6(10):1226–9.

[Dumelie et al., 2008], N. Dumelie, H. Benhayoune et al., In vitro precipitation of electrodeposited calcium-deficient hydroxyapatite coatings on Ti6Al4 V substrate [J], Mater. Charact. 59 (2008) 129–133.

[Emley, 1966], E.F. Emley, Principles of magnesium Technology, Pergamon Press, Oxford, 1966, pp.56-208.

[Fan et al., 2004], Y. Fan, G. Wu, H. Gao, C. Zhai, Current state and development of research on the corrosion of magnesium alloys [J], Foundry Technology 2004, 25(12): 941-942. (in Chinese)

[Fan et al., 2009], Z. Fan, Y. Wang et al., Enhanced heterogeneous nucleation in AZ91D alloy by intensive melt shearing, Acta Materialia 57 (2009) 4891–4901.

[Fan, 2002], Z. Fan, Twin-screw rheoforming technologies for Semisolid Metal processing Magnesium alloys, Proc. 7th Inter. Conf. Semisolid Metal Processing, Tsukuba, Japan, 24-28 Sept. 2002, eds, Y. Tsutsui, M. Kiuchi and K. Ichikawa, pp. 671-676.

[Farbenindustrie, 1942], I.G. Farbenindustrie: Belgian Patent 444,757, 1942.

[Frosch and Stürme, 2006], K.H. Frosch, K.M. Stürmer, Metallic biomaterials in skeletal repair, Eur J Trauma 2006;32:149–59.

[Fulmer et al., 2002], M.T. Fulmer, I.C. Ison et al., Measurements of the solubilities and dissolution rates of several hydroxyapatites, Biomaterials 2002; 23:751–5.

[Gu et al., 2009], X. Gu, Y. Zheng, Y. Cheng, S. Zhong, T. Xi, In vitro corrosion and biocompatibility of binary magnesium alloys, Biomaterials 2009; 30:484–98.

[Hari Babu et al., 2008], N. Hari Babu, S. Tzamtzis, N. Barekar, J. B. Patel and Z. Fan, Fabrication of Metal Matrix Composites under Intensive Shearing, Solid State Phenomena Vols. 141-143 (2008) pp 373-378.

[Harvey et al., 1999], E.J. Harvey, J.D. Bobyn, M. Tanzer, G.J. Stackpool, J.J. Krygier, S.A. Hacking, Effect of flexibility of the femoral stem on bone-remodeling and fixation of the stem in a canine total hip arthroplasty model without cement, J Bone Joint Surg Am A 1999;81(1):93–107.

[Hassel et al., 2006], T. Hassel, F. Bach et al., Magnesium technology in the grobal age, in: 45th Annual Conference of Metallurgists of CIM, Montreal, Quebec, Canada, 2006, pp. 359–370.

[He et al., 2010], W. He, E. Zhang, K. Yang, Effect of Y on the bio-corrosion behaviour of extruded Mg–Zn–Mn alloy in Hank's solution, Materials Science and Engineering C 30 (2010) 167–174.

[Helm et al., 1997], G.A. Helm, J.M. Sheehan, J.P. Sheehan et al., Utilization of type I collagen gel, demineralized bone matrix, and bone morphogenetic protein-2 to enhance autologous bone lumbar spinal fusion, J Neurosurg 1997;86(1):93–100.

[Heublein et al., 2003], B. Heublein et al., Biocorrosion of magnesium alloys: A new principle in cardiovascular implant technology? Heart 89, 651-656 (2003).

[Hodgskinson, et al., 1989], R. Hodgskinson, J.D. Currey, G.P. Evans, Hardness, an indicator of the mechanical competence of cancellous bone, J Orthop Res 1989;7:754–8.

[Hort et al., 2009], N. Hort, Y. Huang, D. Fechner et al., Magnesium alloys as implant materials – Principles of property design for Mg–RE alloys, Acta Biomater 6 (2010) 1714–1725.

[Hu et al., 2010], J. Hu, C. Wang, W.C. Ren, S. Zhang, F. Liu, Microstructure evolution and corrosion mechanism of dicalcium phosphate dihydrate coating on magnesium alloy in simulated body fluid, Materials Chemistry and Physics 119 (2010) 294–298.

[Ilich and Kerstetter, 2000], J.Z. Ilich, J.E. Kerstetter, Nutrition in bone health revisited: a story beyond calcium, J Am Coll Nutr 2000; 19:715-37.

[Janning et al., 2010], C. Janning et al., Magnesium hydroxide temporarily enhancing osteoblast activity and decreasing the osteoclast number in peri-implant bone remodeling, Acta Biomater 6 (2010) 1861–1868.

[Jardim et al., 2002], P.M. Jardim, G. Solorzano, J.B.V. Sande, Precipitate crystal structure determination in melt spun Mg–1.5wt%Ca–6wt%Zn alloy, Microscopy and Microanalysis 2002; 8:487–96.

[Jete and Foote, 1935], E.R. Jete and F. Foote, Precision determination of lattice constants, J. Chem. Phys., Vol 3, 1935, p 605-616.

[Ji et al., 2001], S. Ji, Z. Fan, M.J. Bevis, Semi-solid processing of engineering alloys by a twin-screw rheomoulding process, Materials Science and Engineering A299 (2001) 210–217.

[Kannan and Raman, 2008], M.B. Kannan, R.K.S. Raman, In vitro degradation and mechanical integrity of calcium-containing magnesium alloys in modified-simulated body fluid, Biomaterials 2008; 29(15):2306–14.

[Katayanagi et al., 1990], K. Katayanagi, M. Miyagawa et al., Three-dimensional structure of ribonuclease H from E, coli. Nature 1990; 347(6290):306–9.

[Kuo and Yen, 2002], M.C. Kuo, S.K. Yen, The process of electrochemical deposited hydroxyapatite coatings on biomedical titanium at room temperature, Mater. Sci. Eng. C 20 (2002) 153–160.

[Kuwahara et al., 2001], H. Kuwahara, Y. Al-Abdullat et al., Precipitation of magnesium apatite on pure magnesium surface during immersing in Hank's solution, Mater Trans 2001; 42(7):1317–21.

[Lamolle et al., 2009], S.F. Lamolle, M. Monjo, M. Rubert, H.J. Haugen et al., The effect of hydrofluoric acid treatment of titanium surface on nanostructural and chemical changes and the growth of MC3T3–E1 cells, Biomaterials 2009; 30:736–42.

[Larionova et al., 2001], T.V. Larionova, W.W. Park, B.S. You, A ternary phase observed in rapidly solidified Mg-Ca-Zn alloys, Scr. Mater. 45 (2001) 7–12.

[Li et al., 2006], G. Li, G. Wu, Y. Fab, W. Ding, Effect of the main alloying elements on microstructure and corrosion resistance of magnesium alloys [J], Foundry Technology, 2006, 27(1): 81-82. (in Chinese)

[Li et al., 2008], Z. Li, X. Gu, S. Lou, Y. Zheng, The development of binary Mg–Ca alloys for use as biodegradable materials within bone, Biomaterials 2008; 29:1329–44.

[Lim and Gupta, 2001], S.C.V. Lim, M. Gupta, Enhancing the microstructural and mechanical response of a Mg/SiC formulation by the method of reducing extrusion temperature, MRS Bull 2001; 36:2627–36.

[Liu et al., 2007], C. Liu, Y. Xin, G. Tang, P.K. Chu, Influence of heat treatment on degradation behaviour of bio-degradable die-cast AZ63 magnesium alloy in simulated body fluid, Mater Sci Eng A – Struct 2007; 456(1–2):350–7.

[Lothar, 2000], T. Lothar, Labor und diagnose, 5th ed. Frankfurt: TH-Books; 2000.

[Ma et al., 2001], P. Ma, X. You et al., Progess of research on bioabsorbable synthetic scaffold in bone tissue engineering, Chemistry 07 (2001) 407.

[Majumdar et al., 2008], J. Dutta Majumdar, U. Bhattacharyya, A. Biswas, I. Manna, Studies on thermal oxidation of Mg-alloy (AZ91) for improving corrosion and wear resistance, Surface & Coatings Technology 202 (2008) 3638–3642.

[Ng et al., 2010], W.F. Ng, K.Y. Chiu, F.T. Cheng, Effect of pH on the in vitro corrosion rate of magnesium degradable implant material, Materials Science and Engineering C 30 (2010) 898–903.

[Noda, 1989], M. Noda, In vivo stimulation of bone formation by transforming growth factorbeta, Endocrinology 1989; 124(6):2991–4.

[Okamoto, 1994], H. Okamoto, Comment on Mg–Zn (magnesium–zinc), J Phase Equilibria Diffus. 1994; 15(1):129-30.

[Paris, 1934], R. Paris, Ternary alloys. No.45. Publications Scientifiques et Techniques du minist'ere de L'Air, Ministe` re de L'Air; 1934. p. 1–86.

[Pereda et al., 2010], M.D. Pereda, C. Alonso, L. Burgos-Asperilla et al., Corrosion inhibition of powder metallurgy Mg by fluoride treatments, Acta Biomaterialia 6 (2010) 1772–1782.

[Pérez et al., 2007], P. Pérez, G. Garcés, P. Adeva, Influence of texture on the mechanical properties of commercially pure magnesium prepared by powder metallurgy, Mater Sci 2007; 42:3969–76.

[Porter and Easterling, 1992], D.A. Porter and K.E Easterling, 'Phase Transformation in Metals and Alloys', Best-set Typesetter Ltd., Hong kong, 1992,

pp. 186, 187, 192, 195, 196.

[Pourbaix, 1974], M. Pourbaix, Atlas of electrochemical equilibria in aqueous solutions. 2nd English ed. Houston: National Accociation of Corrosion Engineers, 1974.

[Puleo and Huh, 1995], D.A. Puleo, W.W. Huh. Acute toxicity of metal ions in cultures of osteogenic cells derived from bone marrow stromal cells, J Appl Biomater 1995; 6:109–16.

[Qian and Cao, 2005] M. Qian and P. Cao, Discussions on grain refinement of magnesium alloys bycarbon inoculation, Scripta Mater., 2005, vol. 52, pp. 415-419.

[Qian et al., 2004], M. Qian, D.H. StJohn, M.T. Frost, Heterogeneous nuclei size in magnesium–zirconium alloys, Scripta Materialia 50 (2004) 1115–1119.

[Ramirez et al., 2008], A. Ramirez, M. Qian, B. Davis, T. Wilks and D.H. StJohn, Potency of high-intensity ultrasonic treatment for grain refinement of magnesium alloys, Scripta Materialia 59 (2008) 19–22.

[Rettig and Virtanen, 2007], R. Rettig, S. Virtanen, Time-dependent electrochemical characterization of thecorrosion of a magnesium rare-earth alloy in simulated body fluids, Journal of Biomedical Materials Research Part A 85 (2007) 167.

[Roberts, 1960], C.S. Roberts , Magnesium and Its Alloys, John Wiley & Sons, 1960.

[Scharf et al., 2005], C. Scharf, A. Ditze, A. Shkurankov et al., Corrosion of AZ91 secondary magnesium alloy, Adv. Eng. Mater. 7 (2005) 1134–1142.

[Serre et al., 1998], C.M. Serre, M. Papillard, P. Chavassieux et al., Influence of magnesium substitution on a collageneapatite biomaterial on the production of a calcifying matrix by human osteoblasts, J Biomed Mater Res 1998; 42:626-33.

[Shaw, 2003], B.A. Shaw, Corrosion resistance of magnesium alloys. In: Stephen D, editor. ASM handbook volume 13a: corrosion: fundamentals, testing and protection. UK: ASM International; 2003.

[Shikinami and Okuno, 1999], Y. Shikinami, M. Okuno, Bioresorbable devices made of forged composites of hydroxyapatite (HA) particles and poly L-lactide (PLLA): Part I. Basic characteristics, Biomaterials 1999; 20(9):859–77.

[Song and Atrens, 2003], G. Song, A. Atrens, Understanding magnesium corrosion. A framework for improved alloy performance, Advanced Engineering Materials 5 (2003) 837.

[Song et al., 2008], Y.L. Song, Y.H. Liu, S.R. Yu, X.Y. Zhu, Q. Wang, Effect of cerium addition on microstructure and corrosion resistance of die cast AZ91 magnesium alloy, Appl. Surf. Sci. 254 (2008) 3014–3020.

[Stager and Drickamer, 1963], R.A. Stager and H.G. Drickamer, Effect of Pressure and Temperature on the Electrical Resistance of Eleven Rare-Earth Metals, Phys. Rev., Vol 131, 1963, p 2524-2527.

[Staiger et al., 2006], M.P. Staiger, A.M. Pietak et al, Magnesium and its alloys as orthopedic biomaterials: a review, Biomaterials 2006; 27:1728–34.

[Tamura et al., 2002], Y. Tamura, T. Haitani, E. Yano et al., Grain refinement of high-purity Mg-Al alloy ingots and influences of minor amounts of iron and manganese on cast grain size Mater, Mater. Trans. A, 2002, vol. 33A, pp. 2784-88.

[Turnbull, 1953], D. Turnbull, Theory of catalysis of nucleation by surface patches, Acta Metall. 1 (1953) 8–14.

[Tzamtzis et al., 2009], S. Tzamtzis, N.S. Barekar te al., Processing of advanced Al/SiC particulate metal matrix compositesunder intensive shearing – A novel Rheo-process, Composites: Part A 40 (2009) 144–151.

[Waksman et al., 2008], R. Waksman, R. Pakala et al., Short-Term Effects of Biocorrodible Iron Stents in Porcine Coronary Arteries, Journal of Interventional Cardiology 21 (2008) 15.

[Wang et al., 2008 a], H. Wang, Y. Estrin et al., Bio-corrosion of a magnesium alloy with different processing histories, Materials Letters 62 (2008) 2476–2479.

[Wang et al., 2008 b], Y. Wang et al., Corrosion process of pure magnesium in simulated body fluid, Mater Lett 2008; 62(14):2185–8.

[Wen et al., 2009], C. Wen, S. Guan et al., Characterization and degradation behaviour of AZ31 alloy surface modified by bone-like hydroxyapatite for implant applications, Applied Surface Science 255 (2009) 6433–6438.

[Witte et al., 2005], F. Witte, V. Kaese, et al., In vivo corrosion of four magnesium alloys and the associated bone response, Biomaterials 2005; 26:3557–63.

[Witte et al., 2006], F. Witte et al., In vitro and in vivo corrosion measurements of magnesium alloys, Biomaterials 2006; 27(7):1013–8. 347

[Witte et al., 2007], F. Witte, F. Feyerabend, P. Maier et al., Biodegradable magnesium-hydroxyapatite metal matrix composites, Biomaterials 2007; 28:2163–74.

[Witte et al., 2008], F. Witte, N. Hort, et al., Degradable biomaterials based on magnesium corrosion, Curr Opin Solid State Mat Sci 2008; 12(5–6):63–72.

[Witte et al., 2009], F. Witte, J. Fischer et al., In vivo corrosion and corrosion protection of magnesium alloy LAE442, Acta Biomater Acta Biomaterialia 6 (2010) 1792–1799.

[Xu et al., 2007], L. Xu, G. Yu te al., In vivo corrosion behaviour of Mg–Mn–Zn alloy for bone implant application, J Biomed Mater Res A 2007; 83:703–11.

[Xu et al., 2009], L. Xu, F. Pan, G. Yu, L. Yang, E. Zhang, K. Yang, In vitro and in vivo evaluation of the surface bioactivity of a calcium phosphate coated magnesium alloy, Biomaterials 30 (2009) 1512–1523.

[Yamamoto et al., 2008], A. Yamamoto, T. Terawaki, H. Tsubakino, Microstructures and corrosion properties on fluoride treated magnesium alloy, Mater Trans 2008; 49:1042–7.

[Yang et al., 2006], W. Yang, P. Zhang, J. Liu, Y. Xue, Effect of long-termintake of Y^{3+} in drinking water on gene expression in brains of rats, J Rare Earth 2006;

24(3):369–73.

[Yin et al., 2008], D. Yin, E. Zhang, S. Zeng, Effect of Zn on mechanical property and corrosion property of extruded Mg-Zn-Mn alloy, Trans. Nonferrous Met. Soc. China 18(2008) 763-768.

[Yuan et al., 2003], G. Yuan, M. Liu, W. Ding, Akihisa I. Microstructure and mechanical properties of Mg–Zn–Si based alloys, Mater Sci Eng A 2003; 357:314–20.

[Yun et al., 2009], Y. Yun, Z. Dong, D. Yang et al., Biodegradable Mg corrosion and osteoblast cell culture studies, Materials Science and Engineering C 29 (2009) 1814–1821.

[Zhang and Yang, 2008], E. Zhang, L. Yang. Microstructure, mechanical properties and bio-corrosion properties of Mg–Zn–Mn–Ca alloy for biomedical application, Materials Science and Engineering A 497 (2008) 111–118.

[Zhang et al., 2005], E. Zhang, L. Xu, K. Yang, Formation by ion plating of Ti-coating on pure Mg for biomedical applications, Scripta Mater 2005; 53(5):523–7.

[Zhang et al., 2008 a], E. Zhang, W. He, H. Du, K. Yang, Microstructure, mechanical properties and corrosion properties of Mg–Zn–Y alloys with low Zn content, Materials Science and Engineering A 488 (2008) 102–111.

[Zhang et al., 2008 b], E. Zhang, D. Yin, L. Xu, L. Yang, K. Yang, Microstructure, mechanical and corrosion properties and biocompatibility of Mg–Zn–Mn alloys for biomedical application, Mater Sci Eng C. 29 (2009) 987–993.

[Zhang et al., 2009 a], E. Zhang, L. Yang, J. Xu, H. Chen, Microstructure, mechanical properties and bio-corrosion properties of Mg–Si(–Ca, Zn) alloy for biomedical application, Acta Biomater 6 (2010) 1756–1762.

[Zhang et al., 2009 b], S. Zhang, X. Zhang, C. Zhao et al., Research on an Mg–Zn alloy as a degradable biomaterial, Acta Biomaterialia 6 (2010) 626–640.

[Zhao et al., 2008], M. Zhao, M. Liu, G. Song, A. Atrens, Influence of the b-phase morphology on the corrosion of the Mg alloy AZ91, Corros. Sci. 50 (2008) 1939–1953.

[Zheng et al., 2009], Y. Zheng, X. Gu, Y. Xi, D. Chai. In vitro degradation and cytotoxicity of Mg/Ca composites produced by powder metallurgy, Acta Biomater 6 (2010) 1783–1791.

[Zhou et al., 2009], W. Zhou et al., Effect of heat treatment on corrosion behaviour of magnesium alloy AZ91D in simulated body fluid, Corros. Sci. 52 (2010) 1035–1041.

[Zhuang et al., 2008], H. Zhuang, Y. Han, A. Feng, Preparation, mechanical properties and in vitro biodegradation of porous magnesium scaffolds, Materials Science and Engineering C 28 (2008) 1462–1466.

[Zucchi et al., 2006], F. Zucchi, V. Grassi et al., Electrochemical behaviour of a magnesium alloy containing rare earth elements, J Appl Electrochem. 2006; 36:195.

Acknowledgements

I want to express my sincerest appreciation to a number of people who always encouraged me and who enlightened me in making my research work completed. First and foremost I need to thank my supervisor Dr. Hari Babu Nadendla, who possesses unending source of knowledge. When I encountered some frustration in the project, his valuable suggestions and favourable advices continually guide me out of "troubles". His enthusiastic and optimistic attitude toward science research also deeply affects me. Without his efforts, it is absolutely impossible to accomplish this work for me.

Moreover, I specially would to thank Dr. Yubo Zuo, who is a professional researcher in the field of metallurgy. My experiments during this year are almost conducted under his assistance. The discussions with him have enabled me to solve problems associated with experiments.

I want to take this opportunity to thank Prof. Zhongyun Fan, who is a great expert for advanced solidification technology. I definitely appreciate that he has provided me financial support and the opportunity for me to work at *BCAST* in *Brunel University*. I would like to express my sincere thanks to Professor Fan.

Last but not least, I wish to thank my family for their encouragement and supported during the whole process of my education, particularly to my fiancée, for her waiting and love.